NORSEWInD satellite wind climatology

Hasager, Charlotte Bay; Badger, Merete; Mouche, Alexis; Stoffelen, Ad; Driesenaar, Tilly; Karagali, Ioanna; Bingöl, Ferhat; Pena Diaz, Alfredo; Astrup, Poul; Nielsen, Morten; Hahmann, Andrea N.; Costa, Paulo; Berge, Erik; Bredesen, Rolv Erland

Publication date:
2012

Document Version
Publisher's PDF, also known as Version of record

NORSEWInD satellite wind climatology

DTU Wind Energy E-Report

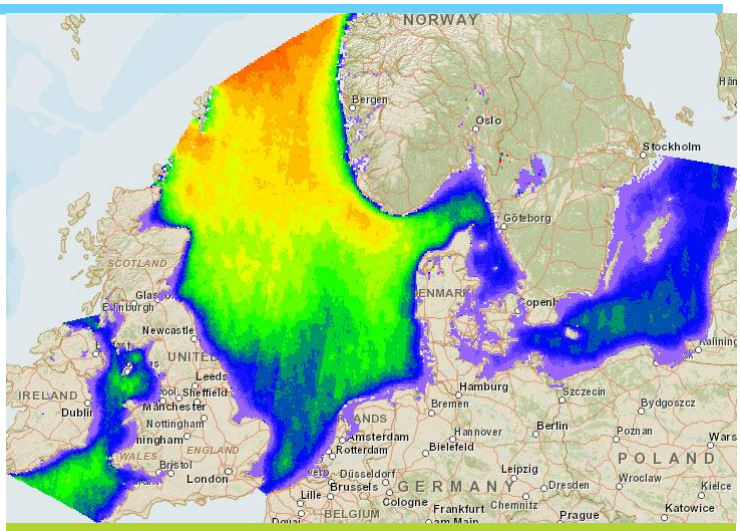

Charlotte Bay Hasager, Merete Badger, Alexis Mouche, Ad Stoffelen, Tilly Driesenaar, Ioanna Karagali, Ferhat Bingöl, Alfredo Peña, Poul Astrup, Morten Nielsen, Andrea Hahmann, Paulo Costa, Erik Berge, Rolv Erland Bredesen

DTU Wind Energy-E-0007(EN)
Publication September 2012

NORSEWInD

2007 - 2013

European Commission

DTU Wind Energy
Department of Wind Energy

Author: Charlotte Bay Hasager, Merete Badger, Alexis Mouche, Ad Stoffelen, Tilly Driesenaar, Ioanna Karagali, Ferhat Bingöl, Alfredo Peña, Poul Astrup, Morten Nielsen, Andrea Hahmann, Paulo Costa, Erik Berge, Rolv Erland Bredesen
Department: DTU Wind Energy

DTU Wind Energy-E-0007(EN)
Publication date September 2012

Abstract (max. 2000 char.): The EU-NORSEWInD project www.norsewind.eu has taken place from August 2008 to July 2012 (4 years). NORSEWInD is short for Northern Seas Wind Index database. In the project ocean surface wind observations from space have been retrieved, processed and analysed. The overall aim of the work is to provide new offshore wind climatology map for the entire area of interest based on satellite remote sensing. This has been based on Synthetic Aperture Radar (SAR) from Envisat ASAR using 9000 scenes re-processed with ECMWF wind direction and CMOD-IFR. The number of overlapping samples range from 450 in the Irish Sea to more than 1200 in most of the Baltic Sea. Wind resource statistics include maps at 2 km spatial resolution of mean wind speed, Weibull A and k, and energy density at 10 m above sea level. Uncertainty estimates on the number of available samples for each of the four parameters are presented. QuikSCAT ocean wind vector observations have been analysed for the same four parameters and ASCAT for mean wind speed. All satellite data has been compared to in-situ observations available in the Norsewind project. SSM/I passive microwave wind speed data from 24 years observed around 6 times per day are used to estimate trends in offshore winds and interestingly a shift in the seasonal pattern is notice. All satellite-based wind products are valid at 10 m, thus it is desirable to lift winds to higher levels for wind energy products. A method has been suggested to lift winds from 10 m to hub-height but more research is needed on this topic. The key wind energy statistical maps based on satellite data in the Norsewind project are publically available at web-sites:
LNEG http://geoportal.lneg.pt//index.php?lg=en&state=Inicio
Norsewind http://www.norsewind.eu/public/index.html
SAR-based results are also available at
SOPRANO http://soprano.cls.fr/ select wind/statistics(L3), Norsewind

ISBN 978-87-92896-12-4

Contract no.:
TREN-FP7EN-219048

Project no.:
43013

Sponsorship: FP7

Cover :
Mean wind speed at 10 m based on 9000 Envisat ASAR WSM images for the Northern European Seas.

Pages: 67
Tables: 8
References: 37

Technical University of Denmark
Department of Wind Energy
Frederiksborgvej 399
4000 Roskilde
Denmark
Telephone +45 46775024
bcar@dtu.dk
www.vindenergi.dtu.dk

Contents

1 Introduction 5

1.1 Study area 6

2 Satellite data sources 7

3 Envisat ASAR 8

3.1 Data set 8
3.2 Processing chain 9
Inversion scheme used for the chain 10
Investigation for new inversion algorithms 10
3.3 Comparisons 11
3.4 Wind resource maps 13
3.5 Lifting winds to hub-height 20
3.6 Summary and perspectives 23

4 QuikSCAT 24

4.1 Background 24
4.2 Comparisons 24
4.3 Wind resource maps 27
4.4 Summary and perspectives 32

5 ASCAT Coastal L3 wind product 33

5.1 Reprocessing of ASCAT L3 coastal wind product for the North Sea and Irish Sea 33
5.2 Comparison of L3 coastal winds and L3 ECMWF winds 34
5.3 Comparison with WRF climatology 39
5.4 Triple collocation of ASCAT L3, WRF and meteorological mast 40
5.5 Wind map comparison 48
5.6 Summary and perspectives 49

6 SSM/I 50

6.1 Wind power trends in the North Sea and the Baltic Sea as found from SSM/I satellite data. 50
6.2 Summary and perspectives 51

7 Summary and conclusion 58

Appendix A 59

Appendix B 61

Appendix C 62

References 64

Preface 5

The EU-NORSEWInD project www.norsewind.eu coordinated by Andy Oldroyd at Oldbaum Services, UK, has taken place from August 2008 to July 2012 (4 years). NORSEWInD is short for Northern Seas Wind Index database. One part of the project was to ensure collection of relevant satellite information, in particular, ocean surface wind observations from space. This part of work was led by Charlotte Bay Hasager at DTU Wind Energy. The overall aim of the work is to provide new offshore wind climatology map for the entire area of interest based on satellite remote sensing. The report summarizes key results on satellite ocean wind observations in respect to the NORSEWInD project.

1 Introduction

In August 2008 the European project "Northern Seas Wind Index Database" (NORSEWInD) started within the seventh framework programme of the European Union http://www.norsewind.eu/public/index.html. The aim of the project is to quantify the wind resource for offshore wind power utilisation. In order to truly understand the quality of the wind resource available, the wind regime will be captured using instrumentation installed at offshore locations in the Baltic, Irish and North Seas. Furthermore a small validation area is selected off Portugal in the Atlantic Ocean. A combination of ground-based remote sensing, satellite-based remote sensing, meteorological masts, computational modelling and forecasting is used in the project. NORSEWInD takes a multi-disciplinary, multi-industrial sector approach to achieve a thorough understanding of offshore wind conditions. The end-product of the project is a comprehensive wind resource database and an offshore wind atlas for (pre-) feasibility, as well as a suite of techniques that can be translated to any offshore location in the world.

One part of the NORSEWInD project was to collect remote sensing observations from space on ocean surface winds in near-real-time (NRT). The overall aim is to provide new offshore wind climatology map for the entire area of interest based on satellite remote sensing. The report describes the activities and key results of the work conducted on satellite remote sensing observations.

The three partners contributing satellite remote sensing data collection and processing are:

- DTU Wind Energy http://www.vindenergi.dtu.dk/
- CLS http://www.cls.fr/welcome_en.html
- KNMI http://www.knmi.nl/

Also partners LNEG http://www.lneg.pt/ and KVT http://www.vindteknikk.no/en/ contributed with analysis and presentation of results.

List of acronyms is found in Appendix B.

We acknowledge QuikSCAT and SSM/I data from Remote Sensing Systems, ASCAT data from KNMI, Envisat ASAR from the European Space Agency. We acknowledge meteorological observations from Horns Rev from DONG energy and Vattenfall, meteorological data from FINO-1 /-2 from BSH, and meteorological data from Greater Gabbard from SSE.

1.1 Study area

The study area is outlined in Figure 1.1.

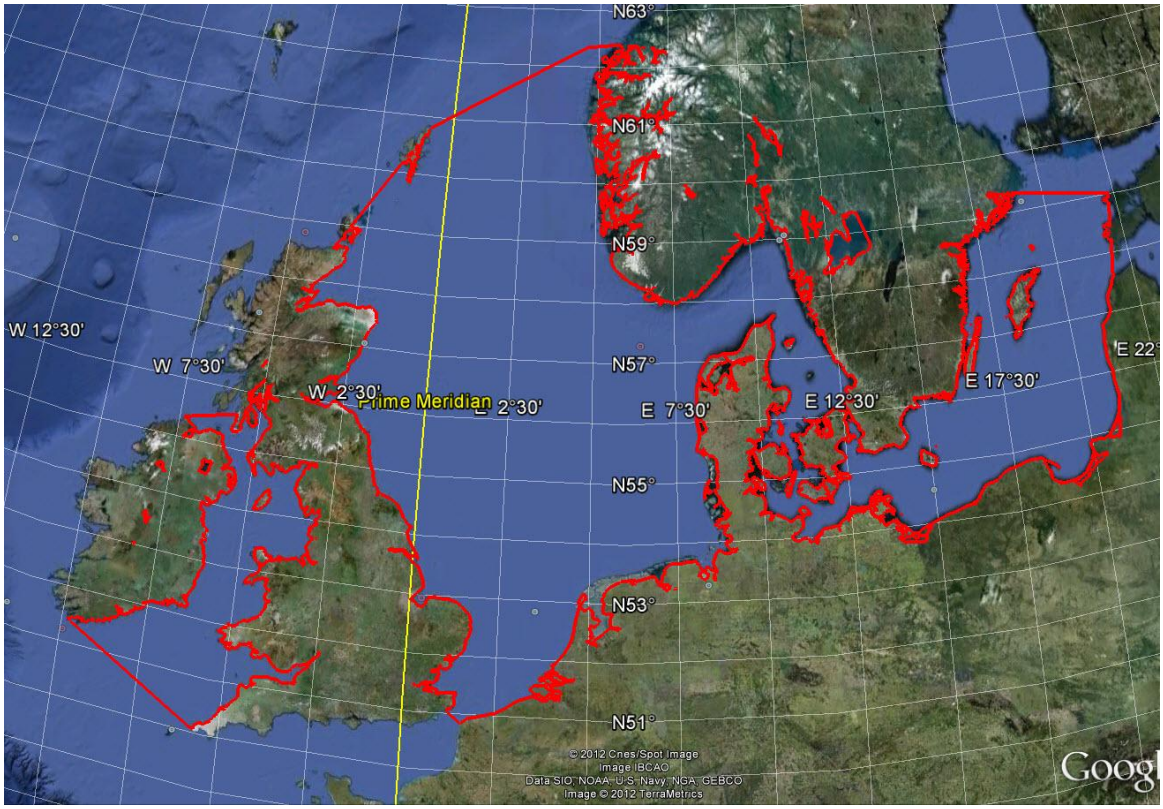

Figure1.1. Outline of the NORSEWInD study area.

The study area includes the Baltic Sea, Irish Sea, and North Sea, roughly of sizes 380.000 km^2, 113.000 km^2, and 705.000 km^2, respectively. In total the Northern European Seas area covered is 1.198.000 km^2.

The NORSEWInD region is currently home for the majority of EU-27 offshore wind farms. According to EWEA (http://www.ewea.org/) the installed cumulative offshore capacity by the end of year 2011 was around ~3.8 GW in 53 offshore wind farms in EU-27. New wind farms projects at preparatory stage sums up to ~3GW total capacity and the consented offshore wind farm projects capacity sums up to ~18 GW.

2 Satellite data sources

The satellite data sources used in NORSEWInD include remote sensing observations from the

- European Space Agency (ESA) satellite Envisat from the Advanced Synthetic Aperture Radar (SAR)
- National Aeronautics and Space Administration (NASA) satellite QuikSCAT with the SeaWinds scatterometer (QSCAT)
- European Organisation for the Exploitation of Meteorological Satellites (EUMETSAT) with the Advanced Scatterometer (ASCAT)
- Defence Meteorological Satellite Program (DMSP) with the Special Sensor Microwave Imager (SSM/I)

The SAR data are granted by ESA. The QSCAT and SSM/I data are from Remote Sensing Systems (RSS) and the ASCAT Coastal data are from Ocean and Sea ice Satellite Application Facility (OSI SAF) at the Royal Netherlands Meteorological Institute.

During the NORSEWInD project all data were collected in NRT. Re-processing and new versions downloads have taken place since.

The report is structured per satellite data type starting with image processing and basic information on the surface ocean wind products, followed by selected results, summary and perspectives.

3 Envisat ASAR

3.1 Data set

Envisat ASAR satellite scenes from ESA were collected in NRT by DTU Wind Energy and CLS during the four years of the NORSEWInD project. We were fortunate to obtain 9256 unique Envisat ASAR scenes in wide swath mode (WSM) for the study area. This means the NORSEWInD study area is covered very well. The distribution of the Envisat ASAR scenes over Envisat's lifetime (2002 to early 2012) is shown in Table 3.1.

Table 3.1 Envisat ASAR scenes per year.

Year											
2002	2003	2004	2005	2006	2007	2008	2009	2010	2011	2012	Total
0	3	19	582	965	1122	1430	1486	1721	1510	418	9256

The monthly distribution of scenes is shown in Table 3.2. The Envisat ASAR scenes are relatively evenly distributed over the year with the highest number of scenes (932) in March and the lowest (641) in June.

Table 3.2 Distribution of Envisat ASAR scenes over the months 1-12 of the year.

Month												
1	2	3	4	5	6	7	8	9	10	11	12	Total
887	775	932	742	777	641	690	772	751	784	729	776	9256

The distribution between ascending (northbound) passes and descending (southbound) passes is almost equal with 4665 and 4591 scenes, respectively. The local overpass time is usually within the time intervals 21:30-22:00 for ascending scenes and 10:30-11:00 for descending scenes. Observations from other times of the day are not available due to the orbital characteristics of the satellite, which operated in a polar sun-synchronous orbit.

In Figure 2.1 the spatial distribution of the SAR scenes is shown. The number of overlapping scenes ranges from approximately 200 for areas west of the UK to 1400 for parts of the Norwegian coastal seas.

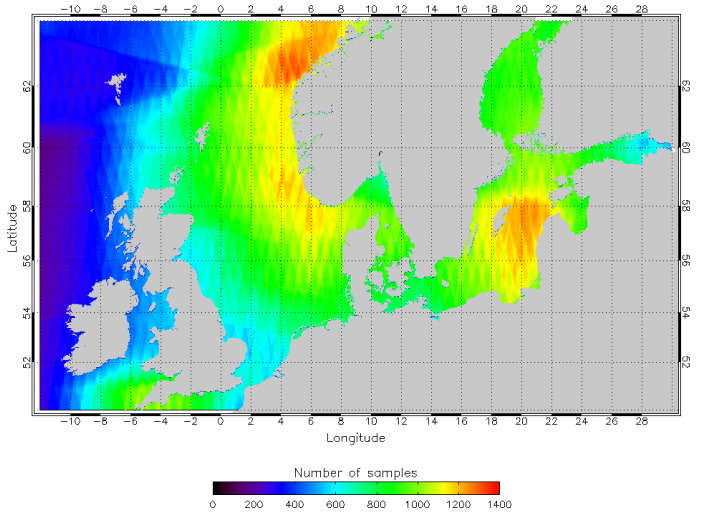

Figure 2.1. Map showing the number of overlapping Envisat ASAR scenes in WSM mode, which was achieved over the NORSEWInD area.

3.2 Processing chain

SAR-based ocean surface wind retrieval was done at both DTU Wind Energy and CLS using different geophysical model functions (GMF) and wind direction inputs for the processing of raw satellite data to 10-m wind speeds. Scientific results have been published (Badger et al., 2010a;Badger et al., 2010b;Christiansen et al., 2008;Hasager et al., 2008;Hasager et al., 2009;Hasager et al., 2010a;Hasager et al., 2010b).

Near the end of the project it turned out that to get a homogeneous dataset which was considered ideal for the final NORSEWInD SAR-based products, a complete re-processing of all the data acquired in the geographical area covered by NORSEWInD with the same methodology was necessary. To this aim, CLS developed a reprocessing chain able to do massive processing and with flexibility in the choice of the parameters. This section briefly describes the system. The data processed is Envisat ASAR wide swath mode (WSM) scenes.

This reprocessing chain is part of Soprano which is a combination of tools developed by CLS to produce L2 ocean products from SAR data. It relies on an infrastructure (CLS VGISAT receiving station) dedicated to the receiving, archiving and processing of satellite data.

The core of the Soprano chain is the L2 processor developed by CLS which generates ocean L2 products from L1 SAR products based on innovative algorithms.

The operation of Soprano and thus the reprocessing also implies the:
- management of the input data mandatory for the L2 processor.
- dissemination of L2 (and higher levels) products for users.

L1 products used as main inputs of the L2 wind are produced by:
- L0 products acquired and processed into L1 products (WS detected products) by the network of ESA receiving ground stations that are made available to CLS via the rolling archive.
- L0 products directly acquired and processed into L1 products (WS detected and complex products) by CLS receiving ground station (VIGISAT).

L1 product files and all L1 into L2 processes are managed by Maestro. Maestro is a software developed by CLS to help satellite (in particular SAR data) project management in a multi-projects and multi-clients context.

L2 products processed in near-real-time can be browsed and downloaded by users thanks to soprano web interface (http://soprano.cls.fr/) hosted on an external web server. L2 products reprocessed are available on the ftp server (ft.soprano.csl.fr) in a directory dedicated to Norsewind project.

The figure 3.2 is a high level description of SOPRANO chain. As observed the left hand side panel is dedicated to the input data necessary for the processing of wind maps that comes from other institutes than CLS. The middle panel describes the tasks that are done at CLS. It encompasses the core of the processing. The left hand side panel is dedicated to the dissemination part of the chain.

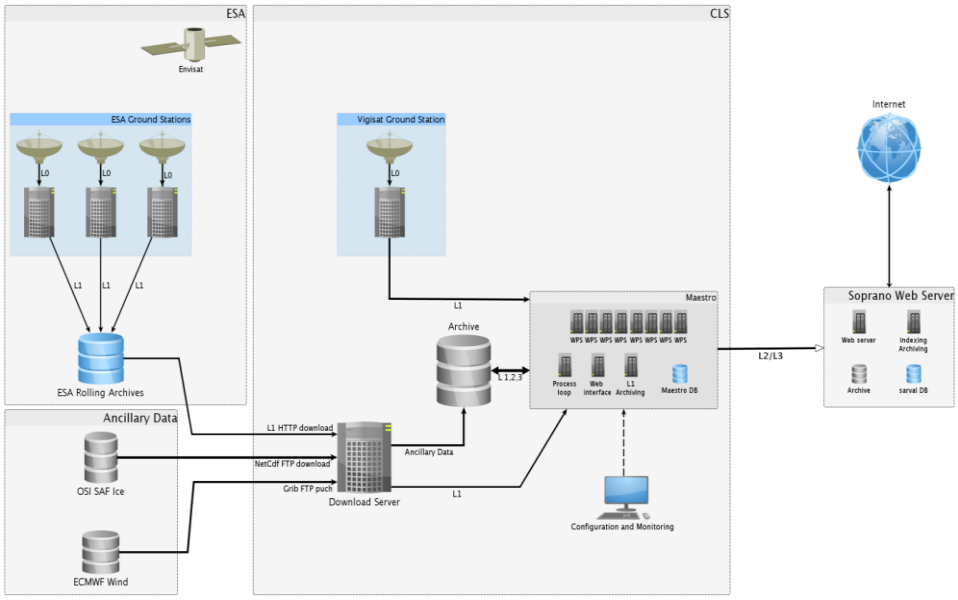

Figure 3.2 SAR wind inversion

This section is dedicated to inversion schemes used for wind maps production from SAR data.

Inversion scheme used for the chain

In two publications (Christiansen et al., 2008) (Hasager et al., 2009) the basic processing into wind maps based on SAR is described. Documentation also exists on the website http://soprano.cls.fr/. The seminal paper from which the method is derived has been written by (Portabella et al., 2002). This methodology has then been revisited by (Kerbaol, 2007). We use this last version of the algorithm for the reprocessing. Ancillary data is given by ECMWF and ice mask by OSI-SAF.

Investigation for new inversion algorithms

In year 2011, we presented how new radar quantities such as the Doppler could benefit wind inversion from SAR data. The paper related to this work is now in press (Mouche et al., 2012).

This year, we decided to investigate the benefit of having a significant amount of SAR data co-located in time and space with a scatterometer such as ASCAT. The idea is to take the ASCAT wind as reference and to investigate the relationship between radar parameters as measured by the SAR and the wind from ASCAT. From this work a geophysical model function to relate normalized radar cross section as measured by SAR in HH polarization to the wind speed and direction has been derived for the first time. It enables to do wind inversion for data in HH polarization without using the so-called polarization ratio and hopefully to get better results, see figure 3.3. This work is in progress.

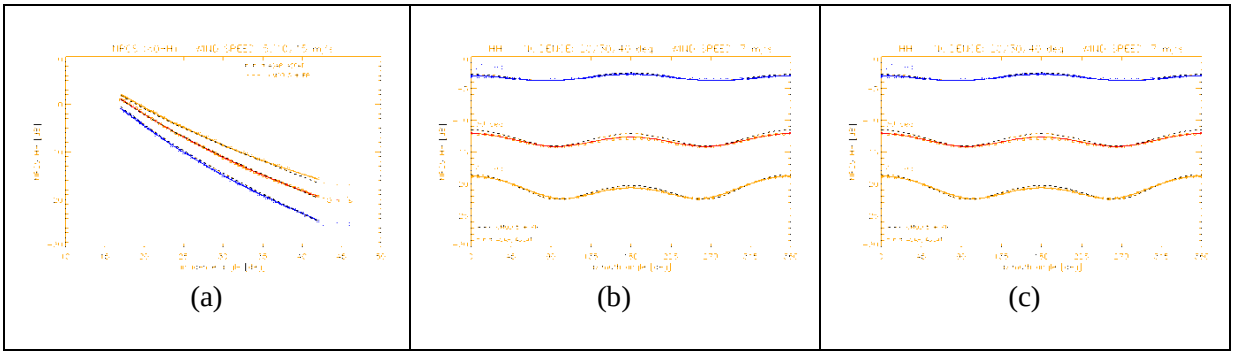

(a) (b) (c)

Figure 3.3 NRCS with respect of (incidence angle), (b) wind speed and (c) radar look angle with respect to wind direction. Dotted line is given by CMOD 5 combined with a PR. Solid line is the Geophysical Model Function (GMF) derived from the data analysis (symbols).

3.3 Comparisons

In the NORSWInD project observations from meteorological masts were kindly provided by several data owners early in the project.

Based on these observations a comparison study between SAR-based wind maps and meteorological observations were performed in the Baltic Sea. SAR-based winds are valid at 10 m above sea level. Thus the wind observations from other heights at the meteorological masts were extrapolated to 10 m before comparison. The meteorological data were corrected for atmospheric stability. In the Baltic Sea the wind speed was found to have root mean square error (r.m.s.) of 1.17 ms^{-1} and the correlation coefficient R^2 of 78. The findings are based on 875 collocated samples from nine offshore meteorological masts in the period 2003 to 2010 (Hasager et al., 2011). The Geophysical Model Function (GMF) used was CMOD5.

In the North Sea later studies from five meteorological masts using three different GMF's have been tested. Selected results are presented in figures 3.4 to 3.6.

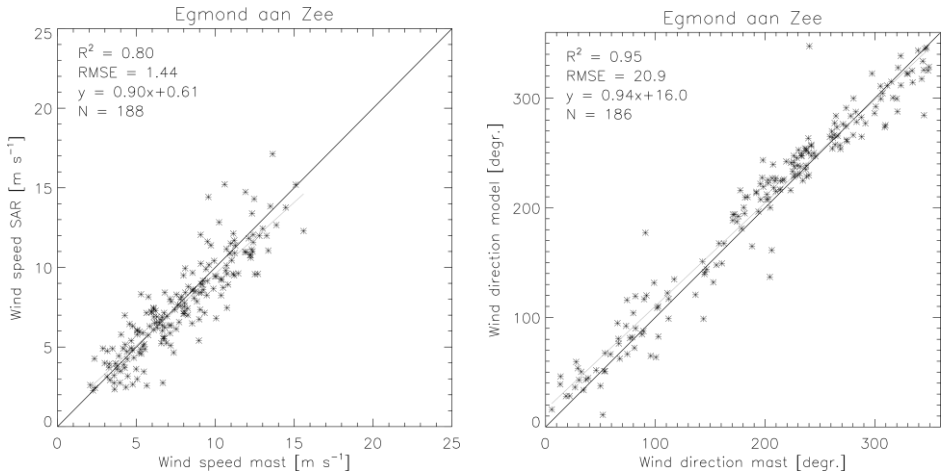

Figure 3.4 Comparison results of wind speed (left) and wind direction (right) of observations at the meteorological mast Egmond aan Zee and SAR-based wind maps using CMOD-IFR2 with stability corrected and the winds are in the range 2-25 ms^{-1}.

Comparison results as graphed in figure 3.4 were obtained for five masts for CMOD-IFR2. In Appendix A is presented the detailed results in table format. It is important to notice that stability correction was only possible at Egmond aan Zee and Horns Rev M2. The results are in Appendix

A table 1. For the other three masts the meteorological mast winds are not stability corrected, Appendix A table 2.

Please refer to (Peña et al., 2012) for further detail on the meteorological mast data.

In figure 3.5 the r.m.s. error and correlation coefficient R^2 are graphed for the five masts for CMOD-IFR2. The lower the r.m.s. error is the better, and the higher the R^2 is the better. From this it is clear that results from Horns Rev M2 and Egmond aan Zee are best. This is as expected as stability correction, which is only possible for these two masts, is important to include in vertical wind extrapolation.

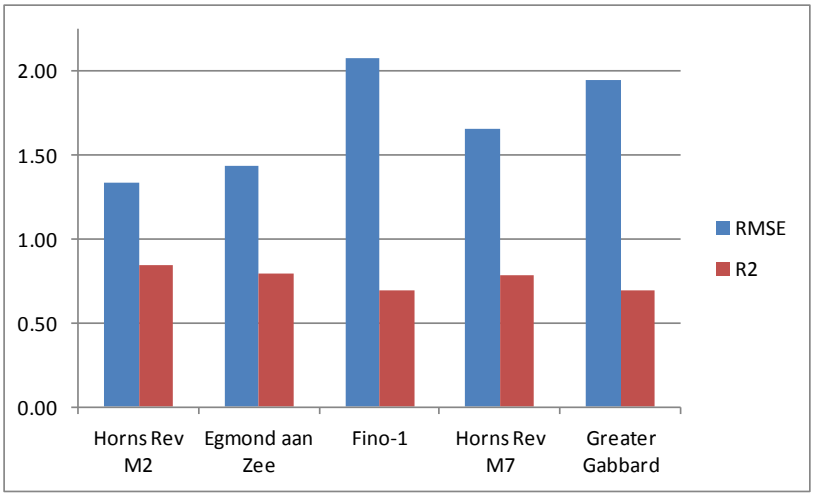

Figure 3.5. Comparison statistics on wind speed observed from offshore meteorological masts and SAR-based wind maps, showing r.m.s.error (m s^{-1}) and correlation coefficients R^2.

Finally we present the comparison results for Horns Rev M2 and Egmond aan Zee versus three GMF's in figure 3.6. The satellite winds retrieved with CMOD-IFR2 and CMOD5 are compared with stability dependent winds (SDW) whereas the winds retrieved with CMOD5.n are compared with equivalent neutral winds obtained from the two masts. From figure 3.6 and Appendix A table 3 the comparison results show that for the wind speed range 2-20 m/s the choice of GMF is not critical, as the results are fairly comparable. The reason for the slightly better agreement between SAR and mast winds at Horns Rev M2 may be influence of a wind farm adjacent to the mast at Egmond aan Zee.

The combined archives of satellite wind maps from DTU Wind Energy and CLS were reprocessed with input wind direction from ECMWF and using the CMOD-IFR2 (see section 3.1).

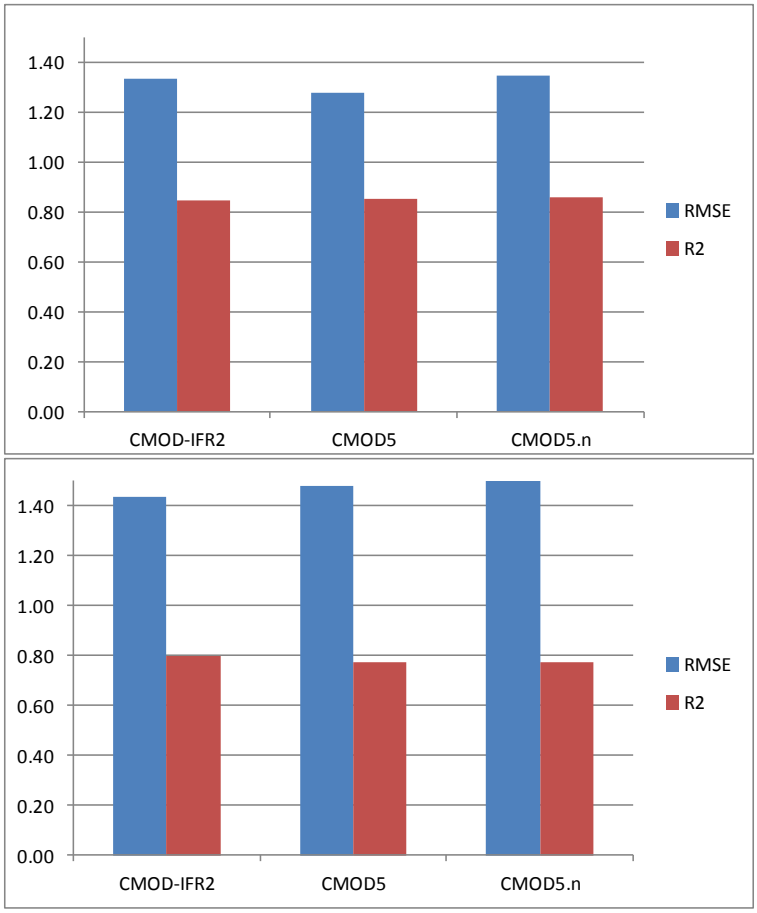

Figure 3.6 Comparison results between meteorological observations from Horns Rev M2 (above) and Egmond aan Zee (below) and SAR-based wind maps using CMOD-IFR2 (SDW), CMOD5 (SDW) and CMOD5.n (ENW) showing r.m.s.error (m s^{-1}) and correlation coefficients R^2.

3.4 Wind resource maps

Wind resource calculation is traditionally based on meteorological observations of hourly values for a least one year, i.e. 8760 observations. The data are used in the Wind Atlas Analysis and Application program (WAsP) www.wasp.dk (Mortensen et al., 2000;Troen and Petersen, 1989). This is de facto standard method. The usual procedure in a WAsP analysis is to divide the data into twelve bins for 30 degree wind direction sectors and determine the Weibull wind-speed distribution for each of these.

The number of satellite ocean wind observation in a single direction bin could be very small due to the observational frequency from space. Thus alternatives were developed (Nielsen et al., 2004) called S-WAsP, short for Satellite-WAsP (Hasager et al., 2008). It was chosen to use the second moment fitting for the Weibull scale (A) and shape (k) parameters (Pryor et al., 2004) (Barthelmie and Pryor, 2003) for the final products in NORSEWInD.

The number of satellite observation in a single directional bin could be small so for the present analysis it was decided to fit a distribution to all data and used the shape parameter for every sector. The scale parameter is then estimated by the average wind speed in each sector. The frequency of occurrence in each sector is uncertain when observations are sparse and there is a risk of observing sectors without any observation and no estimate of the mean wind. An alternative to simple bin-counting is to sort all observations after directions, estimate the probability density between the observations by the angle separating between them, and finally resample the densities in the standard sectors.

The available wind power density, E, (that is proportional to the wind speed cubed), may be calculated from the two Weibull parameters, the scale parameter A and the shape parameter k, using the gamma function Γ, and the air density ρ (~1.245 g/m3 at 10°C) as

$$E = \frac{1}{2}\rho A^3 \Gamma\left(1 + \frac{3}{k}\right). \quad (1)$$

Studies from the North Sea have shown SAR wind maps to be a possible source of information for the estimation of Weibull A and k (Badger et al., 2010b;Christiansen et al., 2006) with accuracy below 5% for Weibull A and below 7% for Weibull k and energy density based on comparison to observations from three meteorological masts. The study in the Baltic Sea showed similar error on Weibull A but up to 16% on Weibull k and even higher for energy density comparing to only one meteorological mast observations.

The final results for NORSEWInD based on Envisat ASAR are shown in figures 3.7 to 3.11, maps of the number of samples, mean wind speed, Weibull A and k, and energy density, respectively. The spatial resolution is 2 km by 2 km. All results are for 10 m above sea level. At http://geoportal.lneg.pt//index.php?lg=en&state=Inicio the digital versions are available.

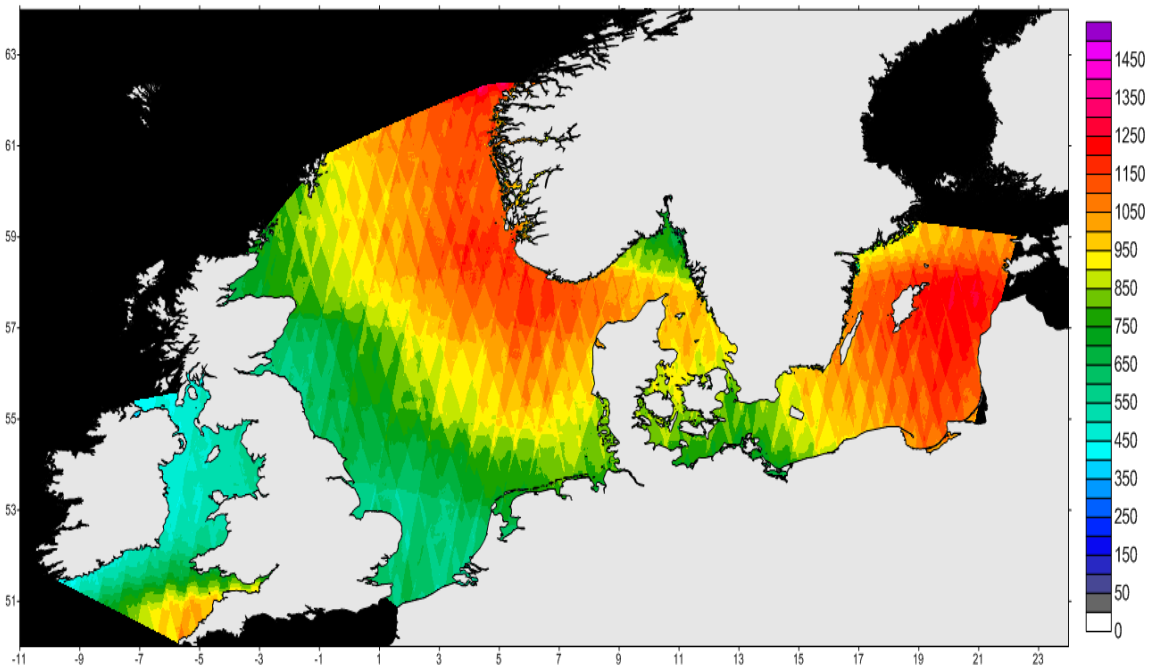

Figure 3.7 Number of overlapping Envisat ASAR WSM scenes used for the SAR-based wind resource estimation for the Northern European Seas.

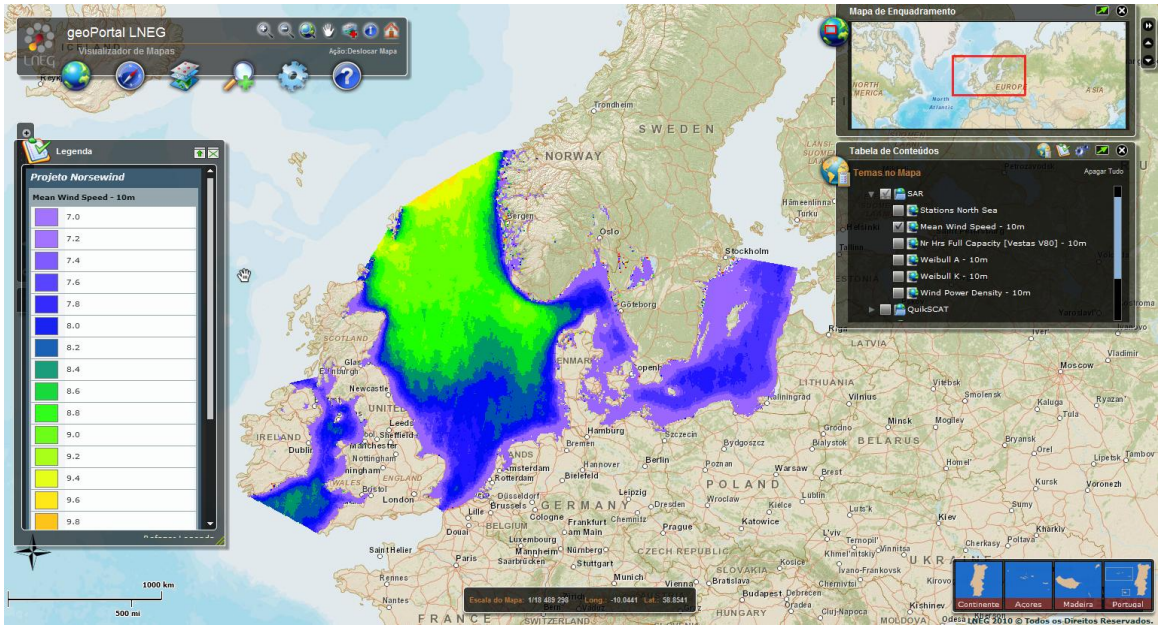

Figure 3.8 Mean wind speed at 10 m observed by Envisat ASAR for the Northern European Seas.

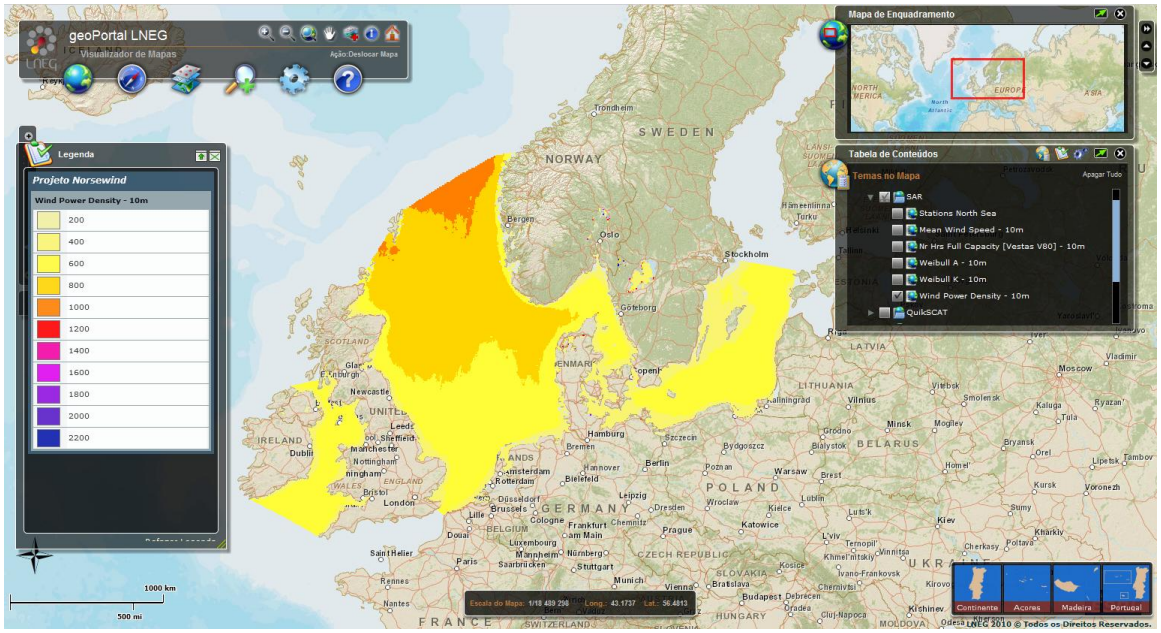

Figure 3.9 Energy density at 10 m observed by Envisat ASAR for the Northern European Seas.

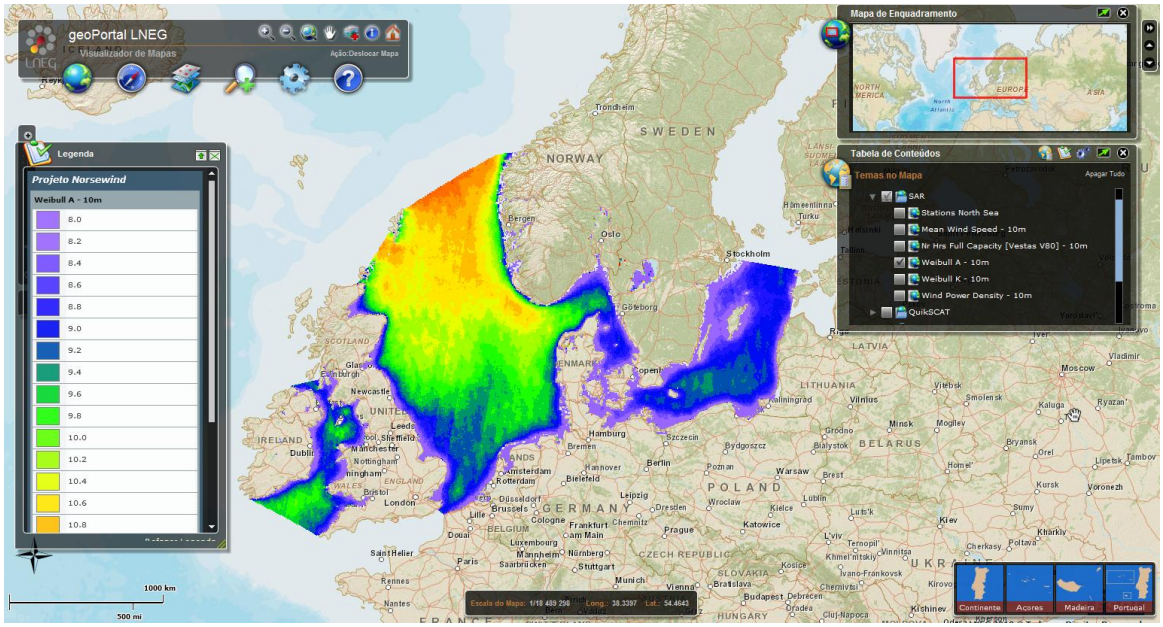

Figure 3.10 Weibull A parameter at 10 m observed by Envisat ASAR for the Northern European Seas.

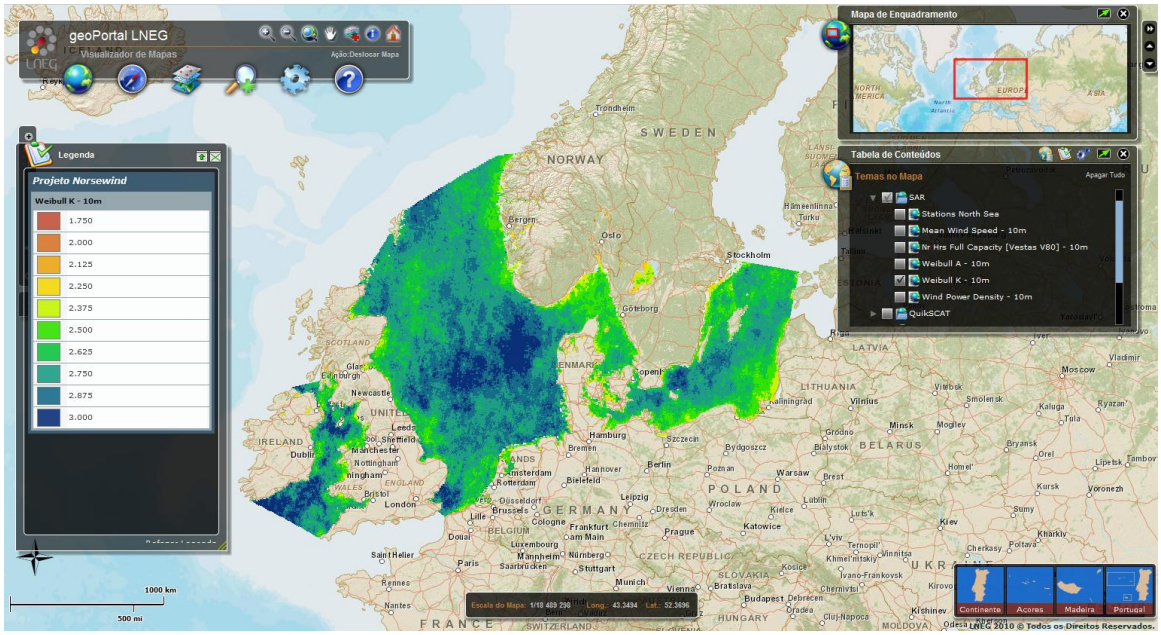

Figure 3.11 Weibull k parameter at 10 m observed by Envisat ASAR for the Northern European Seas.

The number of overlapping scenes (Fig. 3.7) ranges from around 400 in parts of the Irish Sea to more than 1400 in parts of the North Sea and Baltic Sea. The mean wind speed (Fig. 3.8) ranges from around 7 ms^{-1} near many coastlines and in parts of the Baltic Sea up to around 9.8 ms^{-1} in the northern part of the North Sea. There is a clear north to south gradient in the North Sea with lower winds further south. Lee effects of the British Isles are clear too. The energy density (Fig. 3.9) ranges from less than 600 Wm^{-2} in parts of the Baltic Sea to more than 1000 Wm^{-2} in the northern part of the North Sea. The Weibull A parameter (Fig. 3.10) ranges from 8.0 ms^{-1} in the Baltic Sea to 10.8 ms^{-1} in the northern part of the North Sea. The Weibull k parameter (Fig. 3.11) is particularly high in the central part of the North Sea and in the southern part of the Irish Sea.

Also at the web-site http://soprano.cls.fr at link Soprano/wind/statistics(L3) and select Norsewind the SAR-based results are presented. At this site also data outside the focus of study are available for viewing. See Appendix C for these maps. There are indicated ten points of interest at which the wind roses can be viewed at this server. Examples of wind roses from four locations are given in figure 3.12. The positions can be seen in the maps in Appendix C.

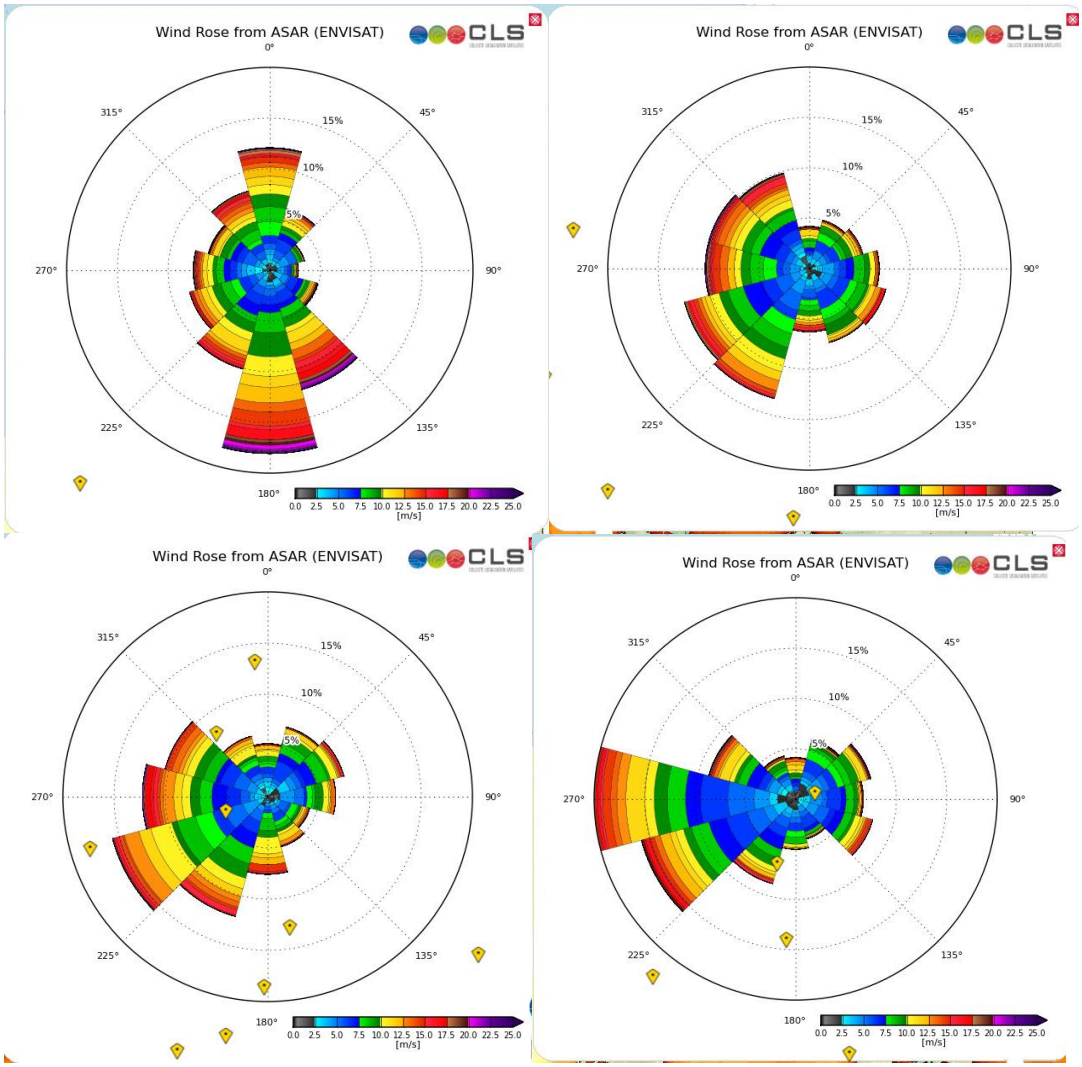

Figure 3.12 Wind roses based on Envisat ASAR from top left near Norway North Sea (3.7E, 61.2N), top right near Denmark North Sea (6.3E, 54.3 N), bottom left Irish Sea (-53.E, 51.4N), bottom right Baltic Sea (17.4E, 55.3 N).

Early in the project is was not clear how many samples would be available for the NORSEWInD region. Thus the wind class sampling method (or hybrid method) (Badger et al., 2010a;Badger et al., 2010b) was considered a possible option in case only few samples would become available. The method is based on relatively few, well-selected wind conditions in the SAR wind maps, and then weighted with long-term wind statistics, e.g. from a meteorological mast and re-analysis model results. The accuracy of results on mean wind speed and the Weibuall scale and shape parameters were considered satisfactory using as little as around 125 well-selected SAR-based

wind maps. In the present study far more overlapping scenes were available and the wind class sampling method was not applied.

The number of samples available for the SAR-based calculation of mean wind speed, Weibull A and k, and energy density are similar. It is, however, necessary with relatively fewer samples to estimate mean wind speed and Weibull A than for Weibull k and energy density to obtain similar certainty (Barthelmie and Pryor, 2003;Pryor et al., 2004). The uncertainties for the four parameters are calculated and the maps are shown in Figures 3.13 to 3.16. The uncertainty calculation estimates the difference of the Weibull A and k fitted function and the measured wind distribution based on the available number of samples. We follow the equations from the appendix in (Pryor et al., 2004). We here assume that each SAR-based wind map is accurate and that the influence of time sampling is insignificant to the estimates. In other words, we assume the diurnal wind pattern to be described accurately using morning and evening observations only.

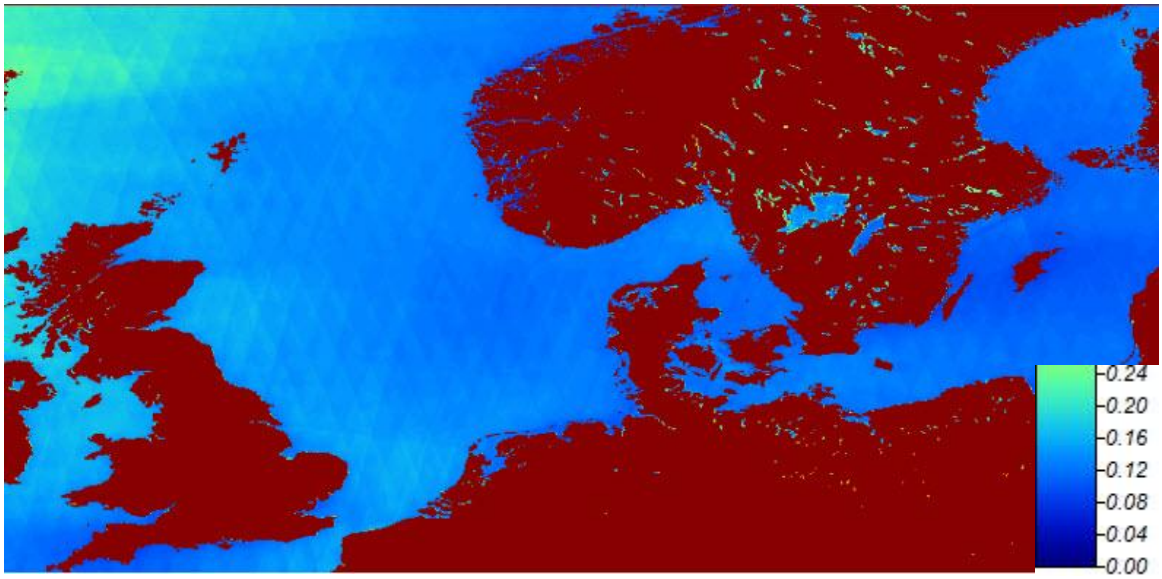

Figure 3.13 Map of uncertainty for mean wind speed in ms^{-1}.

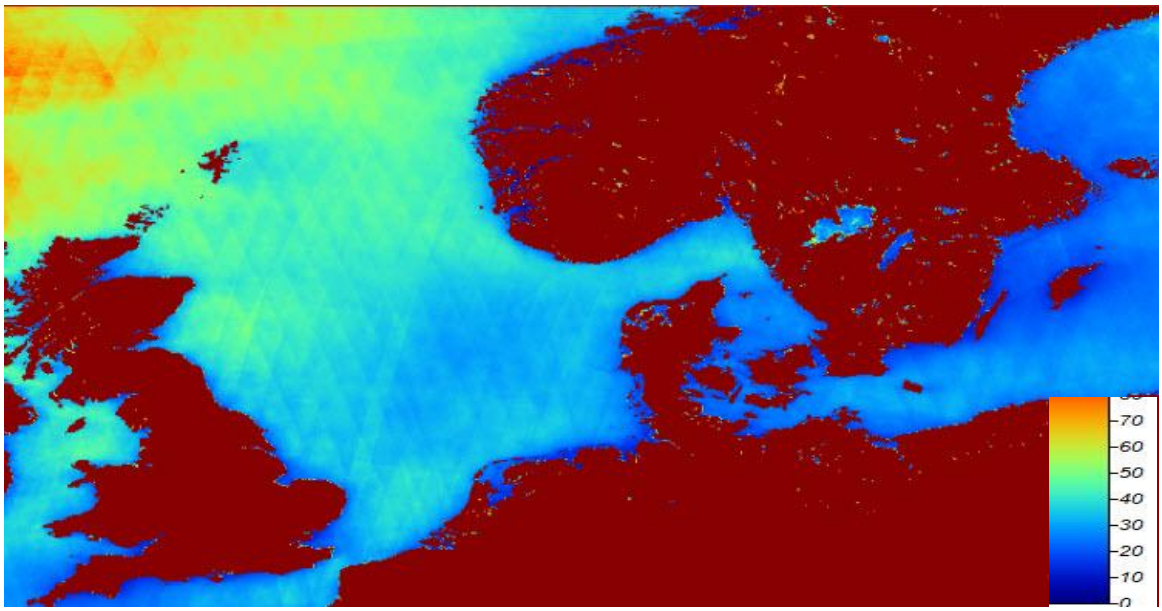

Figure 3.14 Map of uncertainty for energy density in $W\ m^{-2}$.

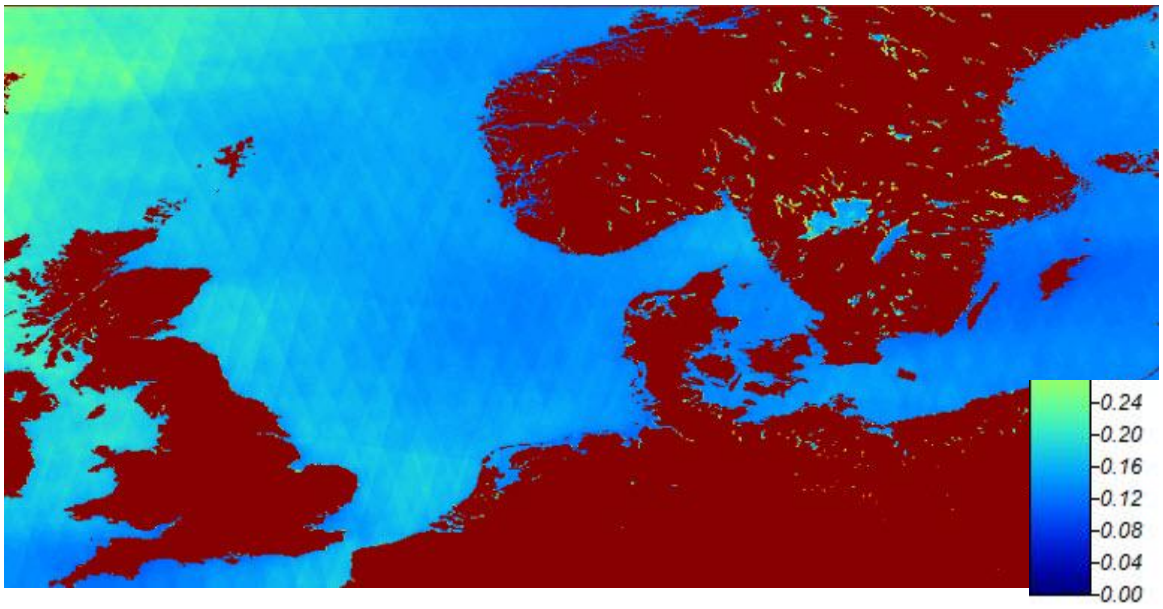

Figure 3.15 Map of uncertainty for Weibull A parameter in ms^{-1}.

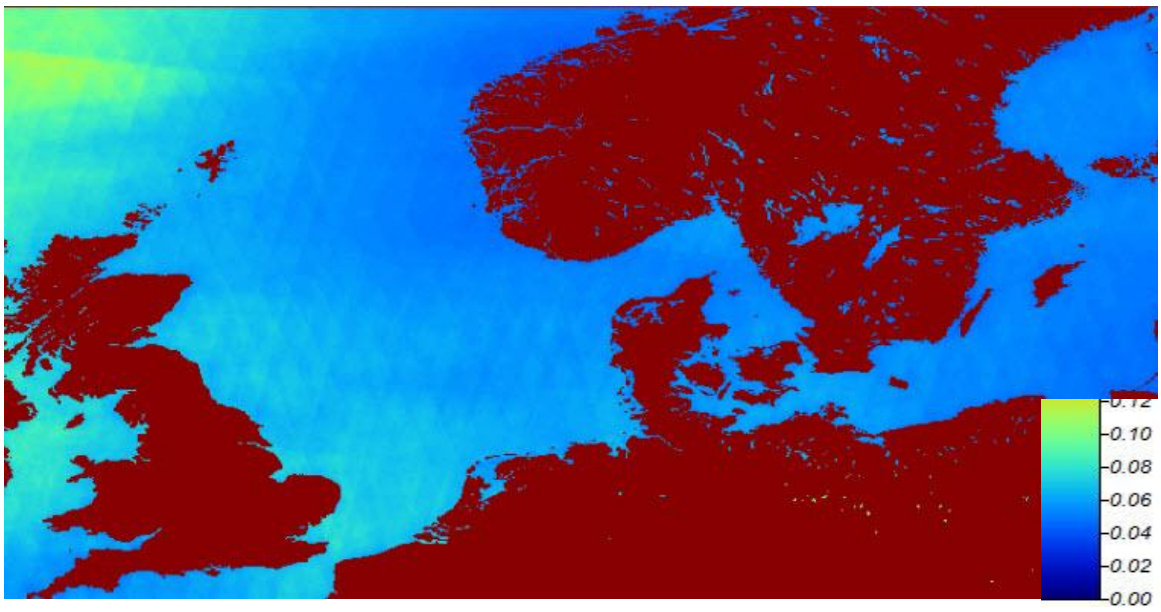

Figure 3.16 Map of uncertainty for Weibull k parameter.

From the results in Figures 3.13 to 3.17 it is seen that the uncertainty on mean wind speed and Weibull A is of the order 0.08 ms^{-1} in most of the study area and around 0.18 ms^{-1} in parts of the Irish Sea (with the fewest samples). The uncertainty of Weibull k is around 0.04 and for energy density from 20 to 50 Wm^{-2}.

Please note the area north of the British Isles is not included in the Norsewind study (see figure 3.7). In figure 2.1 and Appendix C maps show the number of samples also outside the study area.

3.5 Lifting winds to hub-height

The next step for efficient use of satellite ocean wind resource information is lifting of the ocean surface winds from 10 m to hub-height. Work is on-going and preliminary results presented (Badger et al., 2012a;Badger et al., 2012b).

The fundamental principle of the lifting analysis is to combine wind speed information from satellites with information about the atmospheric stability conditions from numerical modelling; in this case from the Weather Research and Forecasting model (WRF). A number of recent advances make the lifting of satellite winds possible:

- A validated description of vertical wind profiles at high levels is available (Peña and Hahmann, 2011) (Peña et al., 2008) (Peña et al., 2012)
- Wind retrieval algorithms can produce Equivalent Neutral Winds (ENW) (Hersbach, H. 2010)
- A large data set of concurrent satellite wind fields, WRF model simulations, and offshore measurements from masts and lidars has been generated in the NORSEWInD project

The first step in our analysis is to derive the friction velocity, u_* from the 10-m wind from SAR. Eq. 2, which describes the logarithmic wind profile for neutral conditions, is combined with Eq. 3, Charnock's equation (Charnock, 1955). Then u_{*SAR} is estimated through iteration:

$$u_{10SAR} = \frac{u_{*SAR}}{\kappa}\left[\ln\frac{10}{z_0}\right] \tag{2}$$

$$z_0 = \alpha_c \frac{u_*^2}{g} \tag{3}$$

κ in Eq. 2 is von Karman's constant of 0.4. In Eq. 3, z_0 is the aerodynamic roughness length, g is the acceleration due to gravity, and α_c is Charnock's parameter of 0.0144.

The second step is to estimate the atmospheric stability expressed as the Obukhov length, L from Eq. 4. Stable conditions occur for $L>0$ and unstable conditions occur for $L\leq 0$. Inputs are u_{*SAR} and the WRF parameters *T2* and *HFX*, which give the air temperature and heat flux.

$$L_{WRF/SAR} = \frac{-u_{*SAR}^3 T2_{WRF}}{g\,\kappa\, HFX_{WRF}} \tag{4}$$

Eq. 5-7 are applied to calculate the stability function, ψ_m for a given height; here the height 100 m is chosen:

$$L>0: \quad \psi_m = -4.7\frac{z}{L_{WRF/SAR}} \tag{5}$$

$$L\leq 0: \quad \psi_m = \frac{3}{2}\ln\left(\frac{1+x+x^2}{3}\right) - \sqrt{3}\arctan\left(\frac{2x+1}{\sqrt{3}}\right) + \frac{\pi}{\sqrt{3}} \tag{6}$$

$$\text{where } x = \left(1-12\frac{z}{L_{WRF/SAR}}\right)^{1/3} \tag{7}$$

Finally, the wind speed at 100 m, u_{100SAR} is estimated from Eq. 8 and 9 using, for stable conditions, the WRF parameter *PBLH* to describe the planetary boundary-layer height.

$$L_{WRF/SAR}>0: \qquad u_{100SAR} = \frac{u_{*SAR}}{\kappa}\left[\ln\frac{100}{z_0} - \psi_{\left(\frac{100}{L_{WRF/SAR}}\right)}\left(1-\frac{100}{2PBLH}\right)\right] \tag{8}$$

$$L_{WRF/SAR} \leq 0: \qquad u_{100SAR} = \frac{u_{*SAR}}{\kappa}\left[\ln\frac{100}{z_0} - \psi_{\left(\frac{100}{L_{WRF/SAR}}\right)}\right] \tag{9}$$

The lifting methodology was applied to satellite SAR data over the North Sea and the Baltic. The numerical modeling over the North Sea covers the one year following 1st of May 2006. Further details about the WRF simulations are found in Badger et al. 2012a and (Berge et al., 2009). A total of 80 concurrent Envisat ASAR scenes could be found for this period.

Figure 3.12 shows (left) the mean wind speed from the lifted SAR wind fields and (right) the mean difference between SAR winds and concurrent WRF simulations at 100 m. The mean difference is less than 1 m/s for the majority of the Norths Sea and always negative (i.e. wind speeds from SAR are lower than those from WRF). Towards the coastline of Germany and the Netherlands, the difference becomes much larger. The research platform Fino-1 is located in this complex area. Statistical results from mast-WRF and mast-SAR comparisons therefore show a negative bias for both the SAR and WRF winds at 100 m with respect to the mast observations (Table 3.3). The bias is larger for the SAR than for the WRF winds.

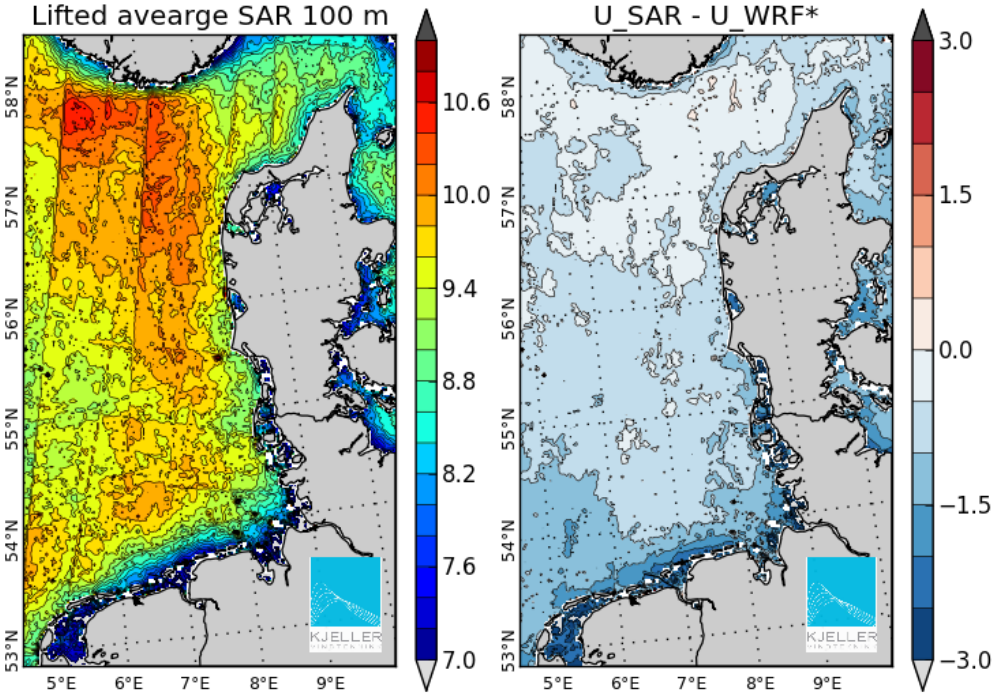

Figure 3.12 Left: mean wind speed (m/s) from a total of 80 SAR scenes lifted to 100 m. Right: Plot of the difference between 100-m SAR and WRF wind speeds (m/s) where U_WRF indicates WRF simulations concurrent with the SAR data acquisitions.*

Table 3.3 Mean wind speed, RMS error, and bias for different wind speed data at Fino-1, 100 m. The RMS error and bias is given for (SAR-mast) and (WRF-mast) using only WRF samples concurrent with the SAR samples.

	U (m/s)	RMS error (m/s)	Bias (m/s)
Mast	10.74	-	-
SAR	9.77	2.22	-0.97
WRF	10.46	1.75	-0.27

For the Baltic, six years of WRF simulations were available (2006-11). This WRF data set is described in (Peña et al., 2011). A total of 323 situations were found where concurrent WRF, SAR, and mast winds at 100-m were available at the research platform Fino-2. The SAR wind fields were taken from DTU's image archive and re-processed with CMOD5.n to give ENW.

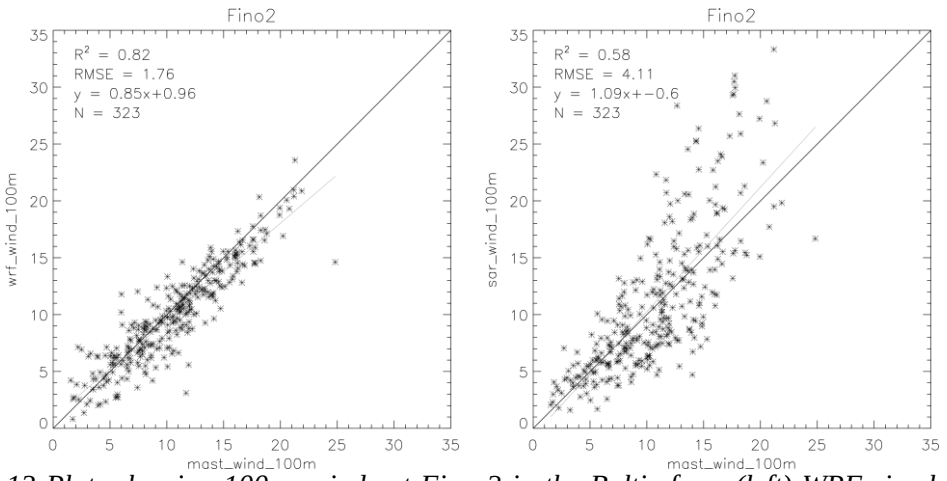

Figure 3.13 Plots showing 100-m winds at Fino-2 in the Baltic from (left) WRF simulations vs. mast observations and (right) lifted SAR vs. mast observations.

Figure 3.13 shows scatter plots of the (left) WRF winds and (right) lifted SAR winds against the mast observations at 100 m. The higher correlation coefficient and lower RMSE which is seen for the WRF-mast comparisons was expected, as the wind speed information from WRF at 100 m is known to be more accurate than the stability information derived from WRF parameters (Peña and Hahmann, 2011). For the SAR-mast comparison, a large amount of scattering is seen. The agreement between lifted SAR and mast winds improves significantly when the data set is narrowed down to show only situations where the initial 10-m wind speeds from SAR and WRF agree well. This means WRF simulates the weather situation captured in the SAR scenes well. For example, a threshold of 2.5 m/s for the SAR-WRF wind speed difference at 10-m improves the results of the SAR-mast comparison at 100 m to R^2 of 0.75 and RMSE of 2.11 m/s.

In figure 3.13 (left) the scattering of SAR winds against mast winds is relatively evenly distributed around a 1:1 line. This indicates that wind fields from SAR lifted by means of WRF stability information may be accurate on a long-term average. Work is in progress to test this hypothesis further.

3.6 Summary and perspectives

The aim of the satellite remote sensing work based on Envisat ASAR is to provide a new offshore wind climatology map for the NORSEWInD area. This has been achieved at high-resolution spatial resolution of 2 km by 2 km based on 9000 unique Envisat ASAR WSM scenes from 2002 to 2012. It was chosen to re-process all scenes with ECMWF winds input and CMOD-IFR2 to have a homogenous data set. The results of mean wind speed, Weibull A and k, and energy density maps are valid at 10 m above sea level.

The perspectives for future use of SAR-based offshore wind maps is to extend the current data set with new observations from Sentinel-1 with an ASAR on-board scheduled to be launched mid-2013 by ESA.

Furthermore, scientific work is on-going on procedures to lift winds from 10 m to hub-height.

4 QuikSCAT

4.1 Background

The SeaWinds scatterometer on board the QuikSCAT platform was a quick recovery mission, launched by NASA in July 1999 to fill the gap created from the failure of the SeaWinds instrument on board the Midori-I platform. At an altitude of 800 km and with a wide swath of 1800 km, QuikSCAT provided daily near global coverage for more than 10 years.

Scatterometers are active radars than transmit microwave pulses towards the Earth's surface and measured the backscattered signal. Scattering occurs differently depending on the type of surface. Bragg scattering is the primary process in the case of water surfaces; the radar signal is scattered due to the small scale ripples on the water surface and a portion of the signal is backscattered to the instrument.

These ripples are assumed to be in equilibrium with the wind stress and by measuring the radar backscatter, a wind speed and direction can be inferred. This occurs through a process known as wind inversion; the backscattered signal is fed into an empirical algorithm, the Geophysical Model Function (GMF). This algorithm describes the wind speed and direction as a function of the frequency and polarization of the radar signal, the angle between the wind and the incidence radar pulse and the incidence angle of the radar pulse measured in the vertical plane.

For SeaWinds, multiple radar backscatter measurements over an area obtained from different viewing angles are organized to wind vector cells. These measurements are fed in the GMF and multiple sets of wind speed and direction estimates are produced; the final selection is performed through a maximum likelihood estimation method. Various processing centers performed wind retrievals from QuikSCAT, using different GMF algorithms. A common characteristic between all is that the physical parameter is the Equivalent Neutral Wind at 10 m above the surface (Liu and Tang, 1996).

For the SeaWinds instrument, operating at 13.4 GHz, rain poses a significant source of error as it scatters and attenuates the radar signal and modifies the ocean surface. It is found that, on average, rain contaminated scatterometer winds are biased towards higher wind speeds (Hilburn K.A. et al., 2006). Thus, care must be taken when using such observations. For the purposes of the NORSEWInD project, all rain-contaminated winds were excluded from the analysis

4.2 Comparisons

In situ measurements from four NORSEWInD nodes were converted to equivalent neutral winds at 10 m above the surface and compared to wind speeds from QuikSCAT. The in situ measurements are converted to ENW according to the methodology described in (Karagali, 2012). Only the 10-min measurement closest to the QuikSCAT overpass time was selected and winds from the QuikSCAT grid cell containing the location of the in situ instrumentation. Wind speeds lower than 3 m/s have been excluded. The overall statistics and the scatter between the in situ and satellite wind speeds are shown in Figure 4.1.

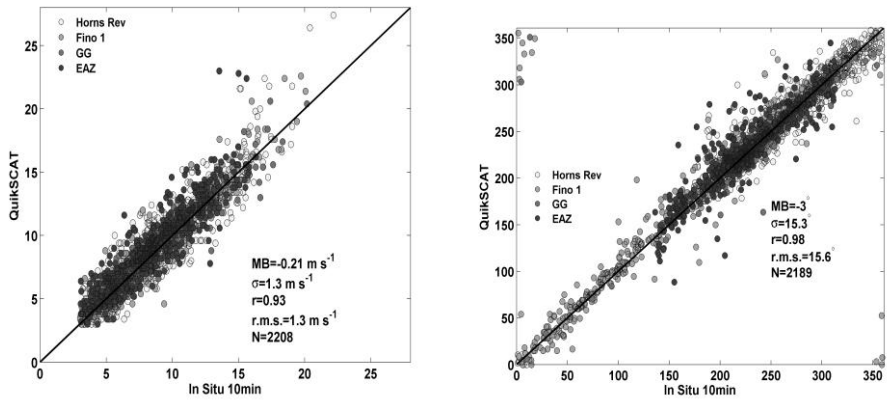

Figure 4. 1: Scatter of wind speed (left) and direction (right), between in situ (horizontal) and satellite (vertical) measurements for 4 different locations

The overall bias is low and negative, indicating higher QuikSCAT wind speeds. The root mean square error is 1.3 m/s and the correlation is 0.93, from a total of 2200 match-ups. The corresponding statistics and scatter for the wind direction are shown in the right panel of Figure 4.1. In this case, wind direction measurements from the meteorological masts are obtained at various heights, most often above 28 m while the satellite wind directions refer to 10 m above the sea surface. In addition, two of the 4 stations are affected by the wind farm wakes and the proximity to land. Therefore only specific sectors are used. For Horns Rev M2, only directions between 174º and 13º are selected, while for EAZ we only use directions between 135º and 315º. The mean bias and the root mean square error meet the mission requirements for both wind speed and wind direction.

In addition, we have also evaluated 10 year long dataset of satellite winds from QuikSCAT against the WRF derived climatography (Hahmann et al., 2010); Peña and Hahmann, 2011). This allows the description of the spatial comparisons between the model outputs and the satellite winds. Figure 2 (left) shows the spatial extend of the mean bias in wind speed, defined as QuikSCAT minus WRF. In most parts of the domain, WRF tends to show higher wind speeds, as the bias ranges from -0.2 up to -1 m/s. Positive biases, indicating higher QuikSCAT wind speeds are found offshore from Neatherlands.

The standard deviation of the mean bias (Figure 4.2, right) shows a south-north component. Standard deviation values are lower in the south part of the domain and increase towards the North. Highest standard deviation values are found in the North Atlantic part of the domain and around the coast of South Norway. In the former area, scatterometer winds are very likely overestimated due to the strong influence of the sea surface temperature and a current. In the latter area, complicated flows around the Norwegian coast are likely not properly resolved by the model.

The correlation coefficient R^2 is presented in Figure 4.3 (left). Lower values are observed around the coastlines, where the scatterometer winds suffer from land contamination to the backscattered signal and the model does not properly resolve the change of surface roughness and its value. In the central part of the North Sea, correlation is around 0.7 while low values (0.5) are observed for the straight between Denmark and Norway (Skagerrak).

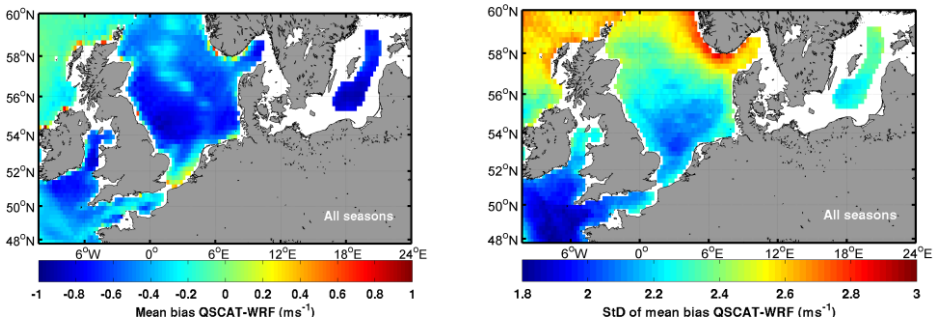

Figure4. 2: Mean bias (left) and standard deviation (right) between QuikSCAT and WRF wind speeds for 10 years of twice daily QuikSCAT overpass times.

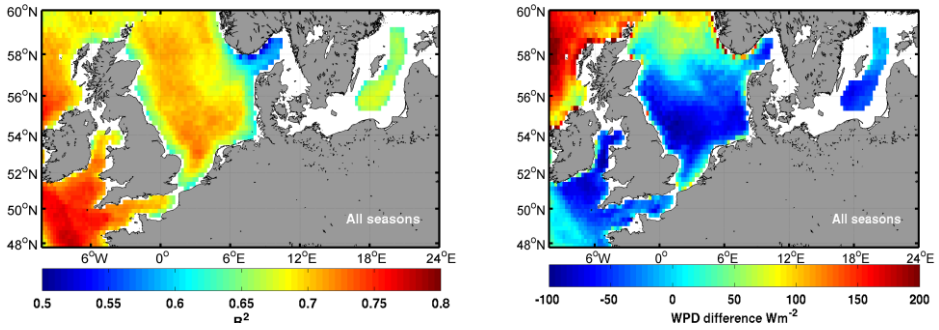

Figure4. 3: Correlation coefficient R^2 between QuikSCAT and WRF (left) and difference in wind power density estimates between coincident QuikSCAT and WRF 10 m neutral winds (right).

One can estimate the wind power density from time-series of observations using Equation 10, where ρ is the air density (~1.245 g/m3 at 10°C) and u is the wind speed.

$$E = 0.5\rho\overline{u^3} \qquad (10)$$

This is done from the coincident QuikSCAT wind retrievals and the WRF derived ones and the wind power estimates are compared. The difference in the estimated density from QuikSCAT and WRF is shown in Figure 4.3 (right). In most parts of the North Sea, the English Channel, the Irish Sea and the Baltic Sea differnces are negative, indicating higher WRF estimates that reach a maximum of 100 W/m^2. In the northern North Sea and the North Atlantic, these differences are positive, indicating higher QuikSCAT estimates and reach up to 200 W/m^2.

4.3 Wind resource maps

The number of available rain-free scatterometer wind retrievals for the 10 years of QuikSCAT's lifetime is presented in Figure 4.4. The North Sea is very well covered with approximatelly 7000 wind retrievals. The central part of the Baltic Sea is also properly covered but the coastal parts of the Baltic basin have almost half the observations, when compared to the North Sea. This is due to the ice mask, applied during the processing from November to April/May. This mask is derived from a passive microwave sensor; to avoid land contamination of the emitted radiation only area far away from the land are ”observed”. Thus, the ice mask only covers the central part of the Baltic Sea and the coastal areas are excluded during winter as no ice information is retrieved there.

With such a large number of satellite wind fields and a consistent return period, many different attributes of the wind field can be explored. Recent studies (Karagali et al., 2012b;Karagali, 2012) (Karagali et al., 2012a) have demonstrated the applicability of QuikSCAT winds for the estimation of the mean wind speed, the wind direction frequency distribution, the Weibull shape and scale parameters and the wind power density.

The number of rain-free QuikSCAT winds lower than 5 m/s is shown in the left panel of Figure 4.5. This threshold is selected as a typical wind turbine cut-in wind speed, below which the turbine does not produce energy. The spatial extend of such occurrences indicates that the North Atlantic and the north part of the English Channel are the areas with the less frequent low winds. Most observations are found in the central Baltic Sea where approximately 30% of the total available wind retrievals are below 5 m/s.

A similar investigation is performed but for wind speeds exceeding the 15 m/s threshold (Figure 4.5, right panel). Note a strong south-north component, where less occurences (maximum 3.5% of the total rain-free retrievals) are observed in the southern North Sea, the Irish Sea, the Skagerrak straight and the central Baltic Sea. In the northern North Sea and the North Atlantic, occurrences of winds higher than 15 m/s reach a maximum of 11% of the total rain free retrievals. In comparison, winds lower than 5 m/s are more frequent than winds higher than 15 m/s.

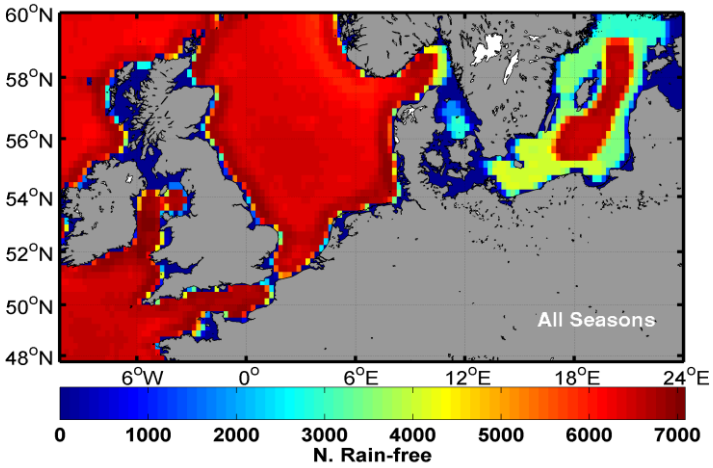

Figure 4.4: Number of QuikSCAT rain-free wind retrievals from August 1999 to October 2009.

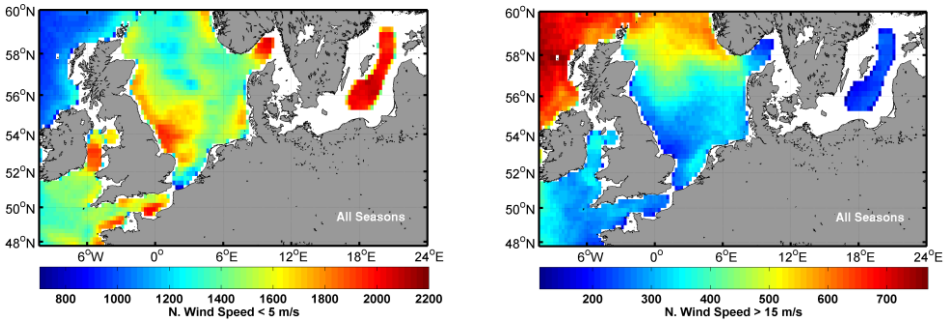

Figure 4.5: Number of rain-free wind retrievals with speed lower than 5 m/s (left) and higher than 15 m/s (right).

Using the grid cells that contain the meteorological masts that were previously used for comparisons with QuikSCAT, the spatial correlation has been estimated and is presented in Figure 4.6. In all cases, correlation higher than 0.9 is limited to a small area around the grid cell containing the meteorological mast. In the case of Horns Rev M2 (top left) and FINO-1 (top right), values higher than 0.6 are computed for a large part of the North Sea basin. The locations of Greater Gabbard (bottom left) and Egmond aan Zee (bottom right) are such that high correlation is limited to a smaller area around the meteorological masts, when compared to the previous cases. In addition, the latter masts are very close to the land and in a semi-closed area where backscatter signal contamination is very likely, thus some scatterometer errors are expected.

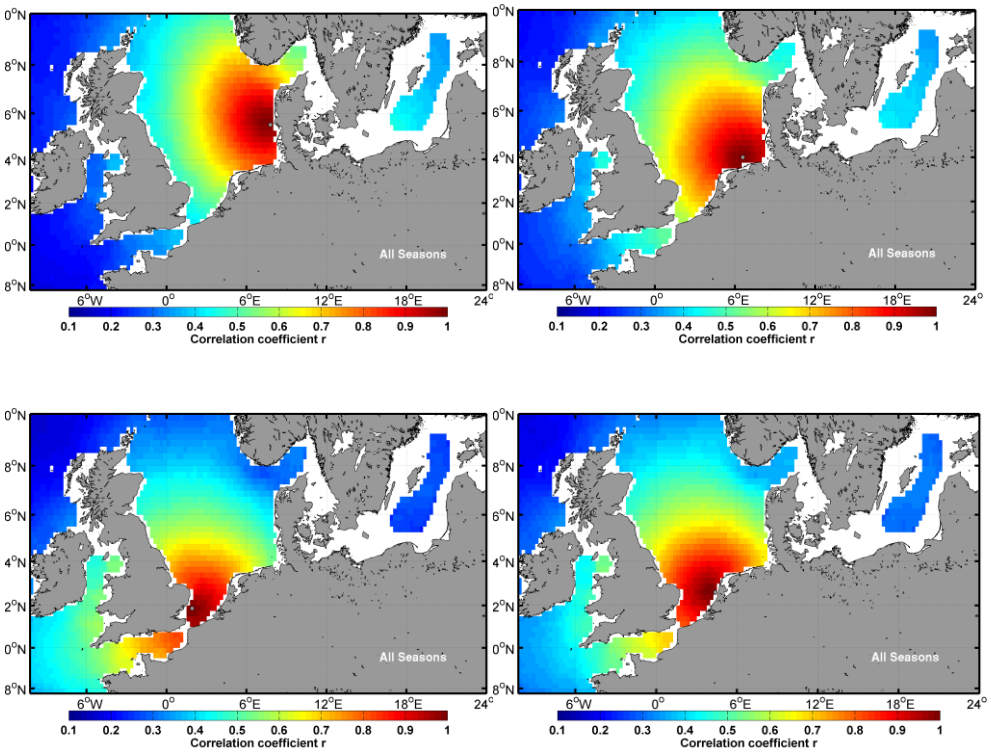

Figure 4.6: Spatial correlation between the QuikSCAT grid cell that contains the Horns Rev M2 mast, FINO-1, Egmond aan Zee (EAZ) and Greater Gabbard (clockwise from upper left corner) and all other grid cells in the domain.

The statistics of mean wind speed, energy density, Weibull A and k based on QuikSCAT are shown for the Northern European Seas in figures 4.7 to 4.10, respectively. Mean wind speeds are around 7.2 ms^{-1} in the central Baltic Sea and ranges from 8 to 9 ms^{-1} in the North Sea. There is a gradient from north to south with higher winds north. The lee effect of the British Isles is clear. Energy density is seen to range from 600 W m^{-2} to more than 1000 W m^{-2}. The Weibull A follows closely the pattern of mean wind speed whereas the spatial distribution of Weibull k appears to have higher values in the southern part of the North Sea, in particular near the English Channel.

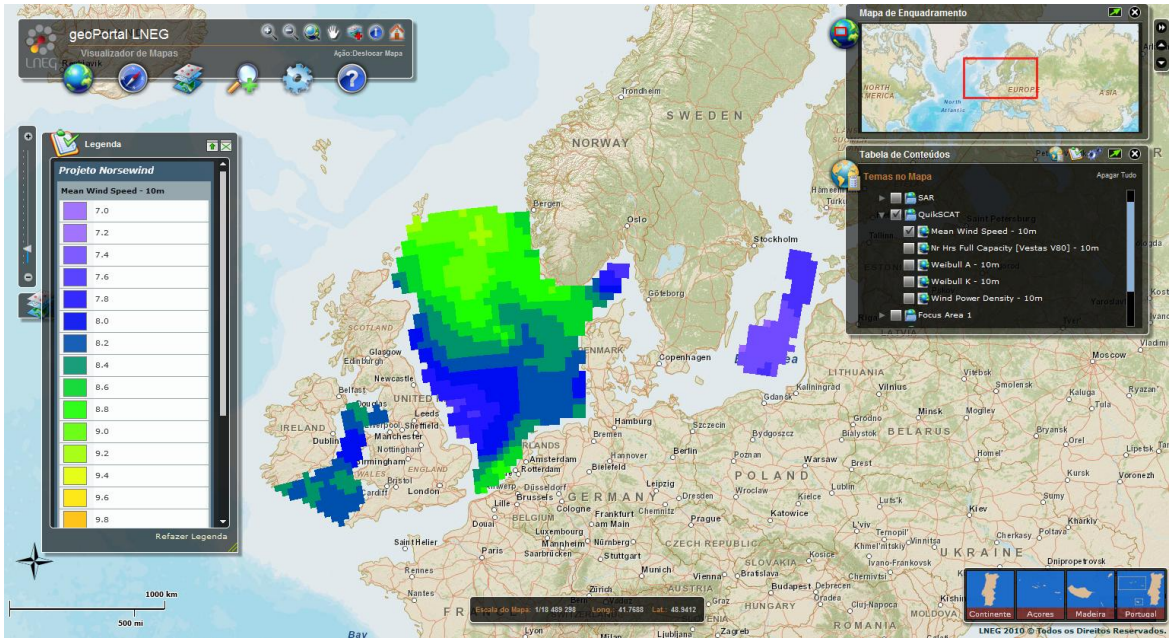

Figure 4.7 Mean wind speed at 10 m observed by QuikSCAT for the Northern European Seas.

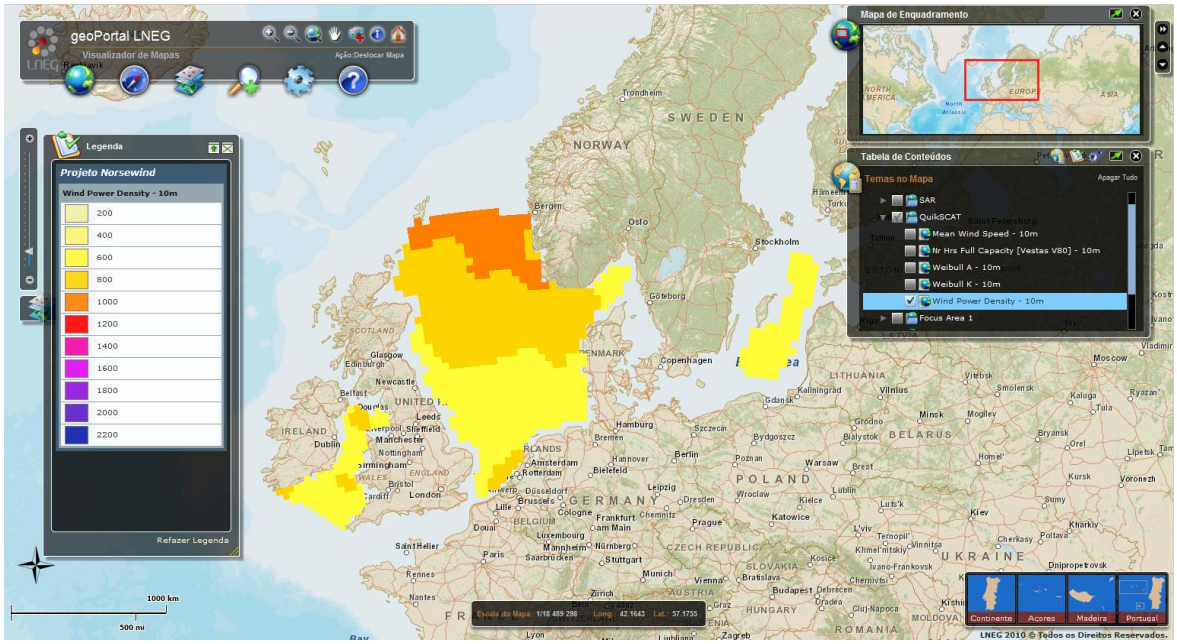

Figure 4.8 Energy density at 10 m observed by QuikSCAT for the Northern European Seas.

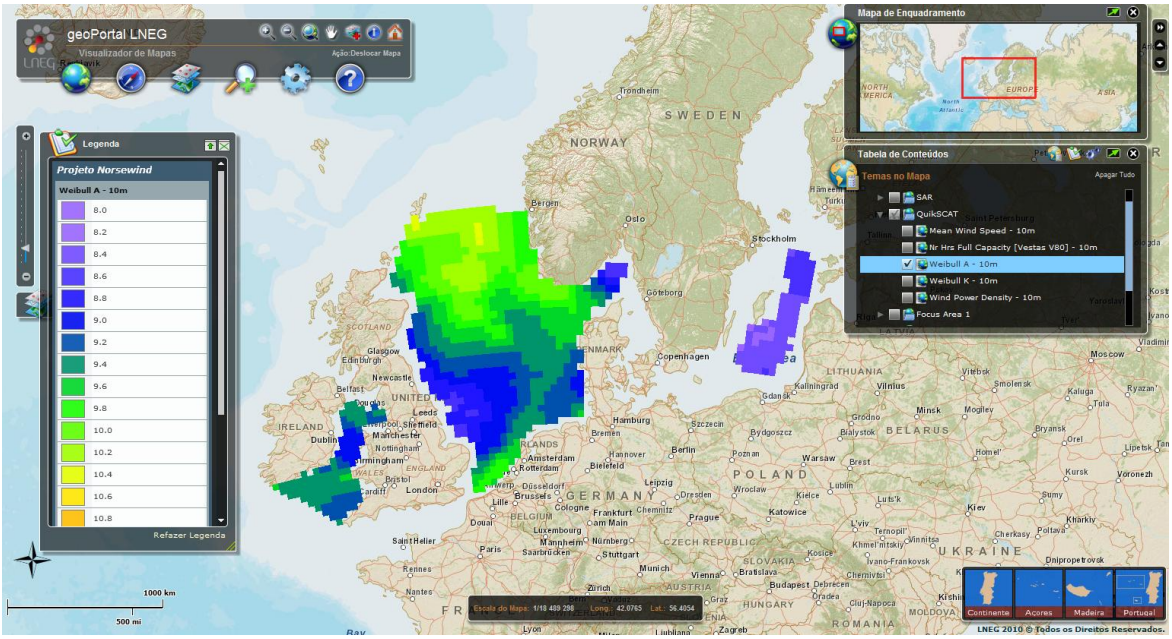

Figure 4.9 Weibull A parameter at 10 m observed by QuikSCAT for the Northern European Seas.

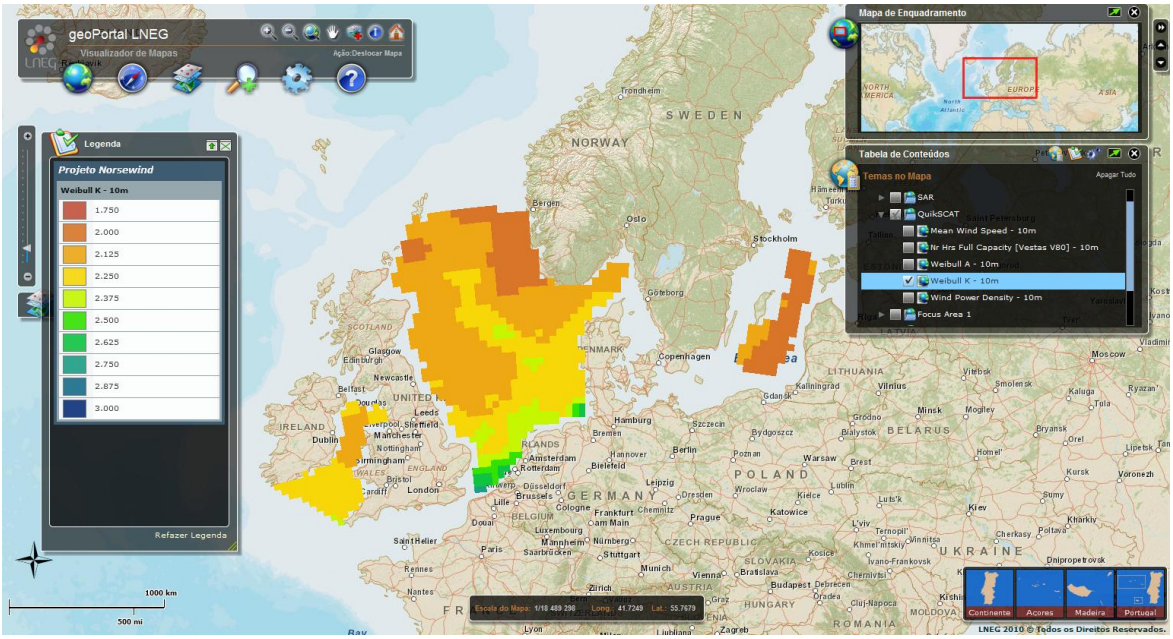

Figure 4.10 Weibull k parameter at 10 m observed by QuikSCAT for the Northern European Seas.

4.4 Summary and perspectives

The aim of the satellite remote sensing work based on QuikSCAT was to use the 10-year long record of twice daily satellite wind fields to investigate the long-term behavior of various wind characteristics in the NORSEWInD focus areas. A new wind atlas at 10-m height has been produced that despite the lower spatial resolution, when compared to the ENVISAT ASAR, hold the advantage of consistent and long spatial and temporal coverage over the North Sea.

QuikSCAT is not operational since 2009 but other scatterometes such as ASCAT and OCEANSAT are currently available, thus creating the possibility for data merging.

5 ASCAT Coastal L3 wind product

5.1 Reprocessing of ASCAT L3 coastal wind product for the North Sea and Irish Sea

KNMI produces since November 2009 the coastal ASCAT scatterometer product within the context of the Eumetsat Ocean and Sea Ice SAF (http://www.osi-saf.org). This product consists of measurements of wind speed and direction (equivalent neutral at 10m) within a wind vector cell of size 12.5 km (see ASCAT Wind Product User Manual at (http://www.knmi.nl/scatterometer) oriented according to the satellite swath. In the context of MyOcean (http://www.myocean.eu) a version of this product is produced on a fixed geographical grid since the beginning of 2012, the MyOcean L3 Global wind product (http://www.myocean.eu).

For the period of 1 June 2007 to 31 December 2008 the Full Resolution product of ASCAT was reprocessed into the ASCAT coastal L2 product (see ref ASCAT product manual) on a grid of 12.5 km. The input ASCAT Full Resolution data was retrieved from the NOAA CLASS archive. The reprocessing was done using the ASCAT Wind Data Processor (AWDP) package version 2.1 of the EUMETSAT NWP-SAF (see AWDP User Manual and Reference Guide v2.0 resp. http://research.metoffice.gov.uk/research/interproj/nwpsaf/). This product was then gridded into the L3 ASCAT 12.5 km product (see Product User Manual for WIND_GLO_WIND_L3_NRT_OBSERVATIONS_012_002) for an area covering the Norsewind areas FA-1 and FA-2.

The gridding is done using the Gouraud shading technique resulting in an ascending and a descending file each day. Only wind vector cells that have successfully passed KNMI Quality control are used in the gridding.

The descending ASCAT swaths pass the North Sea area each day around 09:00 AM UTC and the ascending swaths pass around 22:00 PM.

The L3 product also includes the ECMWF model wind (http://www.ecmwf.int that is used in the near real-time L2 wind processing. This is gridded in exactly the same way as the scatterometer wind, so only using wind information from neighbouring wind vector cells if these contain valid scatterometer winds. Consequently the L3 scatterometer winds and ECMWF model winds suffer the same sampling effect.

The following comparisons have been made:

- Comparison of the L3 coastal winds and the ECMWF model winds in the L3 product. The averaged wind maps of both are compared and overall statistics have been calculated.
- Comparison of the L3 coastal winds with the WRF atlas (15-km grid).
- Triple collocation using the ASCAT L3 coastal winds, data from the Egmond aan Zee met. mast (http://www.noordzeewind.nl), and model data from the WRF atlas (Hahmann et al., 2010).
- The ASCAT data have also been compared with the high-resolution WRF reanalysis for FA-1 of KVT with 2-km grid. In this comparison the 100-m WRF winds are collocated with 10-m equivalent-neutral scatterometer winds by means of collocation for one month. For each L3 scatterometer grid measurement the nearest WRF value is taken in space and time (< 30 minutes). This is not reported here.

5.2 Comparison of L3 coastal winds and L3 ECMWF winds

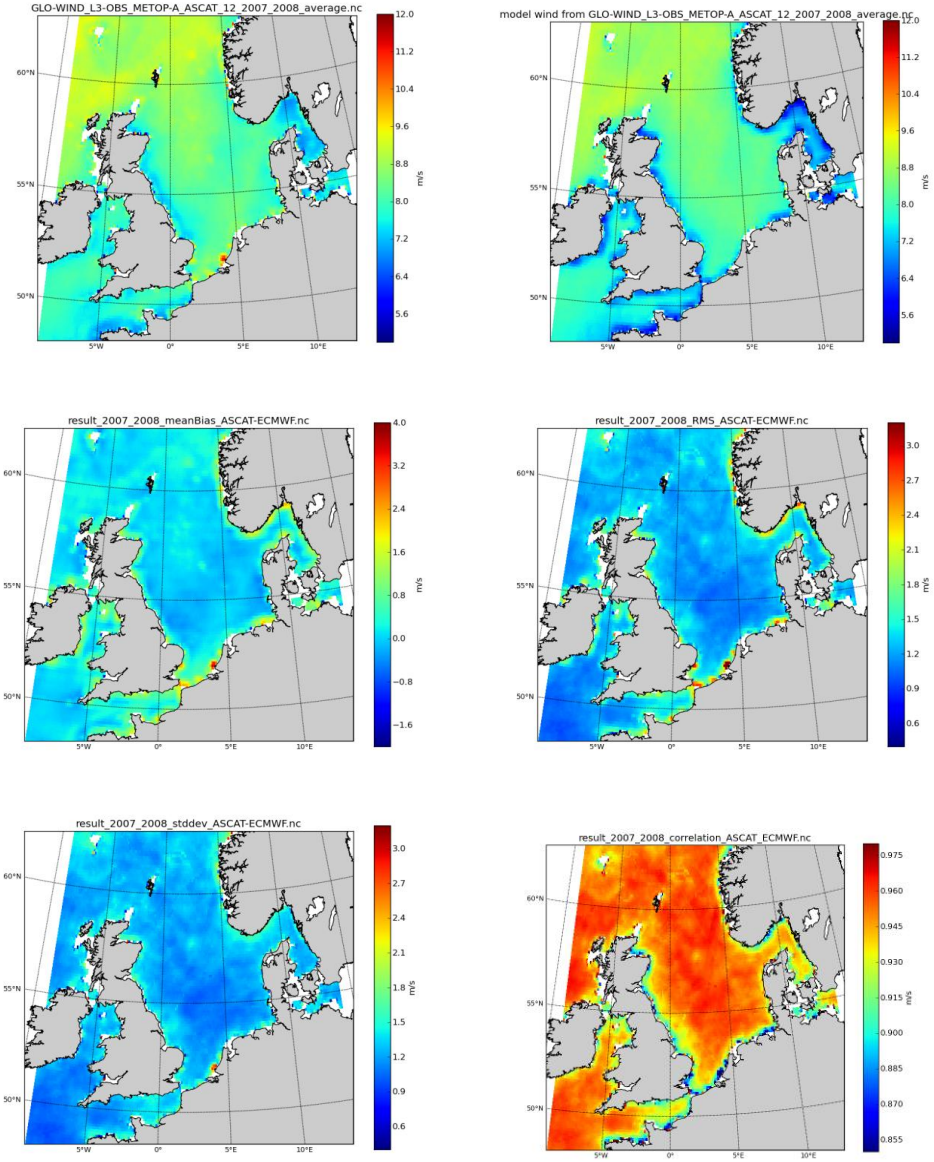

Figure 5.1 Averaged wind speed map for ASCAT L3 coastal winds (top left) and ASCAT L3 ECMWF model winds (top right), mean difference (middle left), RMS difference (middle right) and Standard deviation (lower left) of ASCAT - ECMWF model difference.

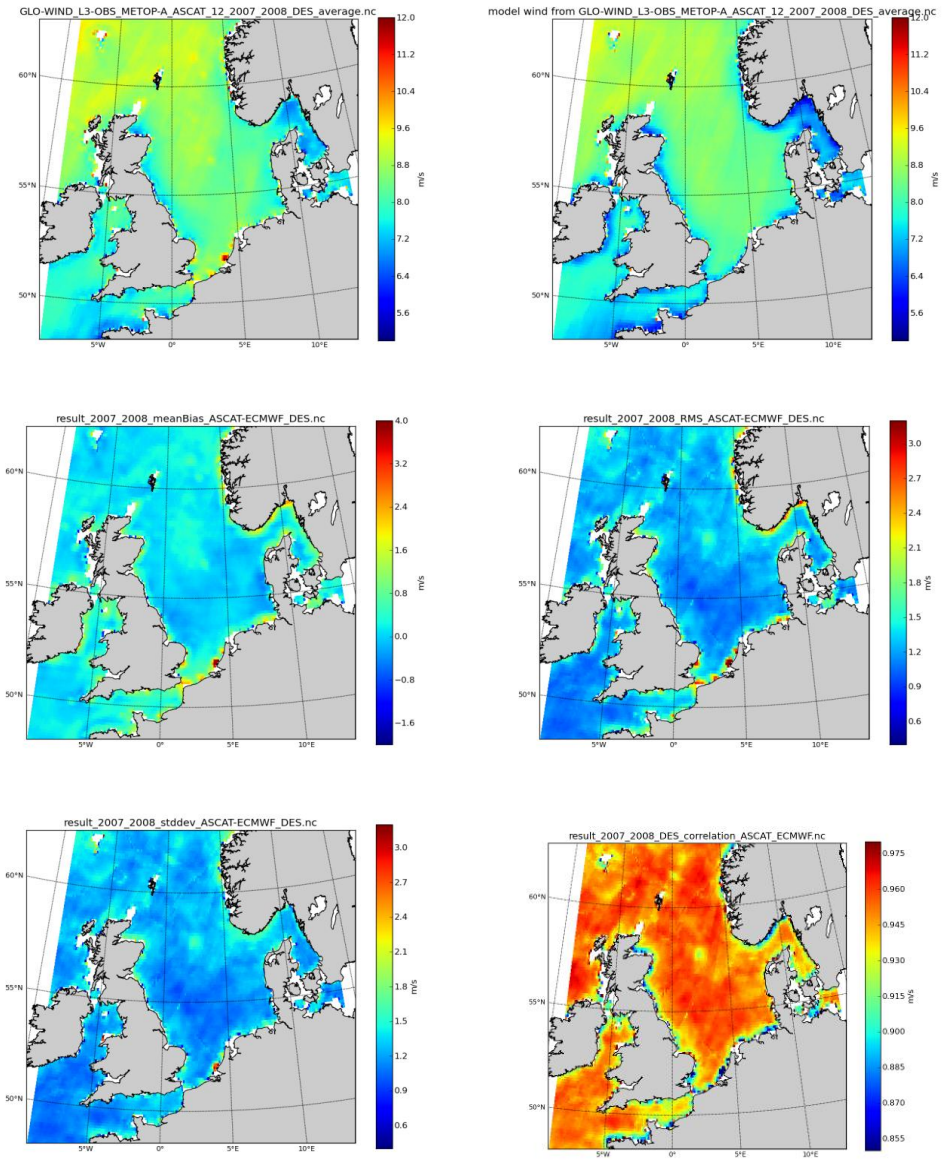

Figure 5.2 Averaged wind speed map of only the descending passes of ASCAT L3 coastal winds (upper left) and ASCAT L3 ECMWF winds (upper right), mean difference (middle left), RMS difference (middle right) , standard deviation (lower left) of ASCAT - ECMWF model differences and correlation of ASCAT L3 and ECMWF winds (lower right). Time of overpass is between 08:00 and 10:00 UTC.

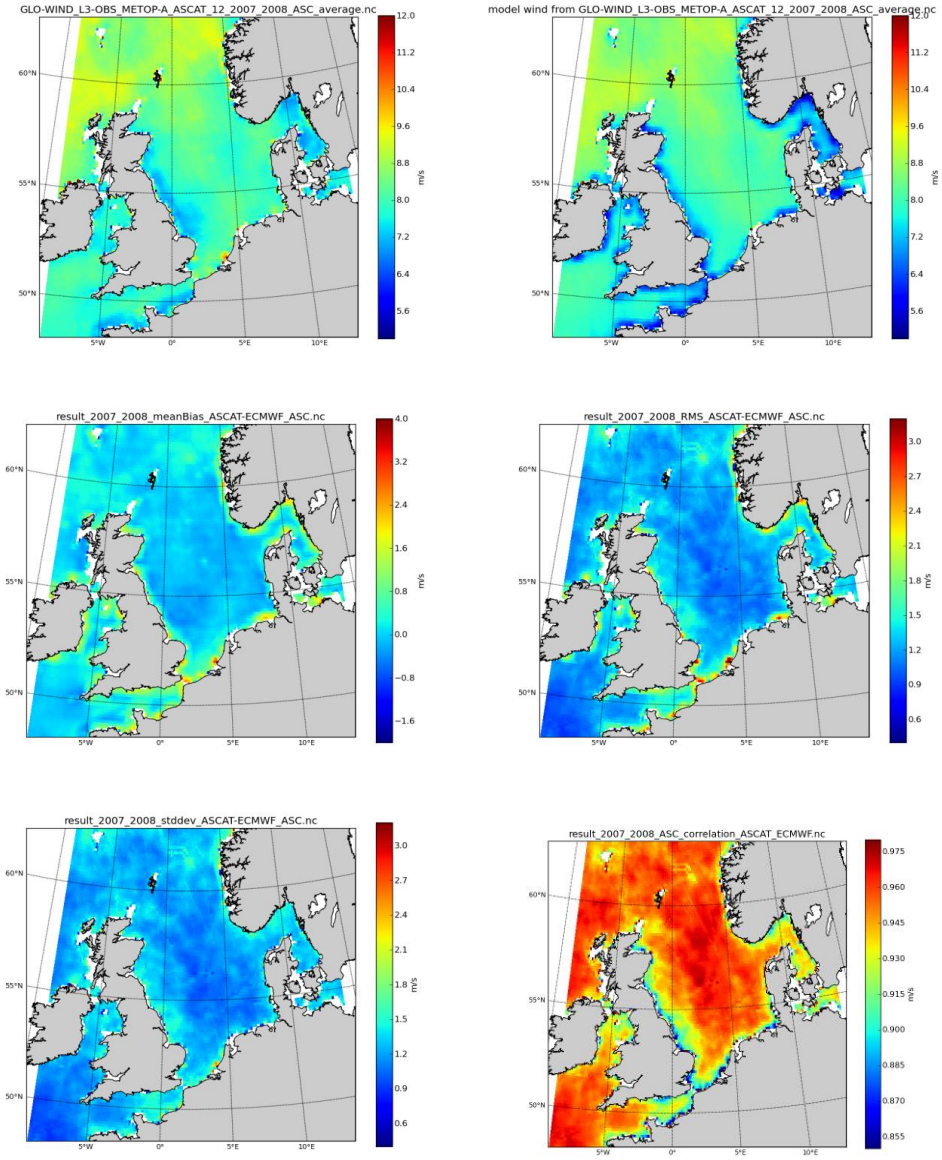

Figure 5.3 Averaged wind speed map of only the ascending passes of ASCAT L3 coastal winds (upper left) and ASCAT L3 ECMWF winds (upper right), mean difference (middle left), RMS difference (middle right) and standard deviation (lower left) of ASCAT - ECMWF model differences, and correlation of ASCAT L3 and ECMWF winds (lower right). Time of overpass is between 21:00 and 23:00 UTC.

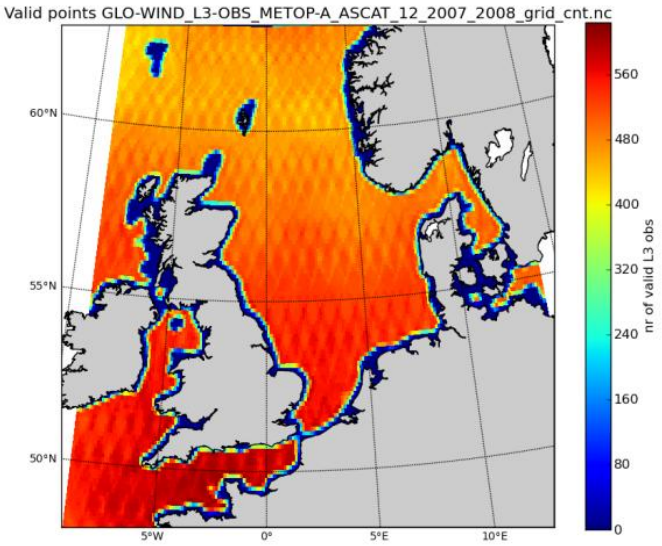

Figure 5.4 Total number of valid grid points used for the calculation of the averaged wind speed map. The Metop-A repeat cycle of 29 days causes the checkered pattern.

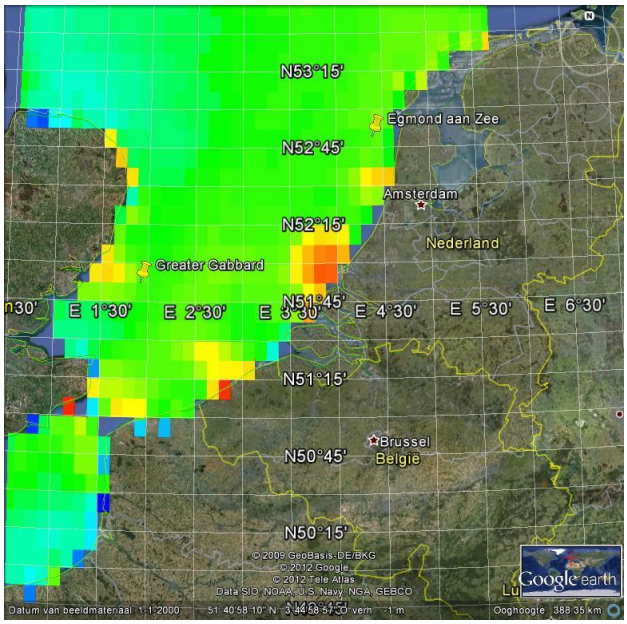

Figure 5.5 Averaged ASCAT winds zoomed in at the Dutch coast. The color scale is the same as in the wind speed maps in the figures above.

When comparing the scatterometer North Sea wind map and the ECMWF wind map we see, as expected, low bias and standard deviation in locations away from the coast. Near the coast, however, we often see larger differences between scatterometer and ECMWF wind speeds, e.g. south of the UK in the straight between Calais (F) and Dover (UK). These effects are slightly different in the evening map (ascending passes) and the morning map (descending passes), the evening passes often showing a larger difference along the coast than the morning passes (see Figure 5.6). The differences are also clear in the correlation plots of ASCAT L3 and ECMWF. Far away from the coast the correlation is very high, around 0.95. Apart from the very low correlation areas near the main ports like Rotterdam (with values below 0.7) there is an area of lower correlation near the coasts. This area appears to be much smaller for the morning passes (descending) than for the evening passes (ascending).

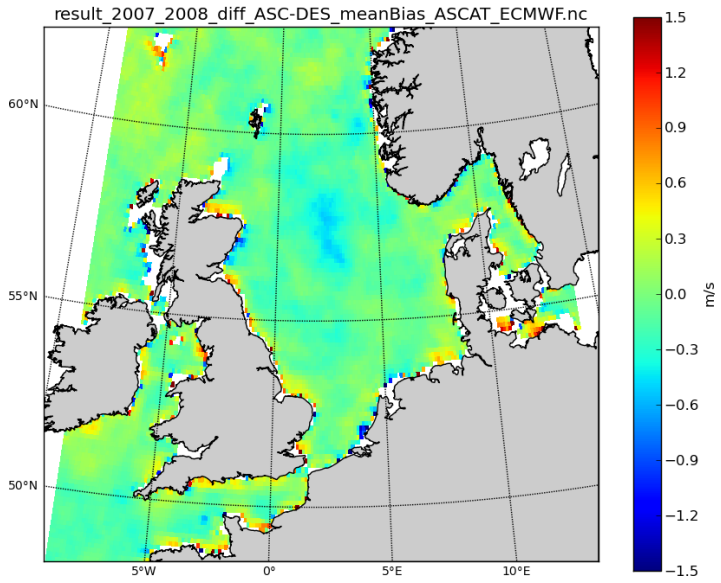

Figure 5.6 Difference of ASCAT L3 - ECMWF for ascending and descending passes. Shown is ascending difference minus descending difference.

Looking closely at the scatterometer wind atlases we can see high wind anomalies for instance before the Dutch coast near the Rotterdam harbour (Eurogeul, Maasgeul). Smaller high wind anomalies can be seen before IJmuiden, Zeebrugge (Belgium), and also near Harwich (UK). This is clear in the zoomed picture in Figure 5.5.

Also a spot can be seen before the coast of Normandie both in the valid grid count plot and in the mean bias plots. This spot collocates with the Guernsey and Jersey isles. This may have something to do with different scattering around these islands due to the rocks in this area.
If we look at the plots showing total number of grid points in Figure 5.4, we can see that the number decreases with increasing altitude. This is due to the overlap of the passes at higher latitudes, and in the L3 only the latest pass is kept.

Comparing wind speed plots and "number of valid grid points" plot, there is a connection between higher wind speeds and lower numbers of valid grid points, i.e., at the mentioned anomalous locations more data is rejected than in other comparable near shore areas.

The anomalies near Rotterdam mainport and other mainports may be related to the anchor areas for freight ships. On http://www.marinetraffic.com/ais real-time monitoring of ships is provided, sailing and anchoring. The anchoring areas near Rotterdam reach about 60 km from the coast. In newspaper articles from 2009 (e.g. http://www.portofrotterdam.com/nl/actueel/pers-en-nieuwsberichten/Pages/20091126_55.aspx) it is mentioned that there was increased number of anchoring ships in 2008 due to the recession. The number of ships waiting is around 100. The ascending and descending data show differences in ASCAT-ECMWF wind speed difference and standard deviation, descending data showing much higher values (see also Figure). This may be related to higher ship density in the morning, but this is to be investigated further.

The corner reflections on such relatively large number of ships will have an effect on the level 2 processing. The quality control screens some of the ship-reflection contaminated observations, but apparently not at high winds (reduced contrast). This will be investigated further by looking more closely at the quality control and comparison with SAR images and ship density maps.

This is the first time that radar reflections on structures are reported to affect scatterometer wind measurements. Since scatterometers strongly oversample the WVCs, the spread of the measurements contributing to a backscatter value may be determined and this is reported in the scatterometer products as so-called Kp noise (Anderson et al., 2012). This opens up the possibility of improved scatterometer quality control at full resolution and screen out data affected by corner reflections on solid structures. This will be further investigated at KNMI in the EUMETSAT OSI SAF.

5.3 Comparison with WRF climatology

The WRF model climatology previously compared to the 10-year long QuikSCAT archive is also used for comparisons with the ASCAT coastal product. The period of investigation is from June 2007 to November 2008. The WRF grid is 15 km thus it has been re-gridded to match the ASCAT 12.5 km grid, using a nearest neighbor interpolation method. Time collocation is performed by selecting the hourly WRF model output that is closest to the ASCAT pass. The number of coincident wind fields is shown in Figure 5.1, left panel. The number of match-ups ranges between 450 and 600 in most parts of the domain and it is reduced to approximately 200 in a narrow coastal zone.

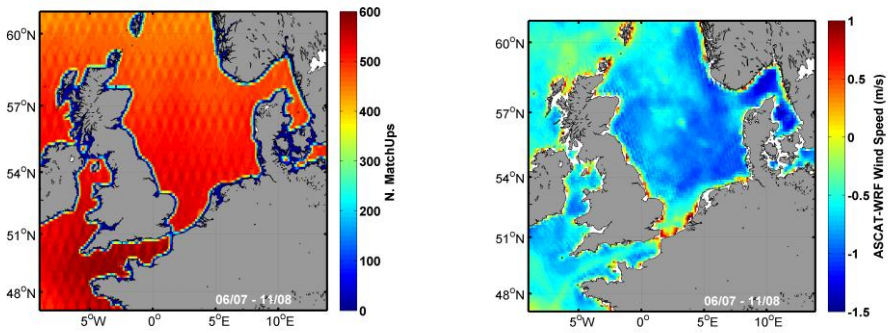

Figure 5.7: Number of ASCAT passes used for comparisons with the WRF model outputs (left) and mean bias between ASCAT and WRF.

The daily ASCAT minus WRF wind speed at 10m above the surface averaged for the entire match-up data set is shown in the right panel of Figure 5.7. Biases are mostly negative, indicating higher WRF speeds, very similar to the QuikSCAT-WRF comparisons. Almost zero biases are estimated for the North Atlantic part of the domain (as in the QuikSCAT-WRF case). Positive biases are restricted to some coastal areas; the highest found off-shore from Netherlands, just like in the ECMWF-ASCAT comparison, probably due to increased backscatter signals caused by the high concentration of ships in the region.

The wind speed RMS error (Figure 5.8, left panel) ranges mostly between 1.8 and 2.8 m/s, highest for the Skagerrak strait between Denmark and Norway. These numbers are much higher than for the ASCAT-ECMWF RMSD (about 1.2 m/s) reported in previous section, suggesting WRF is less accurate than ECMWF (since ASCAT errors are probably very similar in both comparisons). The South-North component, previously found in the QuikSCAT-WRF standard deviation, is also identified in the ASCAT-WRF RMSD. In general, lower RMSD values are found in the south part of the North Sea and increase towards the North. Higher RMSD values, exceeding 3 m/s are estimated for the area off-shore the Rotterdam port.

The correlation R^2 between ASCAT and WRF is shown in the right panel of Figure 5.8. Values range mostly between 0.6 and 0.8, similar to the QuikSCAT-WRF case. A very low correlation is noted for the area with high RMSD off-shore from Rotterdam. Low values are also found in the Skagerrak strait between Norway and Denmark, and the Kattegat strait between Denmark and Sweden. The correlation in most coastal areas is generally 0.7 or higher with some exceptions near the east coast of Scotland, the Irish Sea and the Wadden Sea.

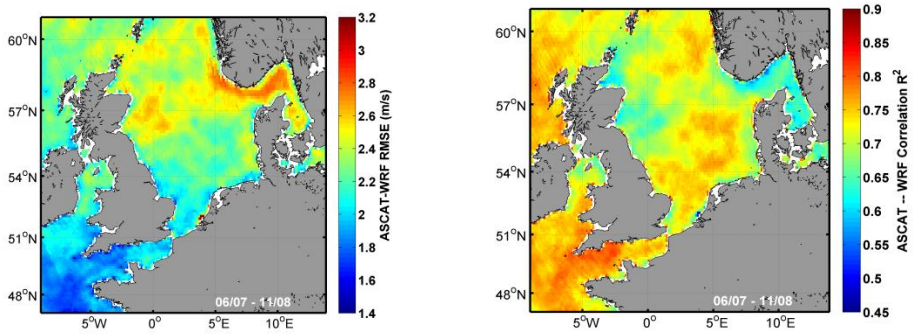

Figure 5.8: Root mean square difference (RMSD) of ASCAT-WRF wind speeds (left) and correlation R^2 between ASCAT and WRF wind speeds.

5.4 Triple collocation of ASCAT L3, WRF and meteorological mast

Triple collocation is a method enabling to characterize systematic biases and random errors in in-situ measurements, satellite observations and model fields. It attempts to segregate the measurement uncertainties, geophysical, spatial and temporal representation and sampling differences in the different data sets by an objective method. The basis for the method is described in Stoffelen (1998) and elaborated by Vogelzang et al. (2012), and software to perform triple collocation is developed within the EUMETSAT NWP-SAF.

Triple collocation has been applied on a set of the ASCAT L3 coastal winds, in-situ data from the Egmond aan Zee meteorological mast, and model data from the WRF climatology run (Hahmann et al., 2010). The period of investigation is from June 2007 to November 2008. The WRF grid is 15 km and has been regridded to match the ASCAT 12.5 km grid, using a nearest-neighbor interpolation method. Time collocation is performed by selecting the hourly model output closest to the ASCAT pass. Wind speed is 10-m equivalent-neutral wind, and wind direction is at 21m height. There is a wake in these in-situ data due to a wind farm in the wind direction sector 315-135 degrees from the meteorological mast.

In Figure 5.9 the location of the Egmond aan Zee mast is shown with respect to the ASCAT L3 grid, and from this plot we can see that the mast is at the border of the coastal zone and it collocated with a L3 grid point close to the coast with a reduced number of valid grid points. Alternatively, the better populated grid point to the northwest may be chosen, but this has not been attempted.

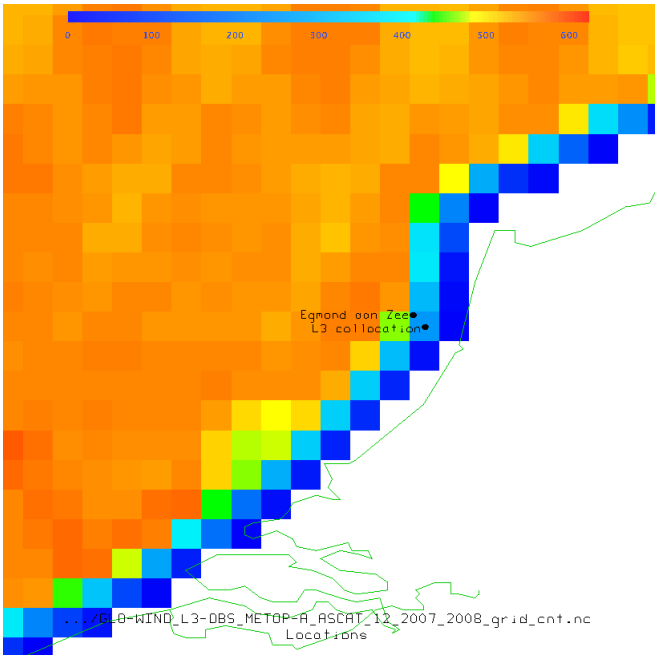

Figure 5.9 Total number of valid grid values for each ASCAT L3 grid cell (starting at 1), zoomed in around the Dutch coast. The location of the Egmond aan Zee meteorological mast and the collocated L3 grid point are indicated on the map. The met mast is clearly in the coastal region with a reduced number of L3 measurements (around 250 in total for the period June 2007-December 2008).

Collocation of the three datasets only provides relatively few collocations, less than 100. So the results are only indicative. The settings used for the triple collocation are the same as used in Vogelzang (2011) where ASCAT L2 data was compared to the ECMWF model and buoy data. The resulting standard deviations for each source are shown in Table 5.1.

Table 5.1 Triple collocation results for in-situ data from Egmond aan Zee mast, ASCAT L3 coastal satellite data observations and WRF model data from the WRF climatology run.

	Mast(E.a.Z.)		ASCAT L3		WRF-DTU	
	sigma_u	sigma_v	sigma_u	sigma_v	sigma_u	sigma_v
Triple collocations excluding wake sector (total 98)	0.9	1.2	1.4	2.1	2.0	1.7
triple collocation including wake sector (total 156)	0.7	1.2	1.6	2.2	2.2	2.0

From Table 5.1 the high accuracy of the Egmond aan Zee measurements stands out. And the high quality is not a surprise considering all the effort that was put into this measurement site and dataset. But it is also partially unexpected as near-coastal winds are expected to be more variable than open ocean winds. This may be due to the small number of collocations.

The ASCAT errors are quite large: at least twice as large as found in other collocation studies (Vogelzang et al., 2011). This may be caused by the interpolation error in the L3 product used here. The other studies use level 2 wind products. The interpolation error may be higher than shown in the Scientific Calibration Report for the level 3 product (2011) because it is on the edge of the interpolation area. This needs to be investigated further.

Furthermore the standard deviation for the components of ASCAT is very skew, sigma u being much lower than sigma v. The dataset is too small to draw any conclusions to this.

The model errors are quite large, which is in line with the high ASCAT-WRF RMSD values found before. Of course there is the uncertainty about the representation error of the model. More information about the model spectra would help here.

Figures 5.10 to Figure 5.15 show the pair-wise correlation between the three sources: Egmond aan Zee vs. ASCAT L3, Egmond aan Zee vs. WRF and ASCAT L3 vs. WRF.

The bias between WRF and ASCAT agrees with the value presented in the WRF - ASCAT comparison in the previous paragraph, both being around 0.9. The correlation value agrees also, being around 0.8 in previous paragraph and 0.84 in the Egmond aan Zee collocation exercise.

We observe a positive bias (1.77 m/s) in the wind speed of ASCAT w.r.t. the mast wind speed (excl. wake). Furthermore does ASCAT observe very few low winds. It would be interesting to find out what is causing this. Maybe we are suffering here the same effect that causes the unrealistic high ASCAT winds at the main-port areas, but now due to the wind turbines in the area?

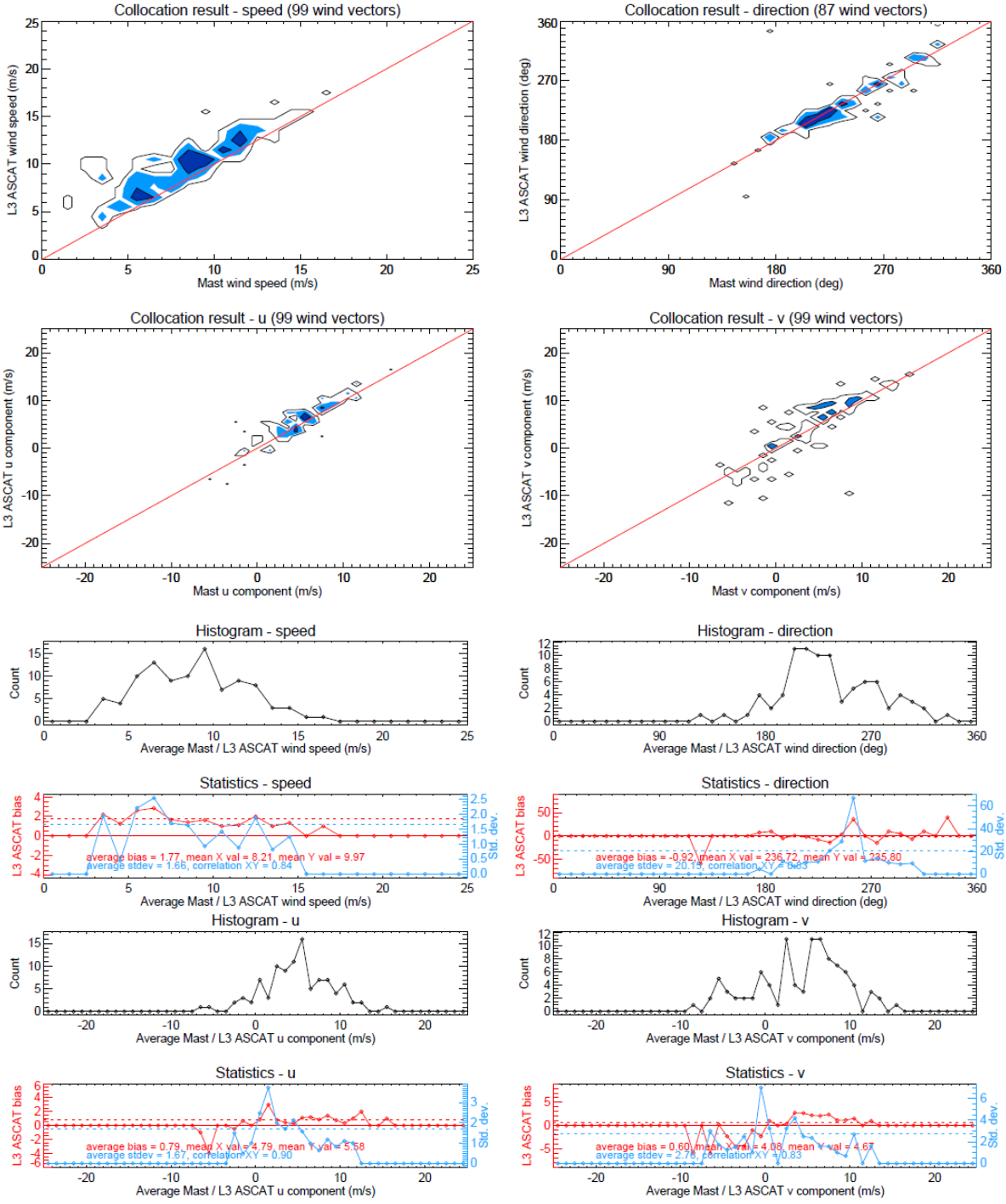

Figure 5.10 Collocation results of Egmond aan Zee vs. ASCAT L3, excluding wake data

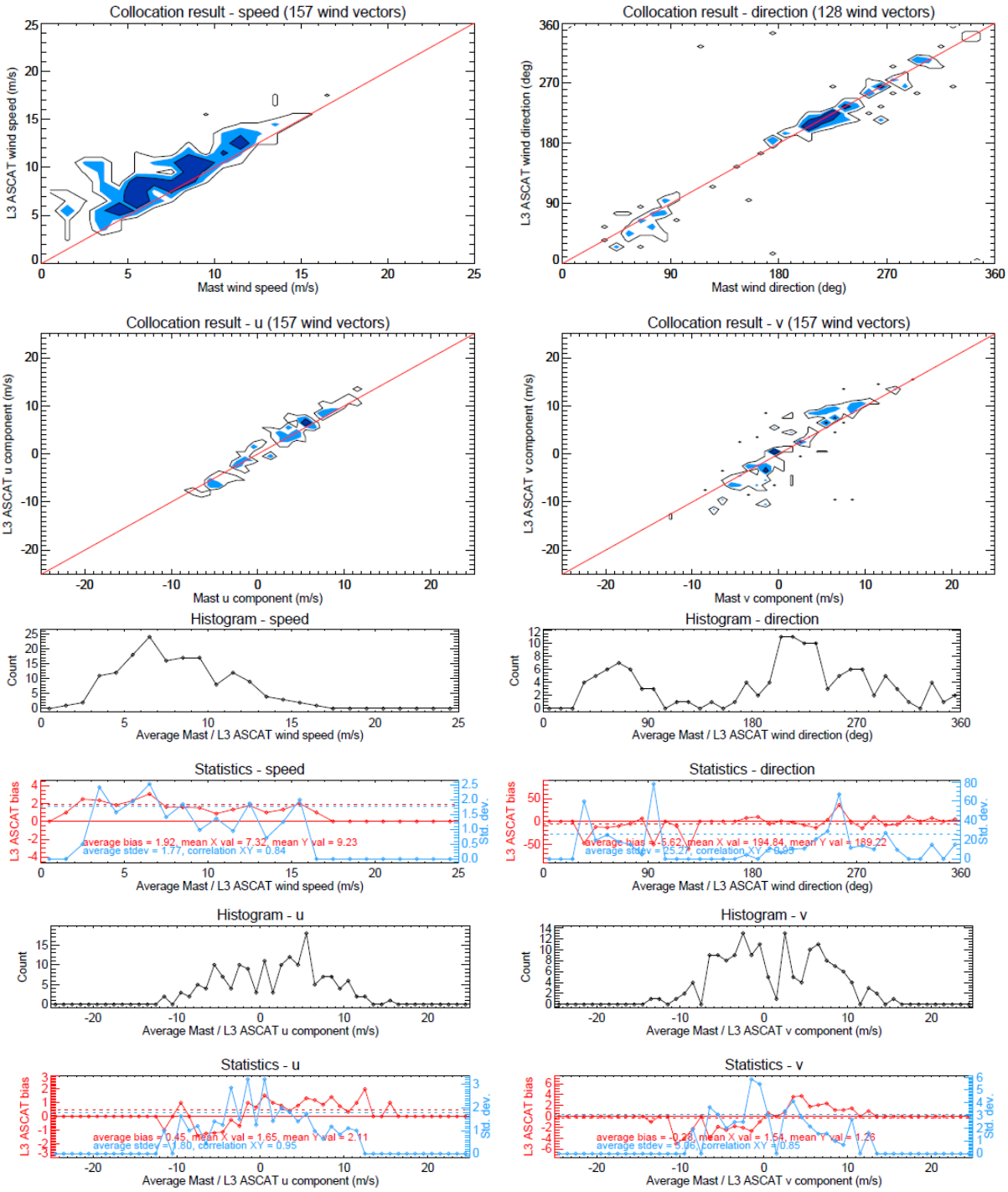

Figure 5.11 Collocation results of Egmond aan Zee vs. ASCAT L3, including wake data.

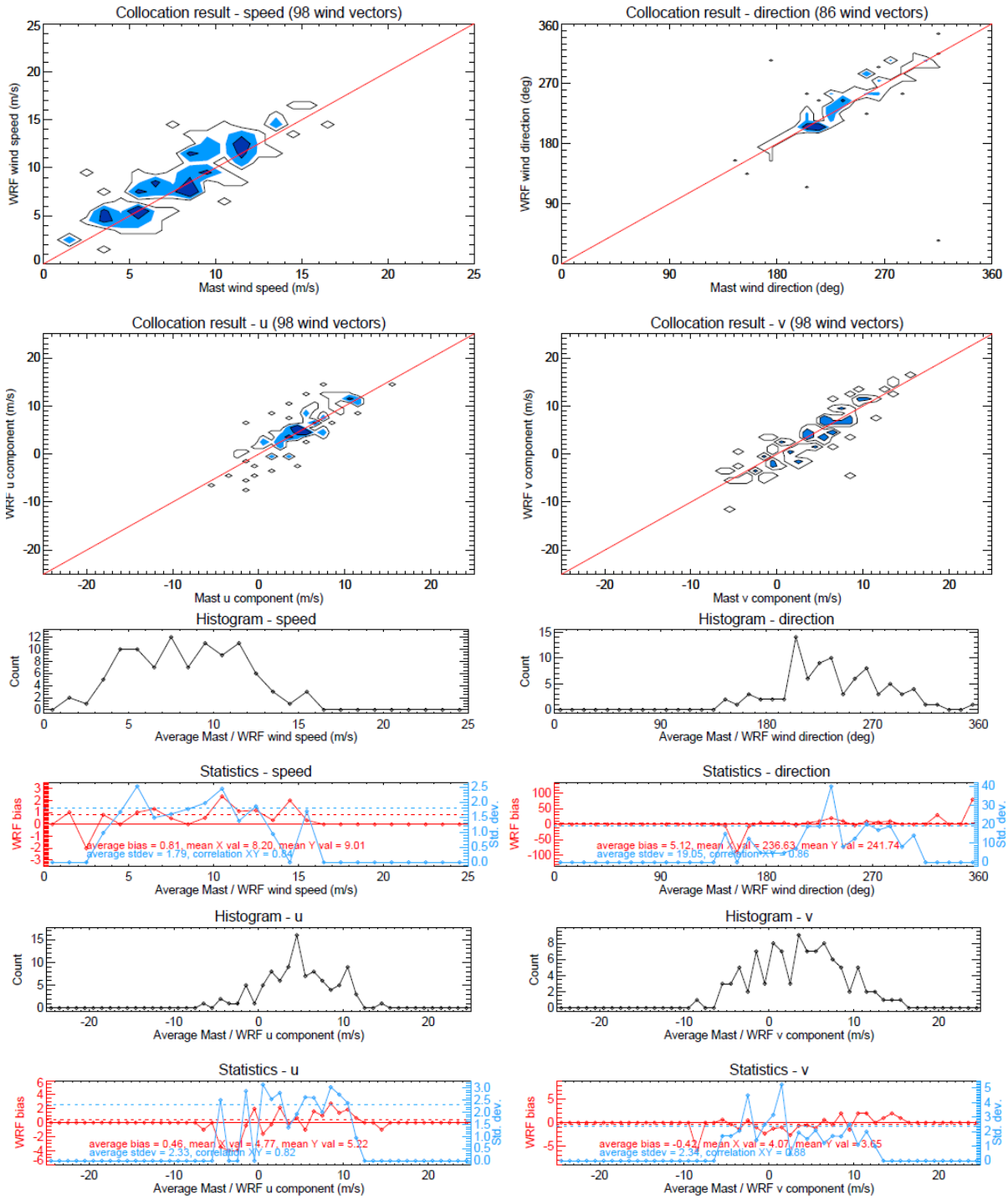

Figure 5.12 Collocation results of Egmond aan Zee vs. WRF, excluding wake data

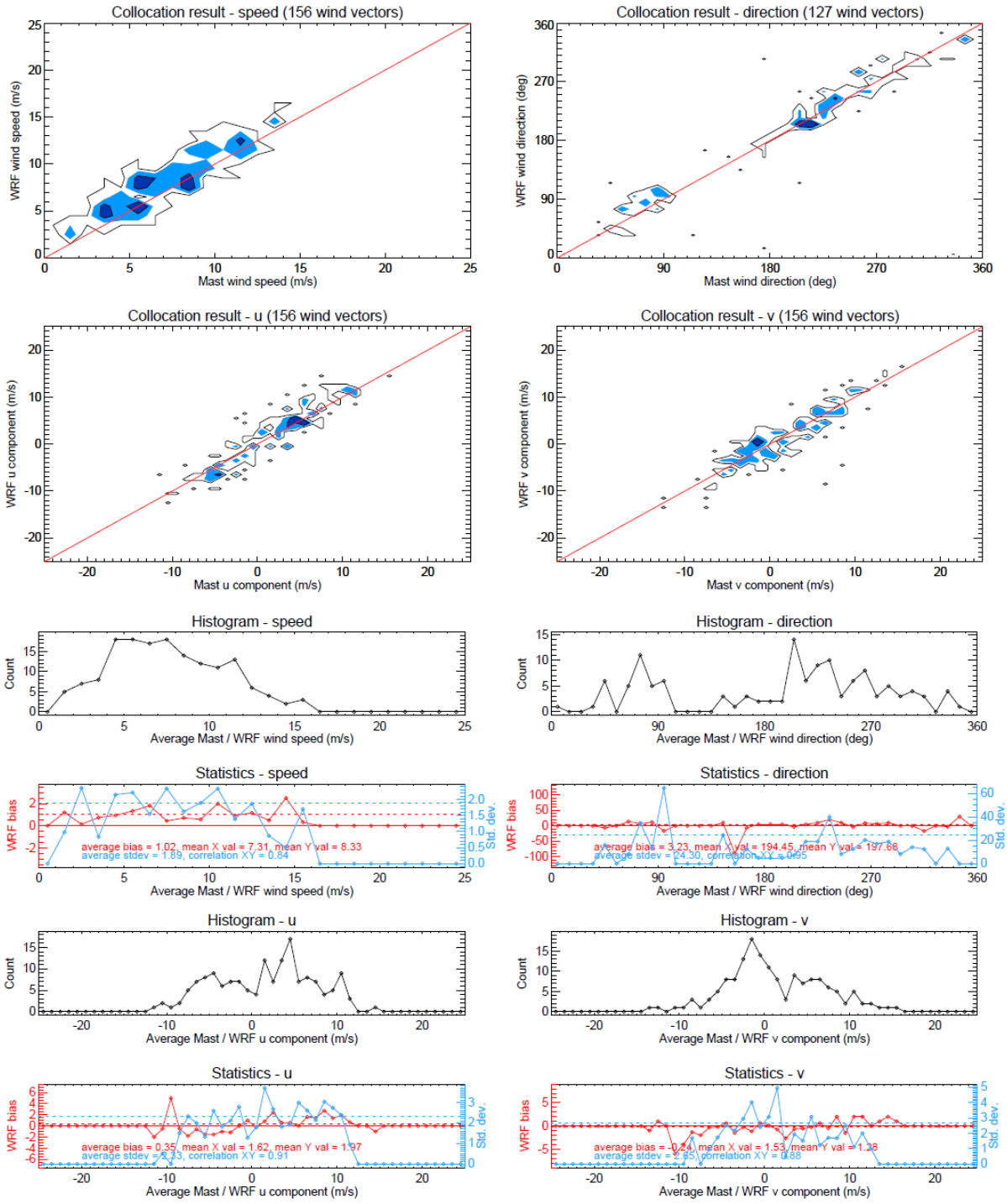

Figure 5.13 Collocation results of Egmond aan Zee vs. WRF, including wake data

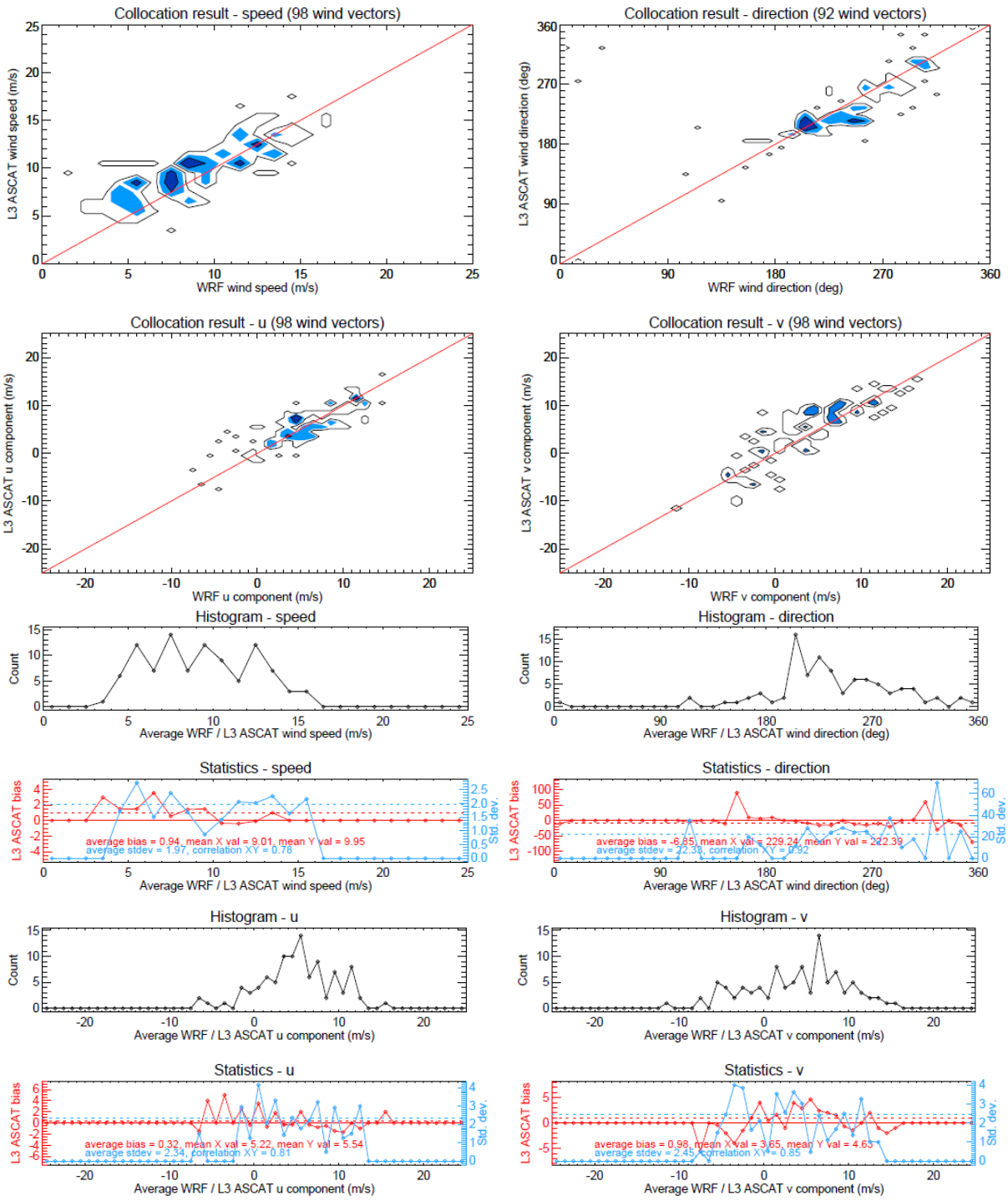

Figure 5.14 Collocation results of WRF vs. ASCAT L3, excluding wake data

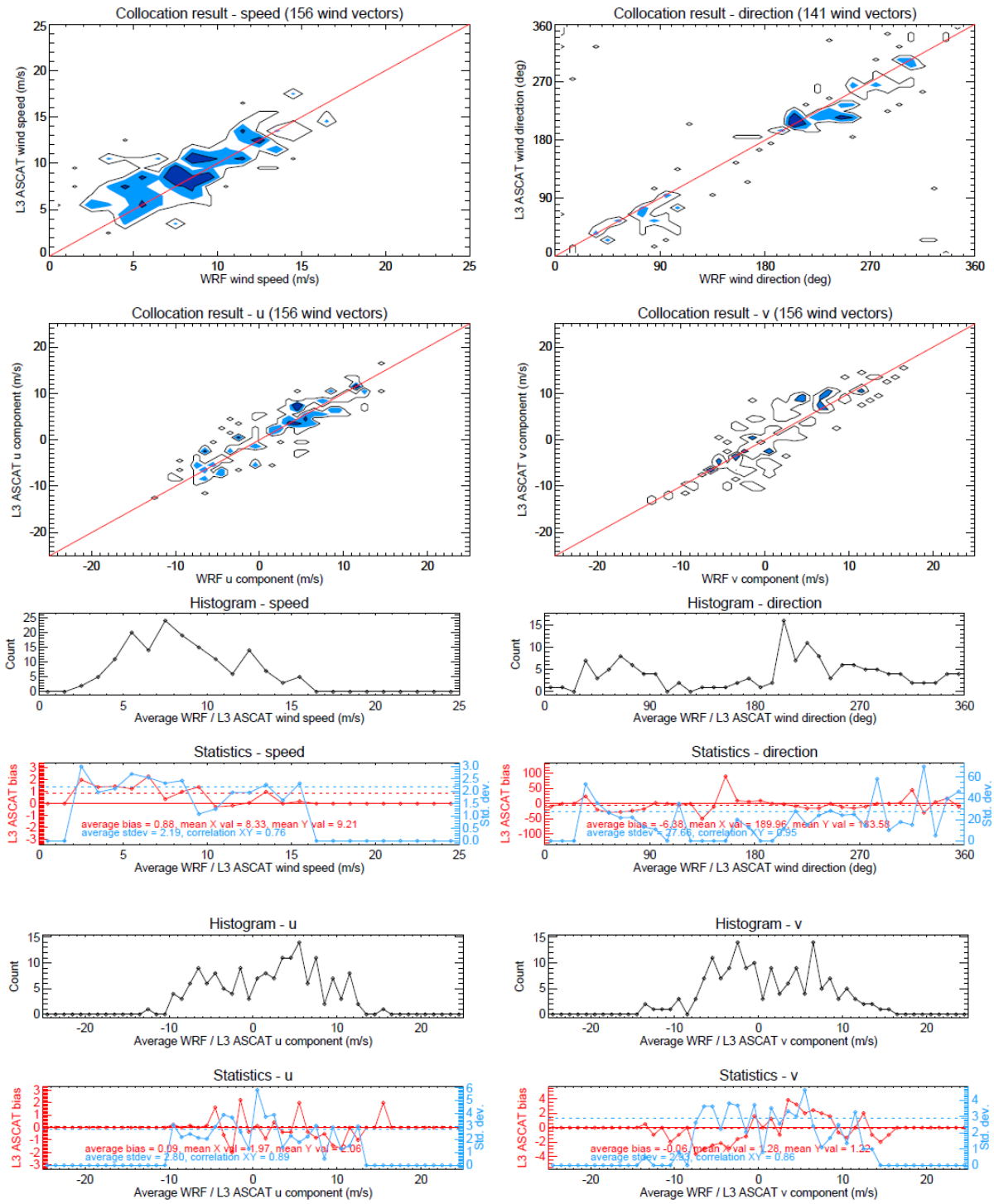

Figure 5.15 Collocation results of WRF vs. ASCAT L3, including wake data

5.5 Wind map comparison

From the available ASCAT wind maps the mean wind speed has been calculated. Figure 5.16 shows this map. The mean wind speed results from QuikSCAT are shown with the same color scale. The two maps cover different periods of time, 2007 to 2008, and 1999 to 2009. Yet there is good agreement in the two results.

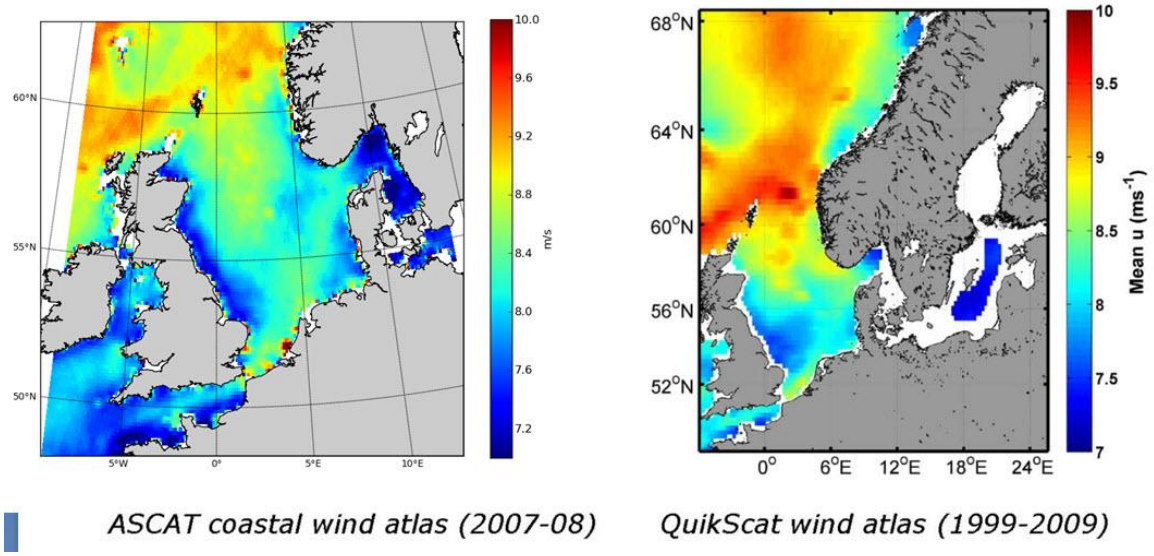

Figure 5.16 Mean wind speed from ASCAT (left) and QuikSCAT (right).

5.6 Summary and perspectives

ASCAT is operating since 2007 and continues to collect ocean surface wind vector observations. ASCAT coastal product fo 12.5 km resolution is compared both to ECMWF, WRF and met-mast data. It is found that anchored ships new Rotterdam Port gives artifact of high wind speed values. There is good agreement in mean winds peed maps for ASCAT and QuikSCAT even though the years used for the maps differ. The combination of QuikSCAT and ASCAT data for longer term estimation of spatial and temporal statistics is of importance.

6 SSM/I

6.1 Wind power trends in the North Sea and the Baltic Sea as found from SSM/I satellite data.

From Remote Sensing Systems (RSS), Internet address www.ssmi.com, SSM/I satellite data products including wind speed have been downloaded for a period from September 1987 until today (May 2012). SSM/I data are produced by Remote Sensing Systems and sponsored by the NASA Earth Science MEaSUREs DISCOVER Project. SSM/I stands for Special Sensor Microwave/Imager and measures the so called brightness temperature at four wavelength and two linear polarizations. From these raw data RSS determines among other parameters the wind speed above the oceans - at 10 m height. Eight satellites have shared the period, each satellite giving two wind speed measurements per day for most of the oceans with 0.25*0.25 degree resolution.

The data for this study is extracted from these measurements as series of two measurements per day, where possible, for the full years 1988 to 2011, for 50 points in the North Sea and 3 in the Baltic Sea, see figure 6.1. At each point the wind speed is taken as an average of the measured wind speeds at the four surrounding 0.25*0.25 degree pixels. The limited number of points in the Baltic Sea is a consequence of the SSM/I data not going close to the coasts.

The long series of data is used to study the trend in wind power potential in the North Sea and Baltic Sea, and to compare the yearly ups and downs to the NAO (North Atlantic Oscillation) index. A previous study on the Danish wind index showed SSM/I winds to be in phase (Hasager et al., 2008). In the present study spatial patterns are investigated also using NAO.

The used wind speed is the SSM/I 10 m wind speed raised to 100 m by anticipating a logarithmic wind speed profile

$$u = \frac{u_*}{\kappa} \ln\left(\frac{z}{z_0}\right)$$

applying Charnock's roughness formula for the open sea

$$z_0 = 0.011 \frac{u_*^2}{g}$$

(Charnock, 1955), and do some iteration.

From the series of 100 m wind speeds a wind power index for a location and period is constructed as

$$P_{period} = \frac{\sum \min(u^2, 15^2)}{15^2 \; N_{meas}} \quad \text{for 5 m/s} < u < 25 \text{ m/s}$$

where N_{meas} is the total number of measurements for the location in the period. This index reflects that wind turbines normally only operate in winds between 5 and 25 m/s, and that their power curves are approximately parabolic until 15 m/s and constant above. The P_{year} so indicates the average fraction of rated power a wind turbine might run at during a full year at the actual location.

Yearly and monthly indexes have been calculated. The yearly indexes has been normalized as

$$P_{year,norm} = \frac{P_{year} N_{years}}{\sum P_{year}}$$

where N_{years} is the number of years, here 24. As this is made for each point individually, these indexes do not contain information about the spatial distribution of potential wind power, but only of the evolution with time.

Figures 6.2 to 6.9 show the variation of normalized yearly wind power indexes as function of time for six of the fifty points in the North Sea plus two in the Baltic Sea, the points indicated with black circles on figure 6.1. Figure 6.2 and 6.6 also show the yearly NAO index (average over the monthly NAO index, figure 6.19, these data taken from http://www.cpc.ncep.noaa.gov/products/precip/CWlink/pna/norm.nao.monthly.b5001.current.ascii

The yearly power index as well as the NAO index seems to vary in a more or less chaotic way, and no correlation is clear between wind power index and NAO index, but while the NAO index has a negative trend over the years the here calculated yearly wind power indexes have positive trends.

The monthly normalized index reads

$$P_{month,norm} = \frac{P_{month} N_{month}}{\sum P_{month}}$$

Based on all monthly indexes for the 24 years this normalized index are generally higher for the wind rich winter month than for the low wind summer month. Figure 6.10 show the variation over the years of the monthly indexes for point 54°N, 4°E, which is indicated on figure 6.1 with a small black square. It is seen - especially from the trend lines - that the season as such seems to have shifted. The high winds in winter and the low winds in summer have shifted towards earlier occurrence. This is also seen at the other investigated points in both North Sea and Baltic Sea.

The trend in the shift of the power wind index has been graphed in Figure 6.11 using the normalized index values per month from the start (1988) to the end (2011) of the data series. It is seen that the power index is shift towards stronger winds earlier in the summer and autumn.

The areal distribution of the wind power index is shown as plots of P_{year}, i.e. the fraction of rated full power production over the year, for years with different NAO indexes, figures 6.12 to 6.18. The power potential is generally highest in the northern part of the North Sea, for some years in the north-eastern part, but there seems to be no correlation with the NAO index.

6.2 Summary and perspectives

The power index calculated from the SSM/I satellite data distributes rather chaotic and it does not seem coupled to the also chaotic NAO index. The power wind index seems to be increasing with time in the period covered, while the NAO index is decreasing.

The monthly indexes reveal a shift towards earlier summer and earlier winter as measured on the wind strength both in the North Sea and Baltic Sea.

Further analysis on trends and statistical significance is relevant to gain more insight to the observed tendencies.

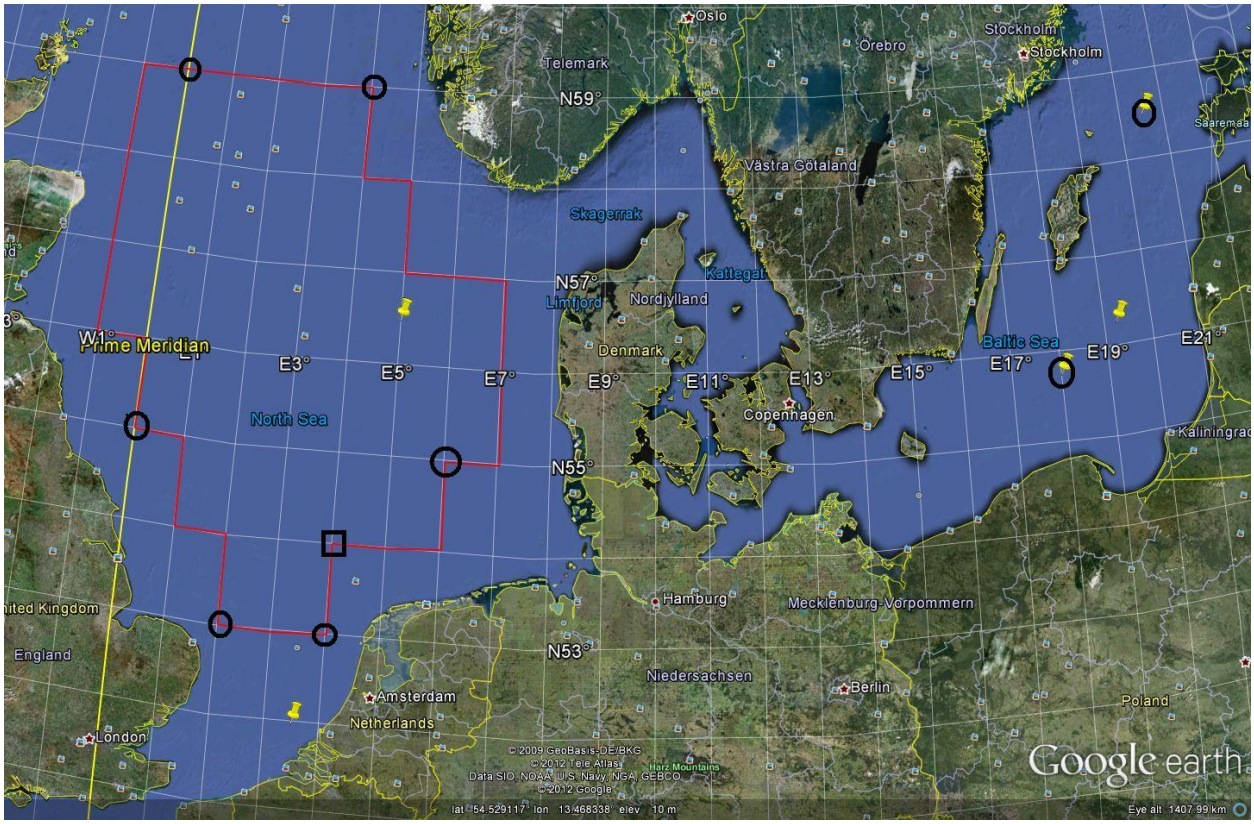

Figure 6.1: Points for wind index calculations: all points at full degrees longitude and latitude at and within the shown red border plus the five points at the yellow Google placemarks (needles).Black circles indicate the points to which figures 6.2 to 6.9 apply, and the black square indicate the point to which figure 6.10 apply.

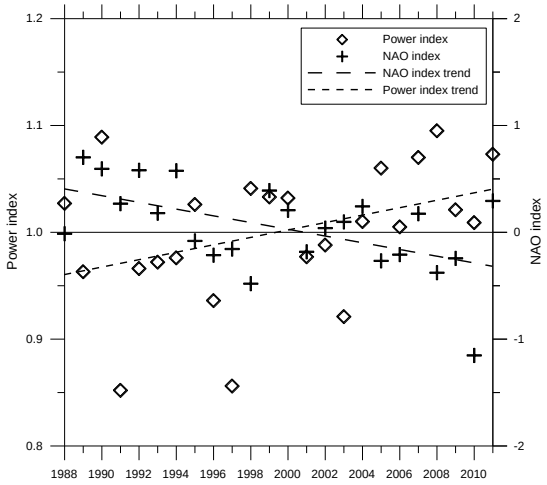

Figure 6.2: Normalized power index at 53N, 2E plus NAO index and linear trends (North Sea)

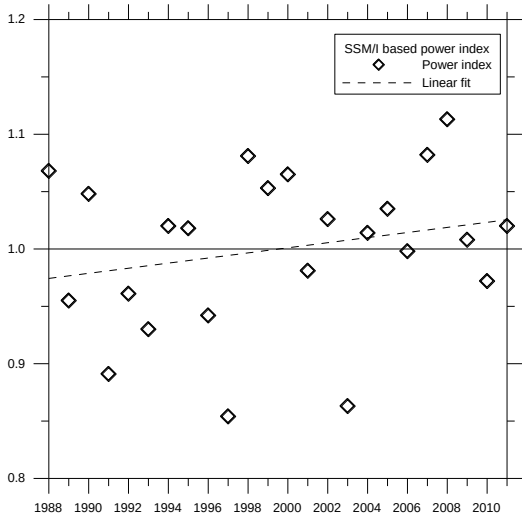

Figure 6.3: Normalized power index at 53N, 4E plus linear trend (North Sea)

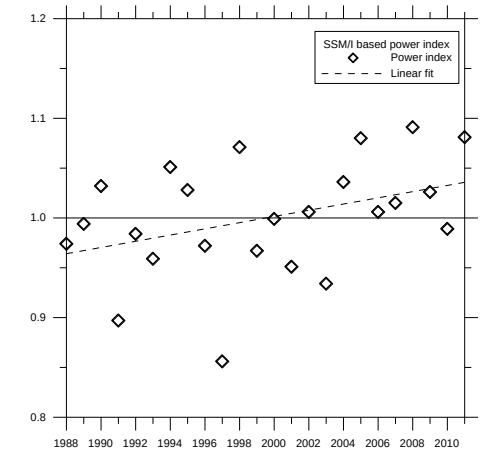

Figure 6.4: Normalized power index at 55N, 0E plus linear trend (North Sea)

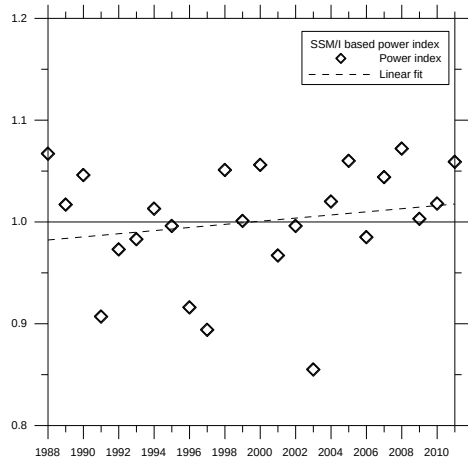

Figure 6.5: Normalized power index at 55N, 6E plus linear trend (North Sea)

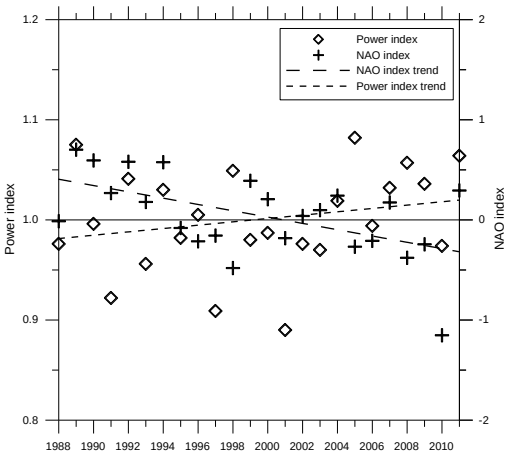

Figure 6.6: Normalized power index 59N, 0E plus NAO index and linear trends (North Sea)

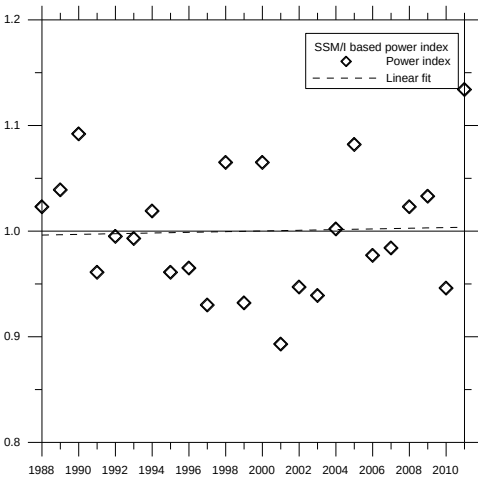

Figure 6.7: Normalized power index at 59N, 4E plus linear trend (North Sea)

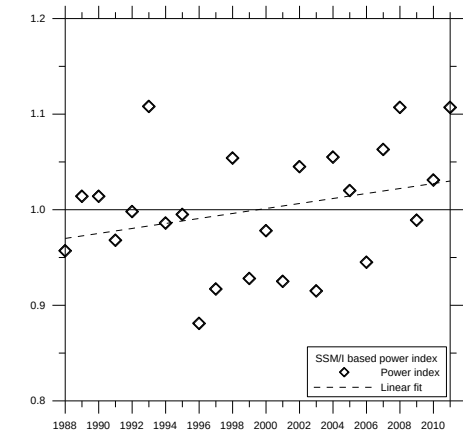

Figure 6.8: Normalized power index at 55.75N, 18E plus linear trend (Baltic Sea)

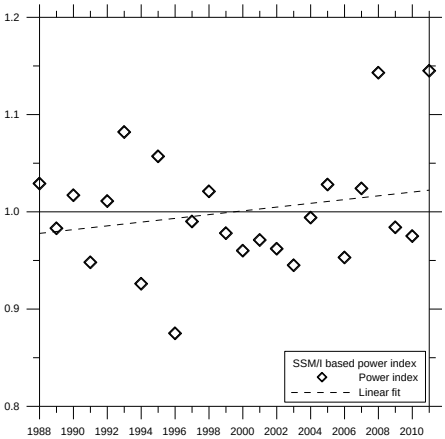

Figure 6.9: Normalized power index at 58.5N, 20.5E plus linear trend (Baltic Sea)

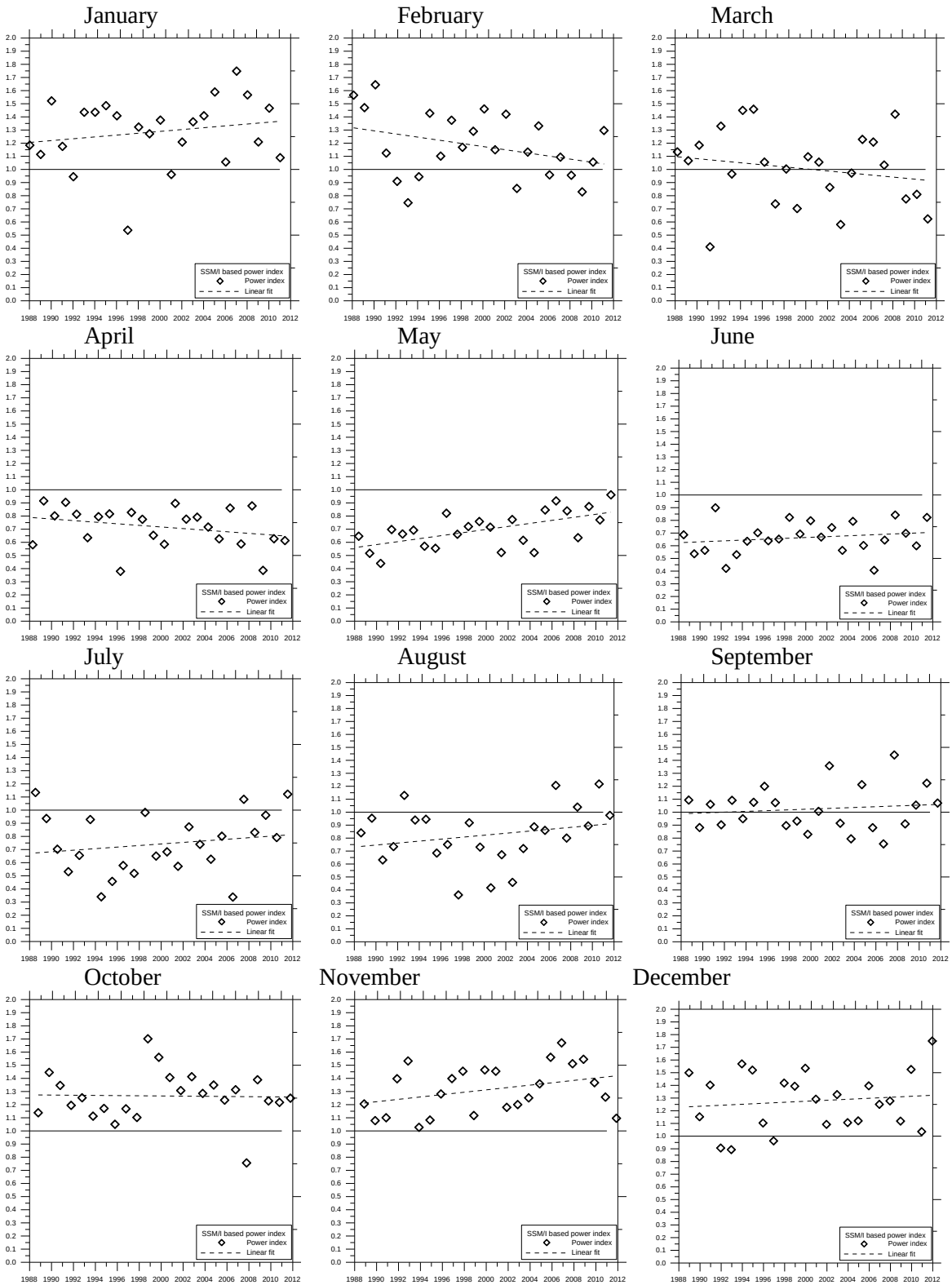

Figure 6.10. Development of the monthly SSM/I based wind power index at 54°N, 4°E over the years 1988 to 2011.

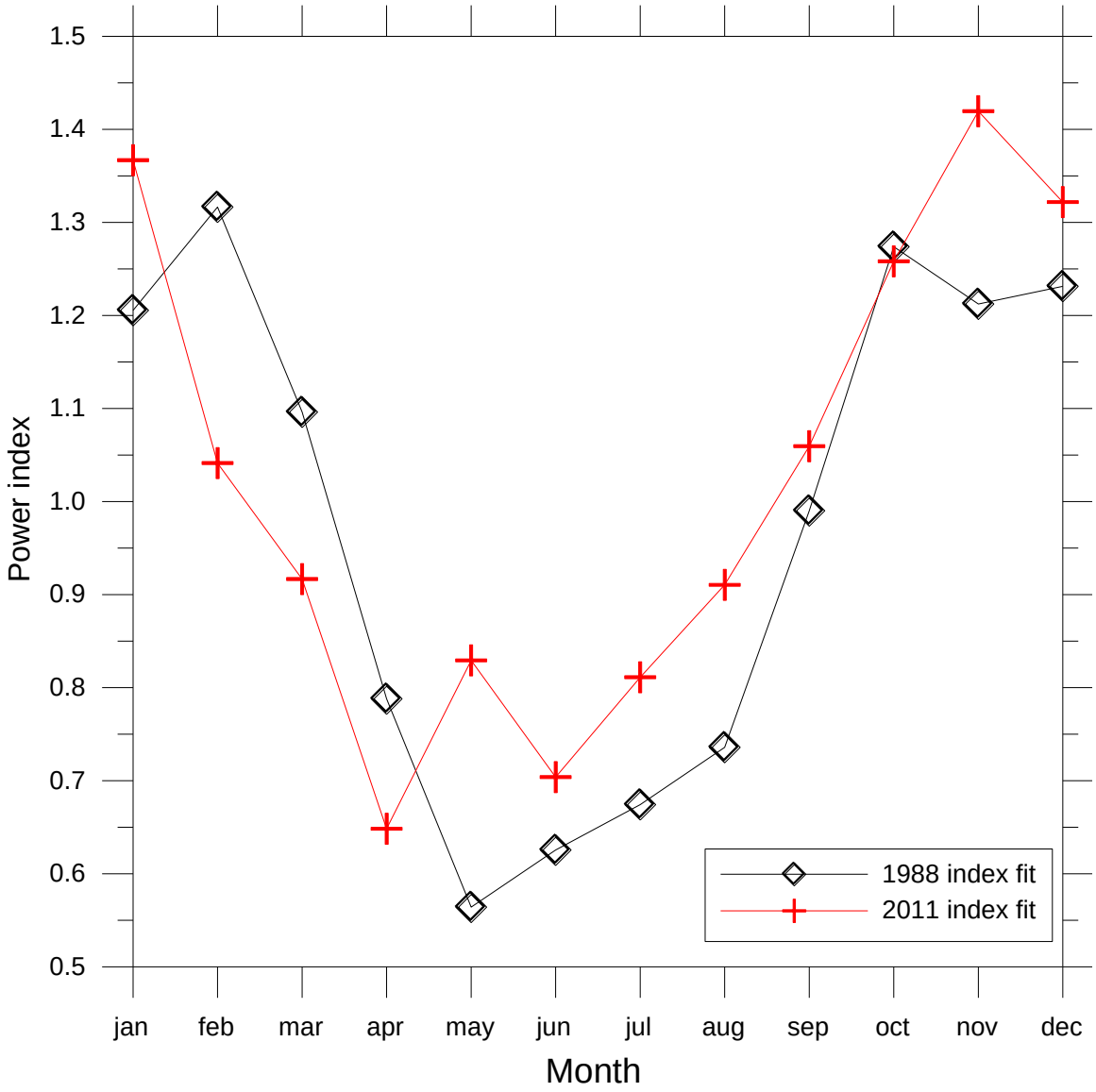

Figure 6.11. Trend of normalized wind power index based on the monthly SSM/I based wind power index at 54°N, 4°E over the years 1988 to 2011.

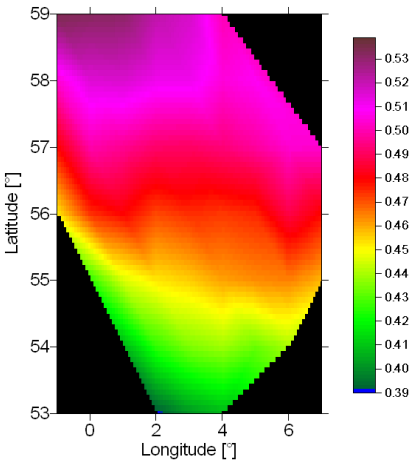

Figure 6.12: 1989 power index distribution with high NAO index

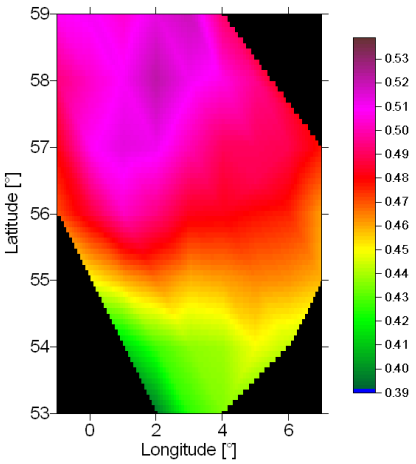

Figure 6.13: 1994 power index distribution with with high NAO index

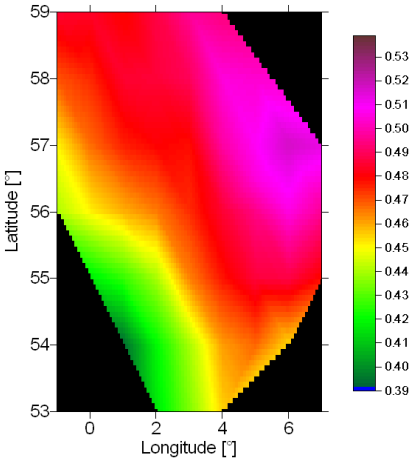

Figure 6.14: 1988 power index distribution distribution with near neutral NAO index

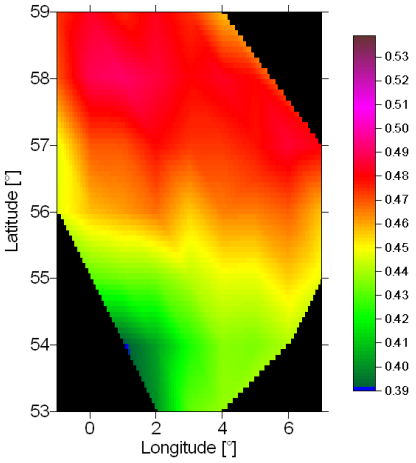

Figure 6.15: 2002 power index with near neutral NAO index

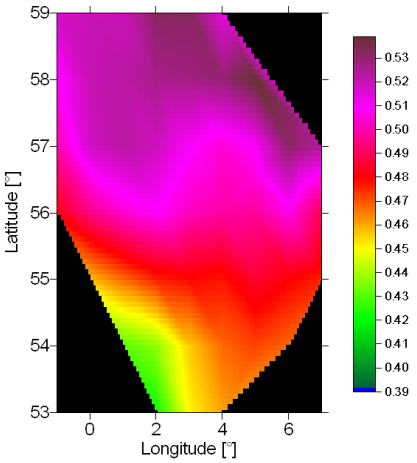

Figure 6.16: 1998 power index distribution distribution with low NAO index

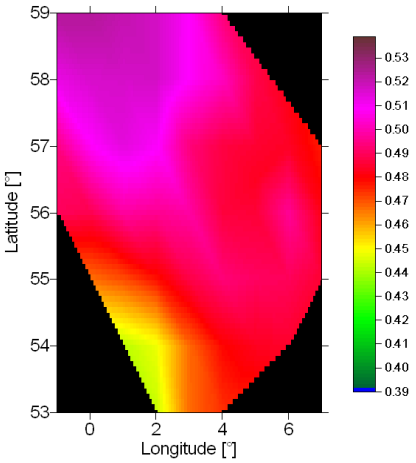

Figure 6.17: 2008 power index with low NAO index

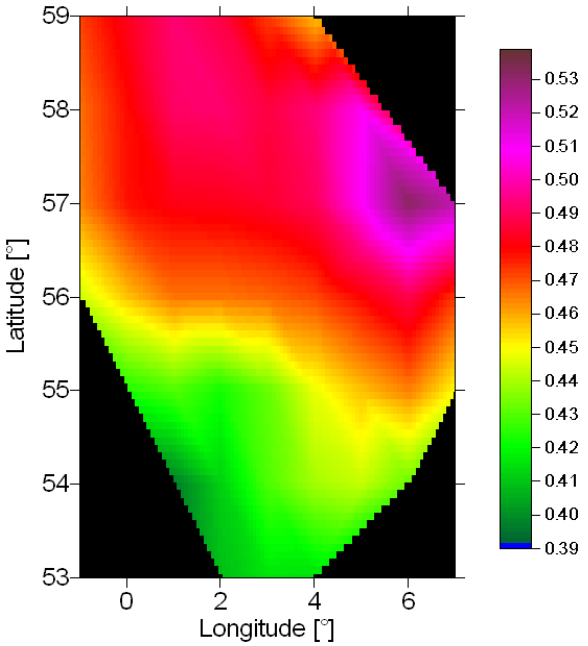

Figure 6.18: 2010 power index distribution with extremely low NAO index

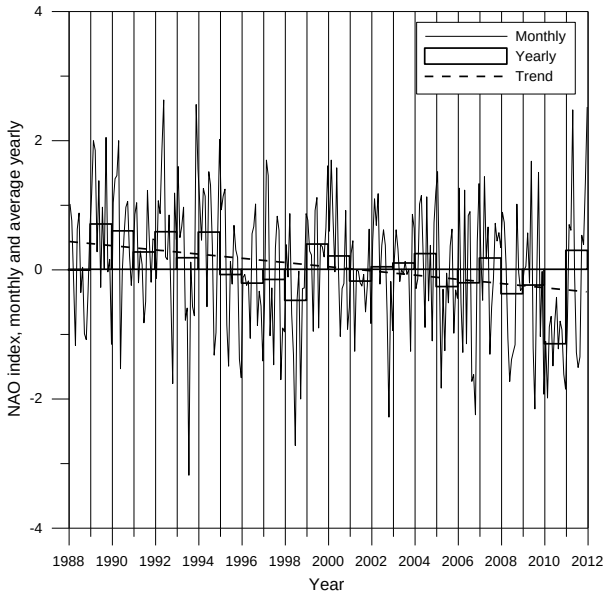

Figure 6.19: NAO index, monthly and yearly averages

7 Summary and conclusion

The analysis of satellite remote sensing products in Norsewind has focused on observations from four sensors: Envisat ASAR, QuikSCAT, ASCAT Coastal and SSM/I. Table 7.1 list some key things about each data set. Number of overlapping samples is a rough estimate. The advantages and limitations for each type of observations are given below.

The advantage of SSM/I is the long-term archive- 24 years – and ~6 samples per day. This allows quantification of long-term variability of wind speed. It is shown that there may be a temporal shift of winds in the Northern European Seas. The limitations of SSM/I are that it is wind speed only, and that the coastal regions are not covered.

QuikSCAT has also the advantage of a long-term archive – 10 years – and two samples per day. In addition, it is the ocean surface vector winds observed. This allows wind roses to be calculated. The data has been used to calculate mean wind speed, Weibull A and k, and energy density maps. Also many other statistical parameters have been calculated, e.g. the spatial correlation maps. Limitations are for the Baltic Sea a sea-ice mask that omits wind along the coasts much of the year in the level 3 product used. The effect of ocean currents may bias results. Close to the coastlines some bias may be found. Rain-flagging is important for the Ku-band scatterometer but it does not seem to be a serious problem for wind resource statistics to omit these data.

ASCAT has the advantage of a coastal wind product of 12.5 km that covers areas closer to the coastlines than QuikSCAT. The observations are very similar to QuikSCAT. ASCAT is in orbit and it will observe for weather applications in the future. ASCAT is C-band and not so affected by rain as Ku-band. This is an advantage. The swath of ASCAT is not as wide as for QuikSCAT therefore the temporal resolution is lower but it is expected that two ASCAT instruments will be in orbit in the future. This will provide temporal coverage similar to QuikSCAT.

Envisat ASAR has the advantage of high spatial resolution. In the Norsewind project we produced maps at 2 km resolution. This allows small-scale features to be identified and the coastal regions to be covered well. Envisat ASAR is giving wind vector information. In our case the wind direction is from ECMWF and the wind speed from the SAR. This combination allows wind roses to be calculated. The number of samples is generally high for the Northern European Seas. One limitation of SAR wind maps is the digital image processing. This has to be done by the end-user (or nowadays for European Seas from CLS Soprano ESA demonstration project). Level 2 wind products are not available from ESA. In contrast, level 3 ocean wind products are available for SSM/I and QuikSCAT and level 2 for ASCAT. It is foreseen that Sentinel-1 with a SAR will provide level 2 wind products in the future.

A disadvantage of all satellite-based wind products is that they are valid at only 10 m above sea level. Thus extrapolation to higher heights is desirable for wind energy. A method has been suggested in the project but more research has to be done.

Table 7.2 Table of satellite ocean wind products with period of observation, spatial resolution and rough estimate of number of samples.

	Period	Resolution (km)	Number of samples
SSM/I	1988-present	25	35000
QuikSCAT	1999-2009	25	7300
ASCAT Coastal	2007-present	12.5	1500
Envisat ASAR	2002-2012	2	1200

Appendix A

Table 1

Comparison of SAR winds (CMOD-IFR2) and mast winds (SDW) extrapolated to 10 m

		Wind speed statistics			Wind direction statistics	
		0-25 m/s	2-25 m/s	2-15 m/s	0-25 m/s	2-25 m/s
Masts with stability information:						
Horns Rev M2	SD_x	3.24	3.18	2.59	-	-
	SD_y	3.44	3.36	2.69	-	-
	R2	0.86	0.85	0.79	-	-
	RMSE	1.33	1.33	1.28	-	-
	Regression_a	0.98	0.97	0.92	-	-
	Regression_b	-0.14	-0.05	0.27	-	-
	N	146	143	136	-	-
Egmond aan Zee	SD_x	3.19	3.06	2.95	92.89	92.17
	SD_y	3.28	3.08	2.91	89.34	89.04
	R2	0.81	0.80	0.80	0.94	0.95
	RMSE	1.48	1.44	1.37	23.48	20.96
	Regression_a	0.92	0.90	0.88	0.93	0.94
	Regression_b	0.36	0.61	0.70	17.90	16.06
	N	197	188	184	195	186

SDW means stability derived winds

Table 2

Comparison of SAR winds (CMOD-IFR2) and mast winds extrapolated to 10 m

		Wind speed statistics			Wind direction statistics	
		0-25 m/s	2-25 m/s	2-15 m/s	0-25 m/s	2-25 m/s
Masts without stability information:						
Fino-1 (large data set)	SD_x	3.65	3.47	2.94	87.87	87.92
	SD_y	3.89	3.68	3.06	89.56	88.99
	R2	0.72	0.69	0.61	0.91	0.92
	RMSE	2.08	2.08	2.00	27.39	25.29
	Regression_a	0.91	0.88	0.81	0.97	0.97
	Regression_b	0.54	0.81	1.25	10.95	10.97
	N	517	489	457	484	461
Horns Rev M7	SD_x	3.37	3.25	2.85	87.21	87.75
	SD_y	3.27	3.09	2.70	86.66	86.78
	R2	0.80	0.78	0.75	0.92	0.93
	RMSE	1.66	1.65	1.59	24.22	23.79
	Regression_a	0.87	0.84	0.82	0.96	0.95
	Regression_b	0.36	0.61	0.77	8.37	8.74
	N	468	450	434	452	437
Greater Gabbard	SD_x	3.40	3.40	2.96	77.82	77.82
	SD_y	3.24	3.24	2.83	73.24	73.24
	R2	0.69	0.69	0.70	0.96	0.96
	RMSE	1.95	1.95	1.68	16.23	16.23
	Regression_a	0.79	0.79	0.80	0.92	0.92
	Regression_b	1.82	1.82	1.56	13.30	13.30
	N	29	29	24	29	29

Table 3

Comparison of SAR winds (CMOD5) and mast winds (SDW) extrapolated to 10 m

		Wind speed statistics			Wind direction statistics	
		0-25 m/s	2-25 m/s	2-15 m/s	0-25 m/s	2-25 m/s
Masts with stability information:						
Horns Rev M2	SD_x	3.24	3.21	2.63	-	-
	SD_y	3.27	3.24	2.57	-	-
	R2	0.85	0.85	0.79	-	-
	RMSE	1.27	1.28	1.22	-	-
	Regression_a	0.93	0.93	0.87	-	-
	Regression_b	0.41	0.43	0.81	-	-
	N	146	145	138	-	-
Egmond aan Zee	SD_x	3.19	3.10	2.99	92.89	92.17
	SD_y	3.07	2.94	2.81	89.34	89.04
	R2	0.78	0.78	0.77	0.94	0.95
	RMSE	1.50	1.48	1.45	23.48	20.96
	Regression_a	0.85	0.84	0.82	0.93	0.94
	Regression_b	1.17	1.31	1.40	17.90	16.06
	N	197	190	187	195	186

SDW means stability derived winds

Comparison of SAR winds (CMOD5.n) and mast winds (ENW) extrapolated to 10 m

		Wind speed statistics			Wind direction statistics	
		0-25 m/s	2-25 m/s	2-15 m/s	0-25 m/s	2-25 m/s
Masts with stability information:						
Horns Rev M2	SD_x	3.30	3.27	2.67	-	-
	SD_y	3.25	3.22	2.48	-	-
	R2	0.86	0.86	0.81	-	-
	RMSE	1.34	1.35	1.26	-	-
	Regression_a	0.92	0.91	0.84	-	-
	Regression_b	1.22	1.24	1.70	-	-
	N	146	145	137	-	-
Egmond aan Zee	SD_x	3.19	3.11	2.97	92.89	92.17
	SD_y	3.06	2.98	2.77	89.34	89.04
	R2	0.78	0.78	0.77	0.94	0.95
	RMSE	1.67	1.66	1.60	23.48	20.96
	Regression_a	0.85	0.84	0.82	0.93	0.94
	Regression_b	1.89	1.93	2.09	17.90	16.06
	N	197	192	187	195	186

ENW means equivalent neutral winds

Appendix B

List of acronyms

ASAR	Advanced Synthetic Aperture Radar
ASCAT	Advanced Scatterometer
BSH	Federal Ministry for the Environment, Nature Conservation and Nuclear Safety, DE
CLS	Collecte Localisation Satellites, France
DMPS	Defence Meteorological Satellite Program
DTU	Technical University of Denmark
ENW	Equivalent Neutral Winds
ESA	European Space Agency
EUMETSAT	European Organisation for the Exploitation of Meteorological Satellites
EWEA	European Wind Energy Association
GMF	Geophysical Model Function
HH	Horizontal transmit, Horizontal receive
KNMI	Royal Netherlands Meteorological Institute
KVT	Kjeller Vindteknikk, Norway
LNEG	Laboratory National for Energy and Geology, Portugal
NASA	National Aeronautics and Space Administration
NORSEWInD	Northern Seas Wind Index database
NRT	Near-Real-Time
OSI-SAF	Ocean and Sea Ice Satellite Application Facility
QSCAT	QuikSCAT
RSS	Remote Sensing Systems
SAR	Synthetic Aperture Radar
SDW	Stability Derived Winds
SSM/I	Special Sensor Microwave Imager
S-WAsP	Satellite-WAsP
VV	Vertical transmit, Vertical receive
WAsP	Wind Atlas Analysis and Application program
WSM	Wide swath mode

Appendix C

Maps at http://soprano.cls.fr soprano/winds/statistics(L3) select Norsewind. The results are based on 9000 Envisat ASAR WSM wind maps collected and processed by CLS and DTU Wind Energy.

The maps are from top to bottom

- Number of samples
- Mean wind speed
- Weibull A parameter
- Weibull k parameter
- Energy density

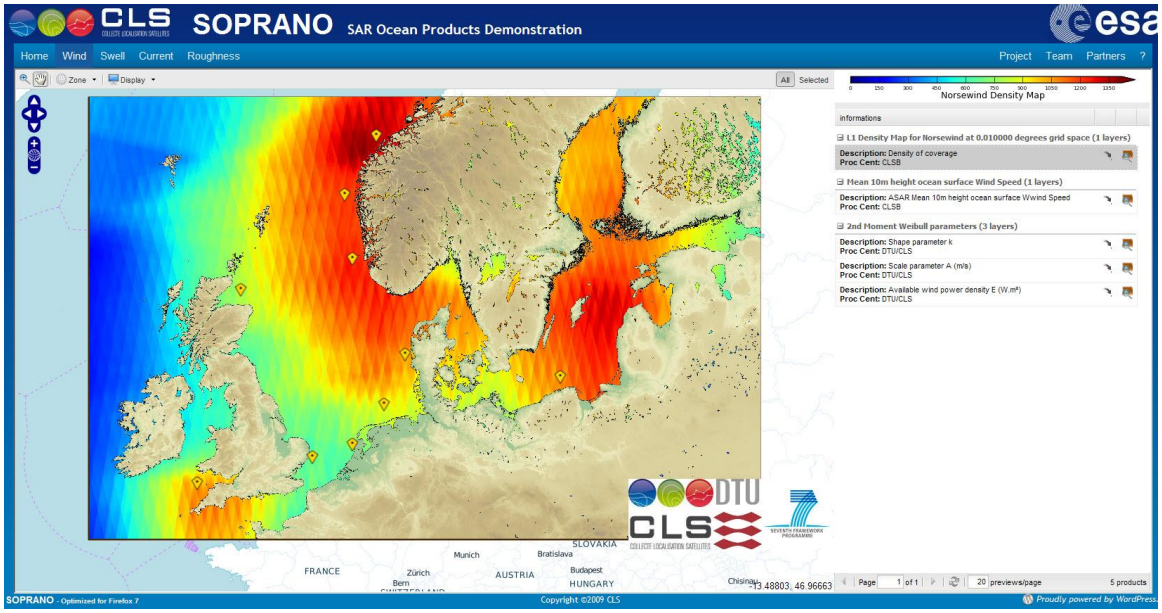

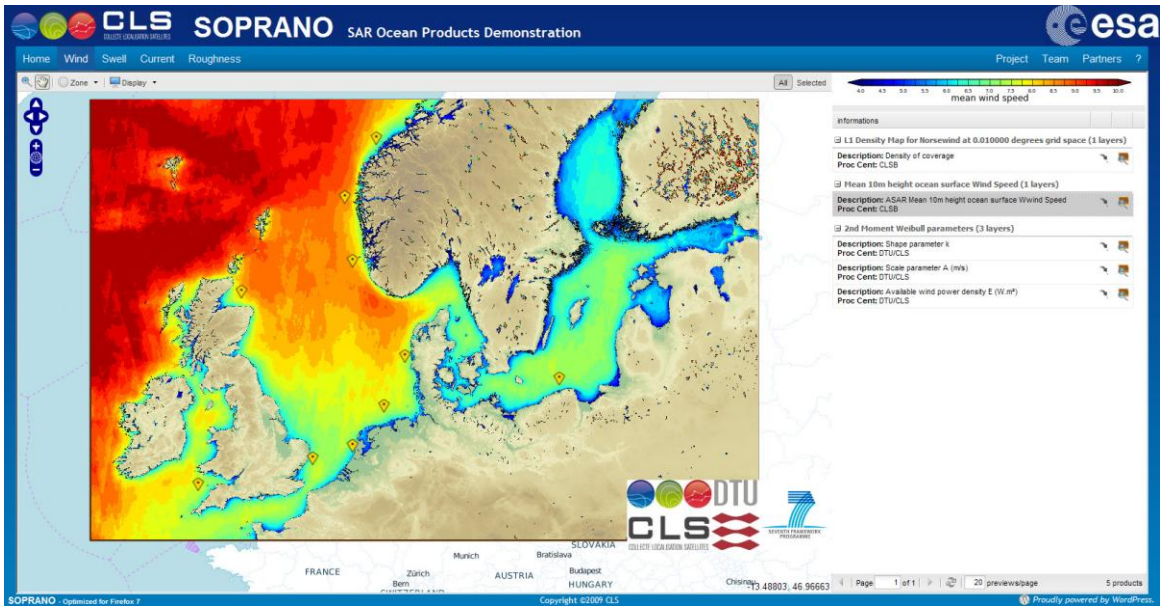

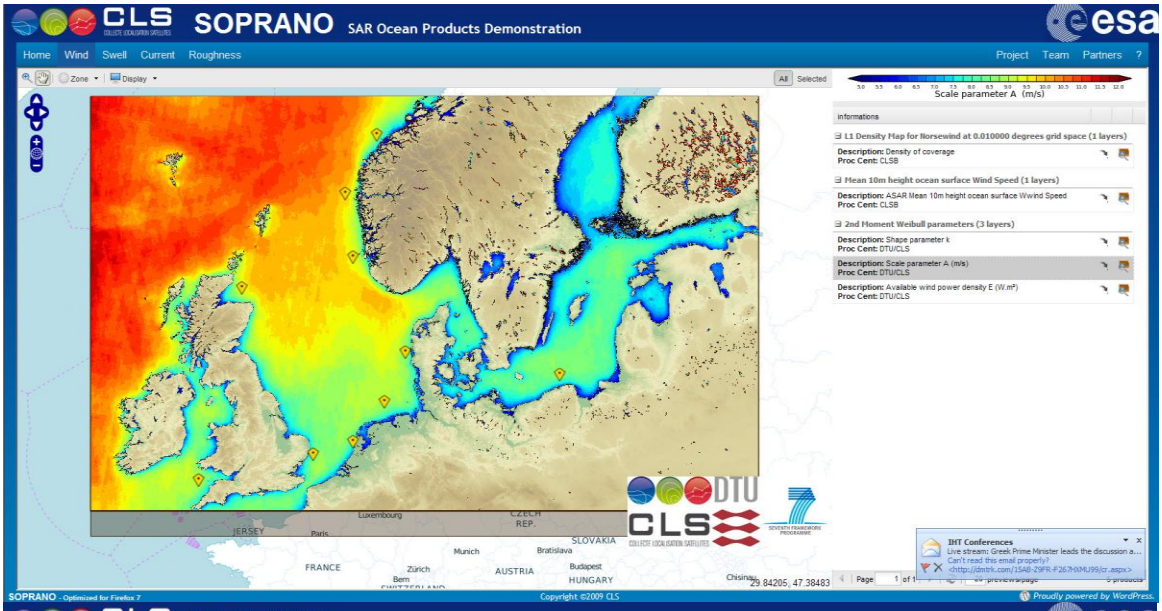
SOPRANO
SAR Ocean Products Demonstration
Home
Wind
Swell
Current
Roughness
Project
Team
Partners
Scale parameter A (m/s)
informations
L1 Density Map for Norsewind at 0.010000 degrees grid space (1 layers)
Description: Density of coverage
Proc Cent: CLSB
Mean 10m height ocean surface Wind Speed (1 layers)
Description: ASAR Mean 10m height ocean surface Wwind Speed
Proc Cent: CLSB
2nd Moment Weibull parameters (3 layers)
Description: Shape parameter k
Proc Cent: DTU/CLS
Description: Scale parameter A (m/s)
Proc Cent: DTU/CLS
Description: Available wind power density E (W.m²)
Proc Cent: DTU/CLS
Luxembourg
CZECH REP.
JERSEY
Paris
SLOVAKIA
Munich
Bratislava
FRANCE
Zürich
AUSTRIA
Budapest
HUNGARY
Bern
29.84205, 47.38483
Copyright ©2009 CLS

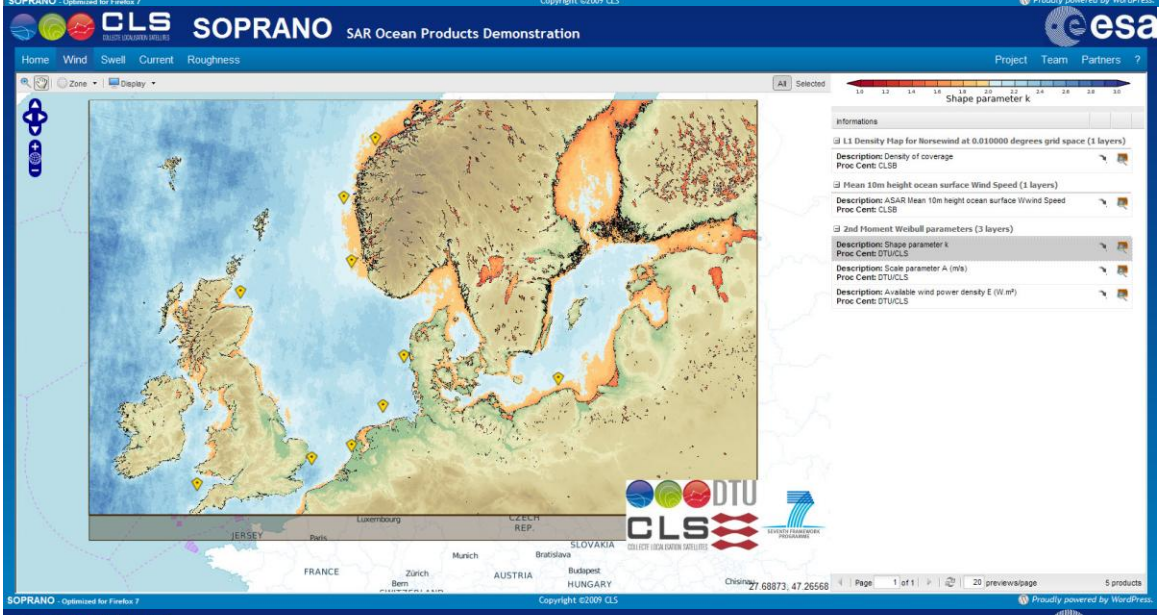
SOPRANO
SAR Ocean Products Demonstration
Home
Wind
Swell
Current
Roughness
Project
Team
Partners
Shape parameter k
informations
L1 Density Map for Norsewind at 0.010000 degrees grid space (1 layers)
Description: Density of coverage
Proc Cent: CLSB
Mean 10m height ocean surface Wind Speed (1 layers)
Description: ASAR Mean 10m height ocean surface Wwind Speed
Proc Cent: CLSB
2nd Moment Weibull parameters (3 layers)
Description: Shape parameter k
Proc Cent: DTU/CLS
Description: Scale parameter A (m/s)
Proc Cent: DTU/CLS
Description: Available wind power density E (W.m²)
Proc Cent: DTU/CLS
Luxembourg
CZECH REP.
JERSEY
Paris
SLOVAKIA
Munich
Bratislava
FRANCE
Zürich
AUSTRIA
Budapest
HUNGARY
Bern
27.68873, 47.26568
Copyright ©2009 CLS

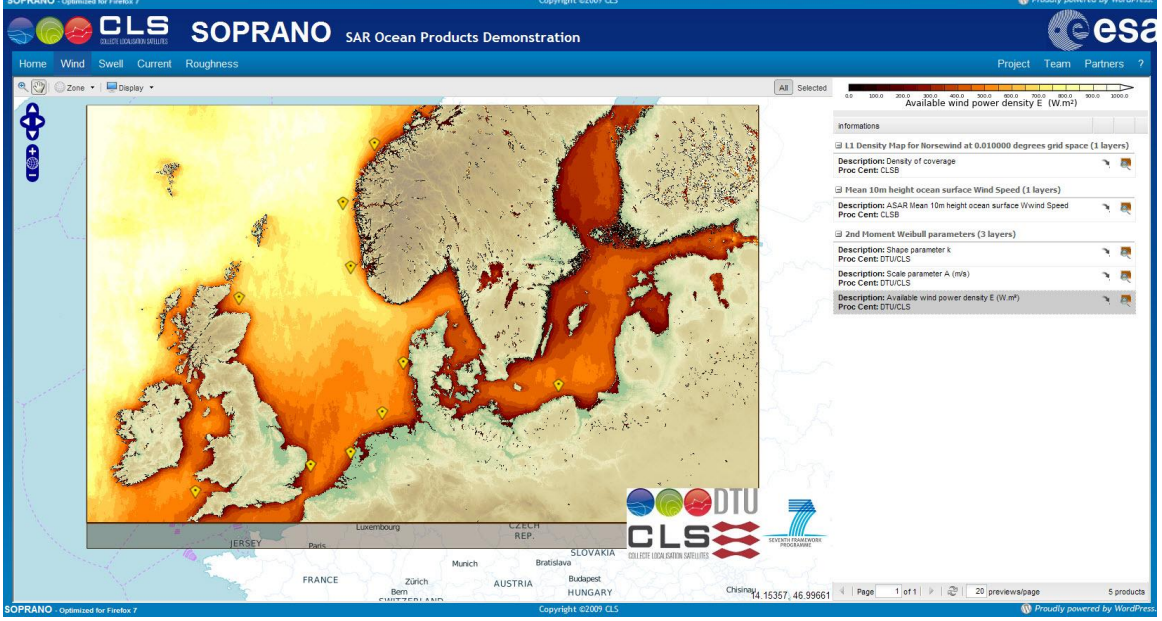
SOPRANO
SAR Ocean Products Demonstration
Home
Wind
Swell
Current
Roughness
Project
Team
Partners
Available wind power density E (W.m²)
informations
L1 Density Map for Norsewind at 0.010000 degrees grid space (1 layers)
Description: Density of coverage
Proc Cent: CLSB
Mean 10m height ocean surface Wind Speed (1 layers)
Description: ASAR Mean 10m height ocean surface Wwind Speed
Proc Cent: CLSB
2nd Moment Weibull parameters (3 layers)
Description: Shape parameter k
Proc Cent: DTU/CLS
Description: Scale parameter A (m/s)
Proc Cent: DTU/CLS
Description: Available wind power density E (W.m²)
Proc Cent: DTU/CLS
Luxembourg
CZECH REP.
JERSEY
Paris
SLOVAKIA
Munich
Bratislava
FRANCE
Zürich
AUSTRIA
Budapest
HUNGARY
Bern
14.15357, 46.99661
Copyright ©2009 CLS

References

References

Anderson, H. Bonekamp, C. Duff, J. Figa-Saldaña, and J. J. W. Wilson, Analysis of ASCAT Ocean Backscatter Measurement Noise, IEEE TRANSACTIONS ON GEOSCIENCE AND REMOTE SENSING, VOL. 50, NO. 7, JULY 2012 2449.

AWDP User Manual and Reference Guide v2.0, NWP-SAF, http://research.metoffice.gov.uk/research/interproj/nwpsaf/scatterometer/AWDP/AWDP_UM_and_RG_v2_0.pdf ,

ASCAT Wind Product User Manual, Ocean and Sea Ice SAF, Version 1.11, March 2012, http://www.knmi.nl/scatterometer/publications/pdf/ASCAT_Product_Manual.pdf
The MyOcean L3 Global Wind Product, http://www.myocean.eu/

Badger, M., J. Badger, M. Nielsen, C. B. Hasager and A. Peña, A hybrid method for offshore wind resource assessment, paper presented at ESA Living Planet Symposium, Bergen 2010, 2010a.

Badger, M., J. Badger, M. Nielsen, C. B. Hasager and A. Peña, Wind class sampling of satellite SAR imagery for offshore wind resource mapping, *Journal of Applied Meteorology, 49*(12), 2474-2491, 2010b.

Badger, M., A. Peña, R. E. Bredesen, E. Berge, A. Hahmann, J. Badger, I. Karagali, C. B. Hasager and T. Mikkelsen, Bringing satellite winds to hub-height, paper presented at EWEA2012 Proceedings, 2012a.

Badger, M., A. Peña, A. Stoffelen, T. Driesenaar, E. Berge and R. E. Bredesen, Bringing ocean winds from 10 m to higher levels, paper presented at IGARSS 2012, 2012b.

Barthelmie, R. J. and S. C. Pryor, Can satellite sampling of offshore wind speeds realistically represent wind speed distributions., *Journal of Applied Meteorology, 42*(1), 83-94, 2003.

Berge, E., O. Byrkjedal, Y. Ydersbond and D. Kindler, Modelling of offshore wind resources. Comparison of a meso-scale model and measurements from FINO-1 and North Sea oil rigs, paper presented at Scientific Proceedings EWEC'09 Marseille, 2009.

Charnock, H., Wind stress on a water surface, *Quarterly Journal of the Royal Meteorological Society, 81*, 639-640, 1955.

Christiansen, M. B., C. B. Hasager, D. R. Thompson and F. Monaldo, Ocean winds from synthetic aperture radar, in Ocean remote Sensing: Recent Techniques and Applications., edited by R. Niclos and V. Caselles, pp. 31-54, Research Singpost Editorial, 2008.

Christiansen, M. B., W. Koch, J. Horstmann and C. B. Hasager, Wind resource assessment from C-band SAR, *Remote Sensing of Environment, 105*, 68-81, 2006.

Hahmann, A., D. Rostkier-Edelstein, T. T. Warner, F. Vanderberghe, Y. Liu, R. Babarsky and S. P. Swerdlin, A reanalysis system for the generation of mesoscale climatographies, *Journal of Applied Meteorology and Climatology., 49*, 954-972, 2010.

Hasager, C. B., M. Badger, A. Peña and X. G. Larsén, SAR-Based Wind Resource Statistics in the Baltic Sea, *Remote Sensing,*((in review)), 2010a.

Hasager, C. B., M. Badger, A. Peña, X. G. Larsén and F. Bingöl, SAR-Based Wind Resource Statistics in the Baltic Sea, *Remote Sensing, 3*(1), 117-144, 2011.

Hasager, C. B., I. Karagali, P. Astrup, M. Badger, A. Mouche and A. Stoffelen, Offshore wind atlas for Northern European Seas, paper presented at ESA Living Planet Symposium, Bergen 2010, 2010b.

Hasager, C. B., A. Mouche, M. Badger, P. Astrup and M. Nielsen, Satellite winds in EU-Norsewind, paper presented at European Wind Energy Conference (EWEC) 2008, Marseilles (FR), 2009.

Hasager, C. B., A. Peña, M. B. Christiansen, P. Astrup, M. Nielsen, F. M. Monaldo, D. R. Thompson and P. Nielsen, Remote sensing observation used in offshore wind energy, *IEEE Journal of Selected Topics in Applied Earth Observations and Remote Sensing, 1*(1), 67-79, 2008.

Hilburn K.A., F. J. Wentz, D. K. Smith and P. D. Ashcroft, Correcting active scatterometer data for the effects of rain using passive radiometer data, *Journal of Applied Meteorology and Climatology., 45*, 382-398, 2006.

Karagali, I., Offshore Wind Energy: Wind and Sea Surface Temperature from satellite observations, Ph.D.Thesis DTU Wind Energy -Ph.D.-003(EN), Technical University of Denmark, 2012.

Karagali, I., M. Badger, A. Peña, A. Hahmann, C. B. Hasager and A. Sempreviva, Spatial and termporal variablity of winds in the Northern European Seas, *Renewable Energy, in review*, 2012a.

Karagali, I., A. Peña, M. Badger and C. B. Hasager, Wind characteristics in the North and Baltic Seas from the QuikSCAT satellite, *Wind Energy, in review*, 2012b.

Kerbaol, V., Improved Bayesian wind vector retrieval scheme using ENVISAT ASAR data: principles and validation results, paper presented at ENVISAT symposium, Montreux (CH), 23-27 Apr 2007, Paris, 2007.

Liu, W. T. and W. Tang, Equivalent neutral wind, National Aeronautics and Space Administration, Jet Propulsion Laboratory, California Institute of Technology, National Technical Information Service, distributor, 1996.

Mortensen, N., D. N. Heathfield, L. Landberg, O. Rathmann, I. TROEN and E. L. Petersen, Wind Atlas Analysis and Wind Atlas Analysis and Application program:WAsP 7.0 Help Facility, pp. 1-277, Risø National Laboratory, Roskilde, 2000.

Mouche, A., F. Collard, B. Chapron, K.-F. Dagestad, G. Guitton, J. Johannessen, V. Kerbaol and M. W. Hansen, On the use of Doppler shift for sea surface wind retrieval from SAR, *IEEE Transactions on Geoscience and Remote Sensing, DOI:10.1109/TGRS.2011.2174998*(in press), 2012.

Nielsen, M., P. Astrup, C. B. Hasager, R. J. Barthelmie and S. C. Pryor, Satellite information for wind energy applications, pp. 1-57, Risø National Laboratory, Roskilde, Denmark, 2004.

Peña, A., S. E. Gryning and C. B. Hasager, Measurements and Modelling of the Wind Speed Profile in the Marine Atmospheric Boundary Layer, *Boundary-Layer Meteorology, 129*(3), 479-495, 2008.

Peña, A. and A. Hahmann, Atmospheric stability and turbulence fuxes at Horns Rev -an intercomparison of sonic, bulk and WRF model data, *Wind Energy*, 2011.

Peña, A., A. Hahmann, C. B. Hasager, F. Bingöl, I. Karagali, J. Badger, M. Badger and N. E. Clausen, South Baltic Wind Atlas, edited by Risø DTU, pp. 1-66, Roskilde, 2011.

Peña, A., T. Mikkelsen, S. E. Gryning, C. B. Hasager, A. Hahmann, M. Badger, I. Karagali and M. Courtney, Offshore vertical wind shear, DTU Wind Energy-E-0005(EN), 2012.

Portabella, M., A. Stoffelen and J. Johannessen, Toward an optimal inversion method for SAR wind retrieval, *Journal of Geophysical Research-Atmospheres, 107*(8), doi:10.1029/2001JC000925, 2002.

PRODUCT USER MANUAL For Sea Ice Wind Thematic Assembly Centre WIND_GLO_WIND_L3_NRT_OBSERVATIONS_012_002, MyOcean, Version 2.0, September 2011, http://catalogue.myocean.eu.org/static/rsources/myocean/pum/MYO-SIW-PUM-012-002-v2.0.pdf

Pryor, S. C., M. Nielsen, R. J. Barthelmie and J. Mann, Can satellite sampling of offshore wind speeds realistically represent wind speed distributions? Part II Quantifying uncertainties associated with sampling strategy and distribution fitting methods., *Journal of Applied Meteorology, 43*, 739-750, 2004.

Scientific Calibration Report (ScCR) for V2, SIW TAC Product: WIND_GLO_WIND_L3_NRT_OBSERVATIONS_012_002, MyOcean, October 2011, http://myocean.met.no/SIW-TAC/index.html

Stoffelen, A., Scatterometry, Thesis: Universiteit Utrecht, 1998
Ad Stoffelen, 1998, Toward the true near-surface wind speed: error modeling and calibration using triple collocation. J. Geophys. Res. 103C4, 7755-7766

Troen, I. and E. L. Petersen, European Wind Atlas, Risø National Laboratory, Roskilde, 1989.

Verspeek, J., M. Portabella, A. Stoffelen, A. Verhoef, Calibration and Validation of ASCAT Winds, OSI-SAF Technical Note SAF/OSI/KNMI/TEC/TN/163, 2011
http://www.knmi.nl/scatterometer/publications/pdf/ASCAT_calibration.pdf

Vogelzang, J., A. Stoffelen, A. Verhoef en J. Figa-Saldana, *On the quality of high-resolution scatterometer winds*, J. Geophys. Res., 2011, 116, doi:10.1029/2010JC006640.

DTU Wind Energy
Technical University of Denmark

Frederiksborgvej 399
4000 Roskilde
Denmark
Phone +45 4677 5024

www.vindenergi.dtu.dk